WILEY-VCH

# Supporting Information

**Stimuli-sensitive linear-dendritic block copolymer-drug prodrug as nano-platform for tumor combination therapy**

*Hao Cai, Ping Tan, Xiaoting Chen, Michal Kopytynski, Dayi Pan, Xiuli Zheng, Lei Gu, Qiyong Gong, Xiaohe Tian, Zhongwei Gu, Hu Zhang, Rongjun Chen, Kui Luo**

Dr. H. Cai, Dr. P. Tan, Dr. D. Y. Pan, Dr. X. L. Zheng, L. Gu, Prof. Q. Y. Gong, Prof. X. H. Tian, Prof. Z. W. Gu, Prof. K. Luo
Huaxi MR Research Center (HMRRC), Department of Radiology, National Clinical Research Center for Geriatrics, Frontiers Science Center for Disease-Related Molecular Network, State Key Laboratory of Biotherapy, West China Hospital, Sichuan University, Chengdu 610041, China. *E-mail: luokui@scu.edu.cn

X. T. Chen
Animal Experimental Center of West China Hospital, Sichuan University, Chengdu, 610041, China

Dr. R. Chen, Dr. M. Kopytynski
Department of Chemical Engineering, Imperial College London, South Kensington Campus, London SW7 2AZ, United Kingdom

Prof. H. Zhang
Amgen Bioprocessing Centre, Keck Graduate Institute, Claremont, CA 91711, USA

Prof. Q. Y. Gong, Prof. K. Luo
Functional and Molecular Imaging Key Laboratory of Sichuan Province, and Research Unit of Psychoradiology, Chinese Academy of Medical Sciences, Chengdu, 610041, China

**Keywords**: tumor microenvironment-responsive, linear-dendritic block copolymer, amphiphilic polymer, nanomedicine, combination therapy

1. Materials and methods ..... 3
1.1. Materials ..... 3
1.2. Synthesis of methacrylate monomers ..... 4
1.2.1. Synthesis of MA-GFLG-($O^tBu$)$_2$ ..... 4
1.2.2. Synthesis of MA-GFLG-($O^tBu$)$_4$ ..... 5
1.2.3. Synthesis of MA-GFLG-(NHNHBoc)$_4$ ..... 5
1.3. Synthesis of linear-dendritic block copolymers ..... 5
1.3.1. Synthesis of macromolecular chain transfer agent POEGMA-CTA ..... 6
1.3.2. Synthesis of POEGMA-GFLG-(NHNHBoc)$_4$ ..... 6
1.3.3 Synthesis of amphiphilic linear-dendritic block copolymer prodrug POEGMA-GFLG-(DOX)$_4$ ..... 6
1.3.4 DOX release evaluation of each block polymer prodrug ..... 7
1.3.5 Critical micelle concentration (CMC) of each block polymer prodrug ..... 7
1.3.6 *In vivo* pharmacokinetics of each dual responsive-block polymer prodrug ..... 7
1.4. Nanopaiticles formation, drug loading, and drug release simulations ..... 8
1.5. Preparation and characterization of LD-DOX/Ce6 NPs ..... 9
1.6. Stability of NPs and *in vitro* release of DOX and Ce6 from NPs ..... 10
1.7. Detection of $^1O_2$ *in vitro* ..... 11
1.8. Cell culture and animal model ..... 11
1.9. Cell uptake and tumor penetration in three-dimensional multicellular tumor spheroids (MTSs) ..... 11
1.10. Intracellular ROS detection ..... 12
1.11. DNA damage assay ..... 12
1.12. *In vitro* cell cytotoxicity and apoptosis ..... 13
1.13. Transcriptome data processing and analysis ..... 14
1.13. 1. mRNA library construction and sequencing ..... 14
1.13. 2. Transcriptome data alignment ..... 14
1.13. 3. Differentiated expressed gene identified ..... 14
1.13. 4. Gene set enrichment analalysis ..... 14
1.13. 5. Visulized with heatmap and volcanplot ..... 14
1.14 Western blots ..... 14
1.15 Acute toxicity in mice ..... 15
1.16 Skin phototoxicity evaluation ..... 15
1.17 *In Vivo* pharmacokinetics and fluorescence imaging ..... 16
1.18. *In vivo* antitumor efficacy of chemo-photodynamic therapy ..... 17
1.19. Statistical analysis ..... 18
2. Supplementary results ..... 19
2.1. Schemes and figures ..... 19
2.2. Tables ..... 58
3. References ..... 60

# 1. Materials and methods

## 1.1. Materials

4-cyanopentanoic acid dithiobenzoate (CTA), poly(ethylene glycol) monomethyl ether methacrylate (OEGMA, Mw = 500 Da), 4-methoxyphenol, 2,2'-[Azobis(1-methylethylidene)]bis[4,5-dihydro-1H-imidazole] dihydrochloride (VA044), methacryloyl chloride, cathepsin B, doxorubicin hydrochloride (DOX·HCl) and chlorin e6 (Ce6) were purchased from Sigma-Aldrich (USA). Boc-glycin (Boc-Gly-OH), methyl L-phenylalaninate hydrochloride (H-Phe-OMe·HCl), Boc-L-Leucine (Boc-Leu-OH·$H_2O$), L-Leucine methyl ester hydrochloride (H-Leu-OMe·HCl), glycine methyl ester hydrochloride (H-Gly-OMe·HCl), L-glutamic acid di-tert-butyl ester hydrochloride (H-Glu(OtBu)-O$^t$Bu·HCl), Boc-hydrazide ($NH_2NHBoc$), 1-hydroxybenzotriazole hydrate (HOBt), N,Ndiisopropylethylamine (DIEA), 2-(7-Aza-1Hbenzotriazole-1-yl)-1,1,3,3-tetramethyluronium hexafluorophosphate (HATU), N1-((ethylimino)methylene)-N3,N3-dimethylpropane-1,3-diamine (EDC) and trifluoroacetic acid (TFA) were obtained from GL Biochem (Shanghai, China). RPMI 1640 medium and fetal bovine serum (FBS) were purchased from Gibco (Thermo Fisher, USA). SupraGel was obtained from Chaotai Biotechnology Ltd. (Nanjing, China). The CCK-8 assay kit was obtained from Dojindo Molecular Technologies (Japan). Singlet oxygen sensor green (SOSG) was purchased from Life Technologies (NY, USA). Reactive oxygen species (ROS) assay kit, Annexin V-FITC apoptosis detection kit and Hoechst 33342 were obtained from Beyotime Biotechnology (Shanghai, China). Primary antibodies for Western Blots including Bax (2772S), Caspase-3 (D3R6Y) (14220S), PARP (9542S) and γ-H2A.X (7631S) were purchased from Cell Signaling Technology (CST); Cleaved caspase-3 (ab2302) from Abcam; GAPDH (7E4) (200306-7E4) from ZEN BIO (Chengdu, China). HRP-conjugated secondary antibodies were from Jackson Lab (115-035-003, 111-035-003).

Characterization and structure confirmation of monomers and polymer conjugates were measured by $^1$H NMR (400 MHz Bruker Avance II NMR spectrometer, Germany). Matrix-assisted laser desorption/ionization time-of-flight (MALDI-TOF) mass spectrometry was performed on a MALDI-7090 TOF-TOF mass spectrometer (Shimadzu, Japan). The weight-average ($M_w$) and number-average ($M_n$) molecular weights of polymers were determined by Gel Permeation Chromatography (GPC) with a GPC column of Shodex Asahipak GF-510 HQ (7.5 mm ID × 300 mmL). The injection volume was 50 μL of 2 mg/mL sample solutions. The mobile phase was 0.2 M lithium chloride sodium solution ($H_2O$: DMF = 35:65, v/v) at a flow rate of 0.5 mL/min (45°C). $M_w$, $M_n$ and dispersity ($Đ$) were measured using Pullulan as a standard. The zeta potential and the hydrodynamic diameter of polymeric conjugates and

nanoparticles (NPs) were measured by dynamic light scattering (DLS, Malvern Zetasizer Nano ZS, UK), and results were analyzed with DTS software version 3.32. The morphology of resulting NPs and their degradation products was observed by transmission electron microscopy (TEM, Tecnai GF20S-TWIN, USA). The drug loading content of DOX and Ce6 in polymer conjugates and NPs were determined by UV-vis absorption spectroscopy (Perkin-Elmer, USA) and fluorescence spectrophotometer (Hitachi F-7000, Japan). High performance liquid chromatography (HPLC) analyses were performed on a Shimadzu prominence HPLC system (column: Shim-pack GIST C18, pore size: 5 μm, dimension: 4.6×250 mm).

## 1.2. Synthesis of methacrylate monomers

N-methacryloyl-glycyl-phenylalanyl-leucyl-glycine (MA-GFLG-OH) was synthesized as previously described.[1] N-methacryloyl-glycyl-phenylalanyl-glycyl- leucine (MA-GFGL-OH) was synthesized following a similar method. The other methacrylate monomers (MA-GFLG-($O^tBu$)$_2$, MA-GFLG-($O^tBu$)$_4$, MA-GFLG-NHNHBoc, MA-GFLG-(NHNHBoc)$_2$, MA-GFLG-(NHNHBoc)$_4$, MA-GFGL-($O^tBu$)$_2$, MA-GFGL-($O^tBu$)$_4$, MA-GFGL-NHNHBoc, MA-GFGL-(NHNHBoc)$_2$, MA-GFGL-(NHNHBoc)$_4$) were synthesized through step-by-step organic synthesis (**Scheme 1** and **Scheme 2**). Synthesis of MA-GFLG-(NHNHBoc)$_4$ was described as a representative procedure.

### 1.2.1. Synthesis of MA-GFLG-($O^tBu$)$_2$

MA-GFLG-OH (**Figure S1** and **S2**) (3.188 g, 6.9 mmol), H-Glu($O^tBu$)-$O^tBu$·HCl (2.46 g, 8.3 mmol), HOBt (1.31 g, 9.7 mmol), and EDC (1.86 g, 9.7 mmol) were dissolved in DMF (40 mL) and stirred in an ice bath under a nitrogen atmosphere for 30 min. Subsequently, DIPEA (6.8 mL, 41.1 mmol) was slowly added to the reaction vial via a syringe. After continuously stirring for 36 h at room temperature, solvents were removed by rotary evaporation, and the residues were dissolved in 300 mL ethyl acetate. The ethyl acetate solution was washed three times with $NaHCO_3$ aq. (satd.), HCl (0.1 M) and NaCl aq. (satd), respectively, then dried with $MgSO_4$. $MgSO_4$ was removed by filtration, and the solvents were removed by rotary evaporation. The obtained crude product was purified by silica gel column chromatography to obtain the intermediate product, MA-GFLG-Glu-($O^tBu$)$_2$, and the yield was 92%. The molecular structure was confirmed by using a matrix assisted laser desorption ionization time-of-light mass spectrometry (MALDI-TOF MS, Autoflex III, Bruker ) (**Figure S3**) and proton nuclear magnetic resonance ($^1$H NMR, **Figure S4**) using 400 MHz Bruker Avance II NMR spectrometer.

### 1.2.2. Synthesis of MA-GFLG-(O$^t$Bu)$_4$

MA-GFLG-(O$^t$Bu)$_2$ (3.9 g, 5.6 mmol) was dissolved in DCM (8.6 mL), and the solution was added with TFA (8.6 ml, 112 mmol) under stirring in an ice bath. The reaction was allowed to proceed at room temperature for 10 h. The solvent was then evaporated under a reduced pressure. The residue was washed with anhydrous diethyl ether. After centrifugation and removal of the supernatant twice, the pellet was dried to yield a white solid.

MA-GFLG-(O$^t$Bu)$_4$ was obtained following a similar procedure for MA-GFLG-Glu-(O$^t$Bu)$_2$, except that MA-GFLG-(OH)$_2$ (3.3 g, 5.6 mmol), H-Glu(O$^t$Bu)-O$^t$Bu·HCl (3.61 g, 12.2 mmol), HOBt (1.93 g, 14.3 mmol), EDC (2.74 g, 14.3 mmol) were dissolved in DMF (40 mL) and DIPEA (10.1 mL, 61.2 mmol) was added for a reaction time of 48 h. The yield of a white product was 90%. The molecular structure was confirmed by MALDI-TOF MS (**Figure S5**) and $^1$H NMR spectra (**Figure S6**).

### 1.2.3. Synthesis of MA-GFLG-(NHNHBoc)$_4$

The -O$^t$Bu group of MA-GFLG-(O$^t$Bu)$_4$ was removed following a similar procedure for MA-GFLG-(O$^t$Bu)$_2$, to produce a white solid. The reaction condition for MA-GFLG-(NHNHBoc)$_4$ was similar to MA-GFLG-(O$^t$Bu)$_2$, but MA-GFLG-(OH)$_4$ (1.50 g, 1.8 mmol), $NH_2NHBoc$ (1.88 g, 14.2 mmol), HATU (5.40 g, 14.2 mmol) were dissolved in DMF (50 mL) and DIPEA (4.8 mL, 28.8 mmol) was added for 48 h of reaction. Subsequently, the solvents were removed by rotary evaporation, and the residues were dissolved in 300 mL ethyl acetate. The ethyl acetate solution was washed three times with $NaHCO_3$ aq. (satd.), HCl (0.1 M) and NaCl aq. (satd), respectively, then dried with $MgSO_4$. $MgSO_4$ was removed by filtration, and the solvents were removed by rotary evaporation. The obtained crude product was purified by silica gel column chromatography to obtain the product MA-GFLG-(NHNHBoc)$_4$ with a yield of 84%. The molecular structure was confirmed by MALDI-TOF MS (**Figure S7**) and $^1$H NMR spectra (**Figure S8**). The characterization of other methacrylate monomers was shown in **Figures S9** to **S30**.

## 1.3. Synthesis of linear-dendritic block copolymers

The amphipathic block polymer prodrugs (POEGMA-GFLG-DOX, POEGMA-GFLG-(DOX)$_2$, POEGMA-GFLG-(DOX)$_4$, POEGMA-GFGL-DOX, POEGMA-GFGL-(DOX)$_2$, POEGMA-GFGL-(DOX)$_4$ ) were synthesized following a similar method (**Scheme 3** and **Scheme 4**). POEGMA-GFLG-(DOX)$_4$ was used as an example to illustrate the procedure.

### 1.3.1. Synthesis of macromolecular chain transfer agent POEGMA-CTA

OEGMA (4.13 g, 8.25 mmol), CTA (23.1 mg, 82.5 μmol), and the VA044 initiator (8.8 mg, 27.5 μmol) were dissolved in 18.7 mL of a binary solvent ($H_2O/CH_3OH$ = 4:1, v/v). The mixture was bubbled with argon for 30 min in an ice bath, and the polymerization reaction proceeded at 44 °C under the sealed condition in the dark for 12 h. The resulting solution was dialyzed (molecular weight cutoff, 3.5 kDa) against deionized water for 1.5 days at 4 °C, and then lyophilized to obtain the product POEGMA-CTA with a yield of 58% (2.42 g). The average molecular weights (MWs) and polydispersity (PDI) of polymers were determined by Gel Permeation Chromatography (GPC), and GPC analyses were performed on a Shimadzu prominence HPLC system (column: Shodex Asahipak GF-1G 7B and Shodex Asahipak GF-510 HQ, detector: Shimadzu RID-20A refractive index (RI) detector, flow rate: 0.5 mL/min, mobile phase: 0.2 M LiCl/DMF = 35:65, v/v, column temperature: 45℃, injection volume: 50 μL).

### 1.3.2. Synthesis of POEGMA-GFLG-$(NHNHBoc)_4$

POEGMA-CTA (1.73 g), MA-GFLG-$(NHNHBoc)_4$ (593.6 mg, 44.4 mmol) and VA044 (6.2 mg, 19.4 μmol) were dissolved in 10.5 mL of a binary solvent ($H_2O/CH_3OH$ =1:4, v/v). The mixture was bubbled with argon for 30 min at 0 °C, the polymerization reaction proceeded at 45 °C under the sealed condition in the dark for 17 h. The resulting solution was dialyzed (molecular weight cutoff, 8 kDa) against deionized water for 2 days at 4 °C, and then lyophilized to obtain the product POEGMA-GFLG-$(NHNHBoc)_4$ with 1.69 g. The Mws and PDI were determined by GPC on a Shimadzu prominence HPLC system as above. **Table S1** enlists the MWD of each copolymer.

### 1.3.3 Synthesis of amphiphilic linear-dendritic block copolymer prodrug POEGMA-GFLG-$(DOX)_4$

POEGMA-GFLG-$(NHNHBoc)_4$ (850.0 mg, 0.27 mmol) was dissolved in DCM (10 mL) and TFA (10 mL), and the solution was stirred in an ice bath. Then, the reaction was allowed to proceed at room temperature for 20 h. The solvents were removed by rotary evaporation. The residue was dissolved in deionized water. After dialysis (MWCO, 2 kDa) for 2 days, the solution was lyophilized to produce the product POEGMA-GFLG-$(NHNH_2 \cdot TFA)_4$.

The de-protected conjugate (500 mg) and DOX·HCl (200 mg) were dissolved in 20 mL of $NH_4OAc$ buffer (0.1 M, pH 5.7). The solution was then stirred in the dark at room temperature for 48 h. Subsequently, the solution was dialyzed (MWCO, 2 kDa) at 4 °C to completely remove excess free DOX. Finally, the solution was lyophilized to produce 530 mg

of the final product POEGMA-GFLG-$(DOX)_4$ (named as LD-DOX). The DOX content determined by UV-vis spectroscopy at 482 nm was 10.8 wt%. Table S2 enlists the drug loading content (DLC), critical micelle concentration (CMC) and size of each copolymer prodrug.

### 1.3.4 DOX release evaluation of each block polymer prodrug

The DOX release profiles of pH or pH/enzyme dual reasonsive prodrugs were investigated by a dialysis method, and POEGMA-GFLG-$(DOX)_4$ was used as an example to illustrate the procedure. Briefly, 3 mL of POEGMA-GFLG-$(DOX)_4$ at a 1 mg $mL^{-1}$ concentration was placed into the dialysis bag (MWCO, 1 kDa) and immersed in 40 mL release media (pH 5.4 with 2.8 μM cathepsin B or pH 7.4 with 2.8 μM cathepsin B) at 37 °C. At predetermined time points, 5 mL of the solution was collected and an equal volume of fresh medium was added. The concentrations of DOX were measured by a fluorescence spectrophotometer (Hitachi F-7000, Japan).

### 1.3.5 Critical micelle concentration (CMC) of each block polymer prodrug

The critical micelle concentration (CMC) of the prodrug was determined with pyrene as a fluorescent probe, and POEGMA-GFLG-$(DOX)_4$ was used as an example to illustrate the procedure. Briefly, 200 μL of pyrene solution ($1.2 \times 10^{-5}$ M) in acetone was added to a 10 mL sample vial. After acetone was evaporated, 2 mL of POEGMA-GFLG-$(DOX)_4$ solution at different concentrations (0.01~1000 μg $mL^{-1}$) was added (n = 3). The solution was then kept at 37 °C for 12 h under gentle stirring. The fluorescence spectra were recorded on a fluorescence spectrophotometer (Hitachi F-7000, Japan) ($\lambda_{ex}$ = 300~380 nm, $\lambda_{em}$ = 390 nm). The ratio of the fluorescence intensity at 339 nm to that at 334 nm was calculated. The CMC value of POEGMA-GFLG-$(DOX)_4$ was determined by the inflection point.

### 1.3.6 *In vivo* pharmacokinetics of each dual responsive-block polymer prodrug

For pharmacokinetic studies, healthy female BALB/c mice (weight: 20 ± 2 g, n = 5) were i.v. injected with POEGMA-GFLG-DOX, POEGMA-GFLG-$(DOX)_2$, POEGMA-GFLG-$(DOX)_4$ and free DOX·HCl via the tail vein at a dosage of 5 mg DOX $kg^{-1}$ mice, respectively. 20 μL of blood was extracted from the orbital sinus at different time points ranging from 1 min to 12 h and stored at -20 °C. After the blood samples were thawed at room temperature, 200 μL of dimethyl sulfoxide (DMSO) was added, and the mixture was vortexed for 5 min and placed at 4 °C overnight. The mixture was vortexed for 1 min before centrifugation at 14,000 rpm for 5 min. Finally, 100 μL of the supernatant was pipetted into a black 96-well plate, and the DOX fluorescence intensity (excitation at 480 nm and emission at 590 nm) was measured using a Varioskan Flash (Thermo Scientific, MA, USA). The content of DOX in

each blood sample was calculated from the standard curve of the free DOX. Blood pharmacokinetic parameters were analyzed by a non-compartment model using PK Solver software.

## 1.4. Nanopaiticles formation, drug loading, and drug release simulations

We use dissipative particle dynamics (DPD) to examine the formation of NPs and drug loading and release from the NPs.[2] DPD is a coarse-grained simulation technique that employs a momentum-conserving thermostat and soft repulsive interactions among beads representing a variety of molecules. This allows for simulations of physical phenomena occurring at relatively large time and spatial scales. Indeed, DPD has been successfully used for simulating the self-assembly of polymers and NPs dispersed in Newtonian fluids.[3]

In DPD, the time evolution of the many-body system obeys the Newton's second law $m\mathrm{d}\mathbf{v}_i/\mathrm{d}t = \mathbf{f}_i$, where $\mathbf{v}_i$ and $\mathbf{f}_i$ are, respectively, the velocity and force on a bead $i$ with mass $m$, and $t$ is time. The equations of motion are integrated using the velocity-Verlet algorithm. The force on a bead is $\mathbf{f}_i = \sum_j(\mathbf{F}^{\mathrm{C}}_{ij} + \mathbf{F}^{\mathrm{D}}_{ij} + \mathbf{F}^{\mathrm{R}}_{ij})$, where the sum runs over all beads $j$ within a cutoff radius $r_\mathrm{c}$ around the bead $i$. The conservative force is given by $\mathbf{F}^{\mathrm{C}}_{ij} = a_{ij}(1-\hat{r}_{ij})\hat{\mathbf{r}}_{ij}$, where $a_{ij}$ is the repulsion between beads $i$ and $j$, $\hat{r}_{ij} = r_{ij}/r_\mathrm{c}$ and $\hat{\mathbf{r}}_{ij} = \mathbf{r}_{ij}/r_\mathrm{c}$ with $r_{\mathrm{ij}} = |\mathbf{r}_i - \mathbf{r}_j|$. The dissipative force is $\mathbf{F}^{\mathrm{D}}_{ij} = -\gamma\omega^{\mathrm{D}}(r_{ij})(\hat{\mathbf{r}}_{ij}\cdot\mathbf{v}_{ij})\hat{\mathbf{r}}_{ij}$ and the random force is $\mathbf{F}^{\mathrm{R}}_{ij} = \sigma\omega^{\mathrm{R}}(r_{ij})\xi_{ij}\Delta t^{-1/2}\hat{\mathbf{r}}_{ij}$, where $\mathbf{v}_{ij} = \mathbf{v}_i - \mathbf{v}_j$. The coefficients $\gamma$ and $\sigma^2 = 2k_\mathrm{B}T\gamma$ determine the strength of dissipative and random forces. Here, $k_\mathrm{B}$ is the Boltzmann constant, and $T$ is the temperature of the system. Moreover, weight functions $\omega^{\mathrm{D}}(r_{ij})$ and $\omega^{\mathrm{R}}(r_{ij})$ are coupled via $\omega^{\mathrm{D}}(r_{ij}) = [\omega^{\mathrm{R}}(r_{ij})]$, and $\xi_{ij}$ is a zero-mean Gaussian random variable of unit variance with $\xi_{ij} = \xi_{ji}$. The relations between weight functions and the strength of dissipative and random forces are set to ensure the thermodynamic equilibrium. The generalized form of the weight function is given by $\omega^{\mathrm{R}}(r_{ij}) = (1-\hat{r}_{ij})^p$ with $p = 1$ for the standard DPD model. In our simulations, we set the time step $\Delta$t = 0.04, $p = 1$, $m = 1$, $r_\mathrm{c} = 1$, $a_{ii} = 25$, $k_\mathrm{B}T = 1$ and the solvent number density $\rho = 3$. For all bead interactions, we set $\gamma = 4.5$. Unless specified otherwise, all dimensional values are given in DPD units.

The coarse-grained model of POEGMA-GFLG-$(DOX)_4$ is shown in **Figure S36 a**. Each polymer chain has a hydrophilic block (blue) and a hydrophobic dendron block connected by a harmonic springs potential $U_{\mathrm{bond}} = K_\mathrm{b}((r-b)/r_c)^2$, where $K_\mathrm{b} = 64\ k_\mathrm{B}T$ and $b = 0.5\ r_\mathrm{c}$ are the bond constant and the equilibrium bond length respectively. The coarse-grained models of the polymers are designed based on the branched structures used in experiments, and each coarse-

grained bead contains almost the same volume and molecular weight. DOX molecules (red) are connected with glutamate dendron (brown) by pH-sensetive bonds and Ce6 molecules (green) are modeled by three connected beads that form triangular shape. The volume fraction of the polymers is set to 10% in all simulations, while fraction of Ce6 molecules is changed. Rectangular simulation boxes of 30× 30× 30 $r_c^3$ with periodic boundary conditions are used. The DPD simulations are performed for 200, 000 time steps with an integration time step of 0.02 to achieve thermodynamic equilibrium and obtain drug-loaded NPs in neutral conditions. Then, to describe the response behavior of polymer chains in different environments, namely, under lower pH condition or existing cathepsin B in the system, we broke some specific chemical bonds (hydrazone bond or GFLG tetrapeptide), leading to DOX or dendrons separated from polymer, respectively. After that, another 100, 000 time steps are used to analyze the drug release process in protonation conditions.

## 1.5. Preparation and characterization of LD-DOX/Ce6 NPs

LD-DOX/Ce6 NPs were prepared in a similar manner as the thin-film hydration method.[4] Briefly, POEGMA-GFLG-$(DOX)_4$ (20 mg) was dissolved in 20 mL of methanol, to which 6.48 mL of acetone containing Ce6 (0.5 mg $mL^{-1}$) was added dropwise under vigorous stirring. After the mixture was further stirred at room temperature for 2 h, the solvent was removed by distillation under a reduced pressure to form a homogeneous thin-film on the wall of the reaction flask. The residual organic solvent was then completely removed by vacuum drying overnight. Subsequently, deionized water was added dropwise to hydrate the Ce6-loaded thin-film. After stirring at 4 °C for 4 h, the resulting mixture was filtered through a membrane filter (0.45 μm) to remove unencapsulated Ce6. The solution obtained by filtration was freeze-dried to obtain POEGMA-GFLG-$(DOX)_4$/Ce6 NPs, which were stored at 4 °C and used for subsequent characterization. The entire experimental process was carried out in the dark. POEGMA-GFLG-$(DOX)_4$/Ce6 NPs with different ratios of POEGMA-GFLG-$(DOX)_4$ and Ce6 was prepared using the same method.

The hydrodynamic diameter and zeta potential of the obtained NPs were measured by dynamic light scattering (DLS, Malvern Zetasizer NANO ZS, UK). The morphology was of the obtained NPs and their degradation products was examined under a transmission electron microscope (TEM, Tecnai GF20S-TWIN, USA). TEM samples were prepared by dropping a solution onto a copper grid.

The loading contents of DOX and Ce6 in polymer conjugates and NPs were determined by UV-vis absorption spectroscopy (Perkin-Elmer, USA). The drug loading content (DLC) and the drug loading efficiency (DLE) were calculated using the following equations:

DLC (wt%) = (weight of drug loaded/total weight of polymer and loaded drug) × 100

DLE (wt%) = (weight of drug loaded/weight of drug fed) × 100

The characterization results of POEGMA-GFLG-$(DOX)_4$/Ce6 NPs at different feeding ratios are summarized in **Table S4**. PTX was used as another model drug to evaluate the ability of LD-DOX as a nano-platform to encapsulate hydrophobic therapeutic agents. PTX was encapsulated using the same method as Ce6. The characterization results of POEGMA-GFLG-$(DOX)_4$/PTX NPs at different feeding ratios are summarized in **Table S5**. The content of PTX was analyzed by HPLC system (column: Shim-pack GIST C18, pore size: 5 μm, dimension: 4.6×250 mm).

## 1.6. Stability of NPs and *in vitro* release of DOX and Ce6 from NPs

The stability of POEGMA-GFLG-$(DOX)_4$/Ce6 NPs (specified as LD-DOX/Ce6) (1.0 mg $mL^{-1}$) was examined under physiological conditions by incubating the NPs in three different buffer solutions in a shaker (100 rpm) at 37 °C: PBS (pH 7.4), PBS containing 10% FBS (pH 7.4) and cell culture medium without FBS. At predetermined time points, the particle size and PDI of the NPs were detected by DLS. Besides, the stability of LD-DOX/Ce6 in long-term storage at 4 °C was also evaluated. The photostability of LD-DOX/Ce6 in different media (PBS or DMSO) was assessed via UV-vis spectra. The sample solution was prepared at a Ce6 concentration of 2 μM and illuminated with a 660 nm laser at 2 mW $cm^{-2}$. The UV-vis absorbance of the samples at 664 nm was read at predetermined time points. The free Ce6 was used as control.

The *in vitro* drug release profiles of LD-DOX/Ce6 were investigated using a dialysis method under different physiological conditions mimicking tumor microenvironments and the blood circulation environment. Briefly, 3 mL of LD-DOX/Ce6 (1.0 mg $mL^{-1}$) was placed in a dialysis bag (MWCO: 1 kDa) and immersed in three media: McIlvaine's buffer (50 mM citrate/0.1 M phosphate, 2 mM ethylene diamine tetraacetic acid (EDTA)) with pH 5.4, McIlvaine's buffer with pH 7.4 and McIlvaine's buffer (pH 5.4) with 2.8 μM cathepsin B. The mixture was incubated in a shaker (100 rpm) at 37 °C. At each time interval, 5 mL of the buffer solution was withdrawn and an equal volume of fresh buffer was added. The concentrations of DOX were measured by a fluorescence spectrophotometer (Hitachi F-7000, Japan). At the same time, another LD-DOX/Ce6 (0.5 mg $mL^{-1}$) sample was incubated in an acidic aqueous solution (pH 5.4) for 24 h and the morphological changes of LD-DOX/Ce6 were observed under a TEM. The drug release properties of LD-DOX encapsulated PTX were determined according to the above method. The concentration of PTX is measured by HPLC (SHIMADZU, Japan).

## 1.7. Detection of $^1O_2$ *in vitro*

To evaluate the photochemical activity of Ce6 in LD-DOX/Ce6, the generation of singlet oxygen was determined using singlet oxygen sensor green (SOSG). The solution of LD-DOX/Ce6, free Ce6, free DOX and LD-DOX in PBS (equivalent Ce6 concentration of 1.0 μg $mL^{-1}$, DOX concentration of 1.0 μg $mL^{-1}$) was mixed with a SOSG solution (2.5 μM), and then the mixture was irradiated by a 660 nm laser (Xi'an Zhongchuan Optoelectronic Technology Co., Ltd., Xi'an, China) at a power density of 5.0 mW $cm^{-2}$ for 4 min. The SOSG fluorescence intensity of the sample was recorded at different time points (0, 30, 60, 120, 180, 240 s) at an excitation wavelength of 490 nm. Ce6 and LD-DOX/Ce6 not irradiated with laser were used as a control.

## 1.8. Cell culture and animal model

The 4T1 murine breast cancer cell line was obtained from Chinese Academy of Science Cell Bank for Type Culture Collection (Shanghai, China) and cultured in RPMI 1640 medium (Life Technologies) with 10% fetal bovine serum (FBS, Gibco, USA) and 1% penicillin-streptomycin (Hyclone, USA) in a humidified atmosphere containing 5% $CO_2$ at 37 °C. Female BALB/c mice (5~8 weeks old, 20 ± 2 g) purchased from Chengdu DaShuo Biological Technology Co., Ltd. were randomly divided and housed in a temperature-controlled room with regularly alternating cycles of light and darkness. The subcutaneous 4T1 tumor model was established by subcutaneous injection of $1.5 \times 10^5$ 4T1 cells suspended in 70 μL PBS into the right lower back of the female BALB/c mice. The orthotopic 4T1 tumor model was established by injection of $1.5 \times 10^5$ 4T1 cells suspended in 70 μL PBS into the right side of each mouse's fourth fat pad of the female BALB/c mice. The tumor volume was calculated as follows: length × $width^2$ × 0.5. All animal procedures were performed in accordance with the Guidelines for Care and Use of Laboratory Animals of West China Hospital, Sichuan University and approved by the Animal Ethics Committee of China.

## 1.9. Cell uptake and tumor penetration in three-dimensional multicellular tumor spheroids (MTSs)

To study cellular uptake of the LD-DOX/Ce6, 4T1 cells were seeded in glass-bottom dishes ($1 \times 10^4$ cells/mL) and incubated for 24 h. Subsequently, the original medium was replaced and fresh medium containing free DOX, free Ce6, LD-DOX or LD-DOX/Ce6 (equivalent to 5.0 μg $mL^{-1}$ of DOX or 5.5 μg $mL^{-1}$ of Ce6) was added separately into each dish. After 4 h incubation, the cells were washed three times with cold PBS, and cell nuclei were stained sequentially by Hoechst33342 according to the standard protocol provided by the supplier.

Intracellular drug distribution of LD-DOX/Ce6 in the 4T1 cells was observed under a confocal laser scanning microscopy (CLSM). The quantitative characterization of cellular uptake was performed with a flow cytometer (Beckman Coulter Cytomics FC-500, USA).

4T1 MTSs were further prepared to uncover tumor uptake and penetration *in vitro*. There was 2 mL molten 2% agarose solution and SupraGel (concentration: 10 mg/mL) added into dishes of a 5 cm diameter. After solidification of the solution, 4 mL 4T1 cell suspension of 5 × $10^6$ cells/mL per dish with fresh RMPI 1640 medium was added on the top of agarose. SupraGel was used to cell spheroid formulation. MTSs were formed after 5-day incubation to reach a diameter of about 200 μm.

To analyze penetration of LD-DOX/Ce6, MTSs were assayed with Hoechst33342 by following the protocol of the manufacturer. The MTSs were co-incubated with LD-DOX/Ce6 for 2, 4 and 6 h. Cells were then observed under a CLSM. The data were further processed by Image J software (National Institutes of Health, Bethesda, MD, USA).

## 1.10. Intracellular ROS detection

For intracellular ROS detection, 4T1 cells were seeded in 6-well plates (5 × $10^5$ cells/mL) and incubated for 24 h. Subsequently, the original medium was replaced and fresh medium containing Ce6 or LD-DOX/Ce6 was added separately at an equivalent Ce6 concentration of 1.0 μg $mL^{-1}$. After 6 h of incubation, the medium was discarded and 4T1 cells were incubated with 1 μM of 2', 7'-dichlorodihydrofluorescein diacetate (DCFH-DA, ROS-sensitive probe) for 20 min. The cells were then irradiated with 660 nm laser (10 mW $cm^{-2}$) for 30 s. Fluorescence signals of intracellular DCF were detected under a fluorescence microscopy (excitation at 488 nm, and emission at 525 nm). In addition, the intracellular ROS levels of various Ce6 formulations were also quantified by flow cytometry. After laser irradiation treatment of 4T1 cells as described above, each group of cells was collected and quantitatively analyzed by flow cytometry (FITC channel). Untreated and no-irradiated cells were used as control groups.

## 1.11. DNA damage assay

γH2A.X staining was used to evaluate DNA double strands breakage. 4T1 cells were seeded in 6-well plates (5 × $10^5$ cells/mL) and incubated for 24 h. Subsequently, cells were treated with free DOX, free Ce6, LD-DOX, LD-DOX/Ce6 (equivalent to 0.3 μg $mL^{-1}$ of DOX or 0.33 μg $mL^{-1}$ of Ce6) and incubated for 12 h. The spent medium was replaced by fresh medium. The cells in the irradiation experiment group were irradiated with a laser of 660 nm for 30 s (10 mW $cm^{-2}$). At 12 h post-laser irradiation, the cells were fixed in 4% paraformaldehyde and permeabilized with 0.2% Trition X-100. After blocking in 5% BSA for

1 h, the cells were incubated with anti-histone γH2A.X rabbit monoclonal antibodies at 4 ◦C overnight and then incubated with a fluorescently labeled goat anti-rabbit secondary antibody in 1% BSA for 1 h. After that, the cells were stained with DAPI to locate cell nuclei and observed with a CLSM. Quantitative analysis of γH2AX foci density (foci/per cell nuclear) were counted using the ImageJ software.

## 1.12. *In vitro* cell cytotoxicity and apoptosis

The cytotoxicity of free Ce6 against 4T1 cells was first evaluated using a CCK-8 assay kit. 4T1 cells were incubated in 96-well plates at a density of $5 \times 10^3$ cells/well and allowed to attach for 24 h before treatment. After the completed RPMI 1640 medium was removed, fresh medium containing various concentrations of Ce6 (0.0005~90 μg $mL^{-1}$) was added and incubation continued for 12 h. Subsequently, cells were washed twice with PBS and fresh culture medium was added. The cells were then irradiated by a 660 nm laser at a power of 10 mW $cm^{-2}$ for different time periods (0 min, 0.5 min, 1 min, 2 min). After laser irradiation, the treated cells were then incubated at 37 °C for 36 h and cell viability was evaluated by the CCK-8 assay. In addition, we also studied the cytotoxicity of 4T1 cells with different laser energy when the concentration of Ce6 was 3 μg $mL^{-1}$.

For chemo-photodynamic combined therapy, 4T1 cells were cultured in 96-well plates and incubated with free DOX, LD-DOX, LD-DOX/Ce6 without laser irradiation (specified as LD-DOX/Ce6) or LD-DOX/Ce6 with laser irradiation (specified as LD-DOX/Ce6 + L) at a DOX concentration ranging from 0.0005 to 90 μg $mL^{-1}$, respectively. After incubation for 12 h, cells treated with LD-DOX/Ce6 for further laser irradiation were replaced with fresh culture medium and then exposed to 660 nm laser for 30 s (10 mW $cm^{-2}$). After laser irradiation, the treated cells were then incubated at 37 °C for 36 h and cell viability was evaluated by the CCK-8 assay. The $IC_{50}$ value was calculated by GraphPad Prism 7 software. The combination index (CI) of LD-DOX and Ce6 + L was calculated by CompuSyn software.[5]

For apoptosis analysis, 4T1 cells were seeded in 6-well plates ($5 \times 10^5$ cells/mL) and incubated for 24 h. Subsequently, cells were treated with various drug formulations (equivalent to 0.3 μg $mL^{-1}$ of DOX or 0.33 μg $mL^{-1}$ of Ce6) and incubated for 12 h. The spent medium was replaced by fresh medium. The cells in the irradiation experiment group were irradiated with a laser of 660 nm for 30 s (10 mW $cm^{-2}$). After 24 h of irradiation, all cells in each experimental group were collected and analyzed by flow cytometry after treatment with the Annexin V-FITC apoptosis test kit according to the protocol provided by the supplier.

## 1.13. Transcriptome data processing and analysis

### 1.13. 1. mRNA library construction and sequencing

The TRIzol reagent (Invitrogen, Carlsbad, CA, USA) was used to isolate and purify the total DNA of each sample. The Dynabeads Oligo (dT)25-61005 (Thermo Fisher, CA, USA) was used to extract the Poly (A) RNA following the manufacturer's recommodation.

### 1.13. 2. Transcriptome data alignment

The adaptors and low-quality reads in raw fasta files were removed by fastp with default parameters. And the processed fatsa files were used to subsequent analysis, including alignemnt, quantification and differneitail identification. Besides, The STAR[6] was used to genertae the alignment files with mouse genome reference mm10.

### 1.13. 3. Differentiated expressed gene identified

The Rsamtools and GenomicAlignments were used to quantify the expression levels of each gene in different samples with singleEnd=FALSE, fragments=FALSE. The DESeq2 was used to normalizased the counts by removing the effect from gene length and library size of each sample. All the visulization and pathways enrichemnt were implmented on these processed data. Besides, the DESeq2 was also used to identify significantly expressed gene with p.adj < 0.05 and |log2-foldchange| > 0.5.[7] .

### 1.13. 4. Gene set enrichment analalysis

The gene otology database (GO) and KEGG enrichment analysis were implemented by clusterprofiler[8] with pvalueCutoff= 0.01, pAdjustMethod=BH and qvalueCutoff=0.05. The log-transformation had been used on expression data after DESeq2 processing. The gene set enrichment analysis was executed by GSEA[9] (java version) software with version 7 gene sets.

### 1.13. 5. Visulized with heatmap and volcanplot

The volcano map and heatmap were used to show the expression patterns of differentiated expressed genes. In volcan map, -log10(p-value) was regraded as the y-axis, and the log2-foldchange values were regraded as the x-axis. And the highlighted genes in volcano map came from significant enriched in version 7 gene sets in GSEA. In the heatmap, the gene were differentiated expressed gene which order by their log2-foldchange. And the genes labled in the heatmap also came from version 7 gene sets in GSEA. Besides, the visualization of volcano map was carried by ggplot2.

## 1.14 Western blots

For western blots analysis, 4T1 cells were seeded in 6-well plates ($5 \times 10^5$ cells/mL) and incubated for 24 h. Subsequently, cells were treated with PBS, free DOX, Ce6 +L or LD-

DOX/Ce6 + L (equivalent to 0.3 μg $mL^{-1}$ of DOX or 0.33 μg $mL^{-1}$ of Ce6), respectively, and incubated for 12 h. The spent medium was replaced by fresh medium. The cells in the irradiation experiment group were irradiated with a laser of 660 nm for 30 s (10 mW $cm^{-2}$). After 24 h of irradiation, cells in each group were harvested, and the cell lysate was immediately prepared. Electrophoresis was performed using 10% SDS-polyacrylamide gel and transferred to Immobilon-P (Millipore) membrane. Primary antibodies were applied at 1:500-1:2000 dilution in 5% BSA and incubated overnight at 4 °C. HRP-conjugated secondary antibodies were applied at 1:10000 dilution. The Immobilon Western Chemiluminescent HRP Substrate (WBKLS0500, MILIPORE) was used for visualization of proteins. Healthy BAlc female mice were subjected to back hair removal treatment 3 days before the light to ensure that the skin damage can be recovered

## 1.15 Acute toxicity in mice

130 healthy BALB/c mice (half male and half male) were randomly divided into 13 groups (n = 10, 5 male and 5 female): one Saline group, three DOX groups (at the dose of 5 mg $kg^{-1}$, 10 mg $kg^{-1}$, 15 mg $kg^{-1}$), three Ce6 groups (at the dose of 10 mg $kg^{-1}$, 20 mg $kg^{-1}$, 30 mg $kg^{-1}$), three LD-DOX groups (at an equivalent DOX dose of 10 mg $kg^{-1}$, 20 mg $kg^{-1}$, 30 mg $kg^{-1}$) and three LD-DOX/Ce6 groups (at the equivalent DOX/Ce6 dose of 10 mg $kg^{-1}$/11.1 mg $kg^{-1}$, 20 mg $kg^{-1}$/22.2 mg $kg^{-1}$, 30 mg $kg^{-1}$/33.3 mg $kg^{-1}$). The mice were fasted for 12 h before tail vein administration of above formulations. Mice were monitored for 4 h on the day of administration, and the body weight, general behavior changes and death of the mice were recorded every other day for 14 days. The mice in each group were sacrificed at the end of the experiment. The blood of mice in the saline group, the DOX group (10 mg $kg^{-1}$), the Ce6 group (10 mg $kg^{-1}$), the LD-DOX group (10 mg $kg^{-1}$) and the LD-DOX/Ce6 group (equivalent DOX/Ce6 dose of 10 mg $kg^{-1}$/11.1 mg $kg^{-1}$) was obtained for blood routine tests and biochemical analysis, and their main organs were stained with hematoxylin and eosin (H&E).

## 1.16 Skin phototoxicity evaluation

Healthy BALB/c female mice were depilated 3 days before laser irradiation to ensure that all injures had recovered. The shaved mice were randomly divided into four groups (n = 4): (a) injection with saline without laser irradiation; (b) laser irradiation; (c) injection with free Ce6 with laser irradiation (at a Ce6 dose of 2 mg $kg^{-1}$); (d) injection of LD-DOX/Ce6 with laser irradiation (at an equivalent Ce6 dose of 2 mg $kg^{-1}$). Immediately after administration oft he above formulations, the anesthetized mice were irradiated by a 660 nm laser (200 mW $cm^{-2}$, 4 min), and the back of the mice with an area of ~1 $cm^2$ area were exposed to laser irradiation.

The skin on the back in these groups was photographed at day 1, 2, 3, 4 and 5 after irradiation, respectively. The Paraffin sections of skin were stained with H&E.

## 1.17 *In Vivo* pharmacokinetics and fluorescence imaging

To measure pharmacokinetics of LD-DOX/Ce6, three normal female BALB/c mice were *i.v.* injected with free Ce6 or LD-DOX/Ce6 via the tail vein at a dosage of 5 mg Ce6 per kg mice. 20 μL of blood was extracted from the orbital sinus at different time points ranging from 1 min to 24 h and stored at -20 °C. After the blood samples were thawed at room temperature, 100 μL of acetonitrile was added, and the mixture was vortexed for 5 min and placed at 4 °C overnight. The mixture was vortexed for 1 min before centrifugation at 14,000 rpm for 5 min. Finally, 100 μL of the supernatant was pipetted into a black 96-well plate, and the Ce6 fluorescence intensity (excitation at 400 nm and emission at 660 nm) was measured using a Varioskan Flash (Thermo Scientific, MA, USA). The content of Ce6 in each blood sample was calculated from the standard curve of the free Ce6. Blood pharmacokinetic parameters were analyzed by a non-compartment model using PK Solver software.

A 4T1 subcutaneous xenograft tumor model was established to map the *in vivo* distribution of LD-DOX/Ce6. When the tumor reached a volume of approximately 100 $mm^3$, the mice were randomized into 3 groups (n = 3), each of which was intravenously injected with free saline, free Ce6 or LD-DOX/Ce6 at equivalent concentration of 5 mg Ce6 $kg^{-1}$ mice. The mice in each group were euthanized at 1 h, 3 h, 6 h, 12 h, 24 h, 48 h and 72 h after administration. Heart, liver, spleen, lungs, kidneys and tumor were separated and immediately subjected to *in vitro* fluorescence imaging on a Maestro In-Vivo imaging system. A similar procedure as above was performed for another batch of 4T1 tumor-bearing mice. The mice were euthanized at 1 h, 12 h, 24 h, 48 h and 72 after administration, and the tumors were immediately excised for preparation of frozen sections. Tumor sections were stained for nuclei and blood vessels with DAPI and anti-CD31 antibodies, respectively, and then observed under CLSM.

Biodistribution of LD-DOX/Ce6 in tumor was further evaluated via fluorescence imaging after injection of LD-DOX/Ce6 into mice bearing orthotopic 4T1 tumor. The mice with a tumor volume of about 150 $mm^3$ were injected with LD-DOX/Ce6 at 5 mg Ce6/kg mice for each mouse via tail veins. Three mice of each group were continuously taken fluorescence imaging at 1, 6, 24 and 48 h post-injection. The CLSM was also used to investigate the penetration of NPs from tumor vascular into tumors. When orthotopic 4T1 tumor volumes reached 150 $mm^3$ , mice were intravenously administrated with LD-DOX/Ce6 (5 mg Ce6/kg mice). After the mice were anesthetized, the skin on the surface of the tumor was uncovered,

and the fluorescence change of the tumor site was immediately observed using a fluorescence microscope. During the whole experiment, mice were anesthetized with isoflurane.

## 1.18. *In vivo* antitumor efficacy of chemo-photodynamic therapy

The subcutaneous 4T1 tumor model and orthotopic 4T1 tumor model was established as described above. For subcutaneous tumor model, when the tumors of female BALB/c mice reached a volume of approximately 70 $mm^3$, mice were divided into 9 groups (n = 7) to receive one of the following treatments: saline (G1), laser alone (G2), free Ce6 + L at a dose of 8.9 mg Ce6 $kg^{-1}$ mice (G3), free DOX at a dose of 4 mg DOX $kg^{-1}$ mice (G4), LD-DOX/Ce6 without laser irradiation (DOX = 4 mg $kg^{-1}$, Ce6 = 4.4 mg $kg^{-1}$) (G5), LD-DOX/Ce6 without laser irradiation (DOX = 8 mg $kg^{-1}$, Ce6 = 8.9 mg $kg^{-1}$) (G6), LD-DOX/Ce6 with laser irradiation (DOX = 4 mg $kg^{-1}$, Ce6 = 4.4 mg $kg^{-1}$) (G7), LD-DOX/Ce6 with laser irradiation (DOX = 8 mg $kg^{-1}$, Ce6 = 8.9 mg $kg^{-1}$) (G8) and free DOX at a dose of 8 mg DOX $kg^{-1}$ mice (G9) by tail injection on day 1, 5, 9, and 13. For the laser irradiated group, mice were irradiated with a 660 nm laser (250 mW $cm^{-2}$) at 24 h post-injection for 20 min after each administration. During entire experimental period, body weight and tumor volume of each mouse were recorded every 2 days. On day 21, all mice were euthanized and the major organs and tumors were dissected separately. Tumors of each group were weighed and the tumor growth inhibition (TGI) was calculated using the formula: $TGI = (1-W_1/W_2) \times 100\%$, where $W_1$ and $W_2$ represented the mean tumor weight of the treated and control groups. H&E staining was performed for each group of organs and tumors to observe the morphological and pathological characteristics. Tumor tissue was further used for immunohistochemical analysis in a similar way as described in previous reports.[10]

For orthotopic 4T1 tumor model, when the 4T1 tumor volume reached approximately 70 $mm^3$, the mice were divided into 6 groups and treated with saline, free Ce6 + L (8.9 mg $kg^{-1}$ mice), free DOX (4 mg $kg^{-1}$ mice), LD-DOX (DOX = 8 mg $kg^{-1}$), LD-DOX/Ce6 without laser irradiation (DOX = 8 mg $kg^{-1}$, Ce6 = 8.9 mg $kg^{-1}$) and LD-DOX/Ce6 +L (DOX = 8 mg $kg^{-1}$, Ce6 = 8.9 mg $kg^{-1}$), respectively by tail injection on day 1, 5, 9, and 13. For the laser irradiated group, mice were irradiated with a 660 nm laser (250 mW $cm^{-2}$) at 24 h post-injection for 20 min after each administration. The body weight and tumor volume were monitored as above. The survival rate was recorded for 30 days (When mice body weight lost more than 20% or the longest diameter of the tumor was greater than 12 mm, the mice were considered dead). On day 21, the tumor metastasis in the lungs of each group of mice was detected by a Quantum GX Micro-CT Imaging System (Quantum GX, PerkinElmer, USA). The micro-CT scanning parameters were as follows: voltage, 80 kV; current, 100 μA; pixel

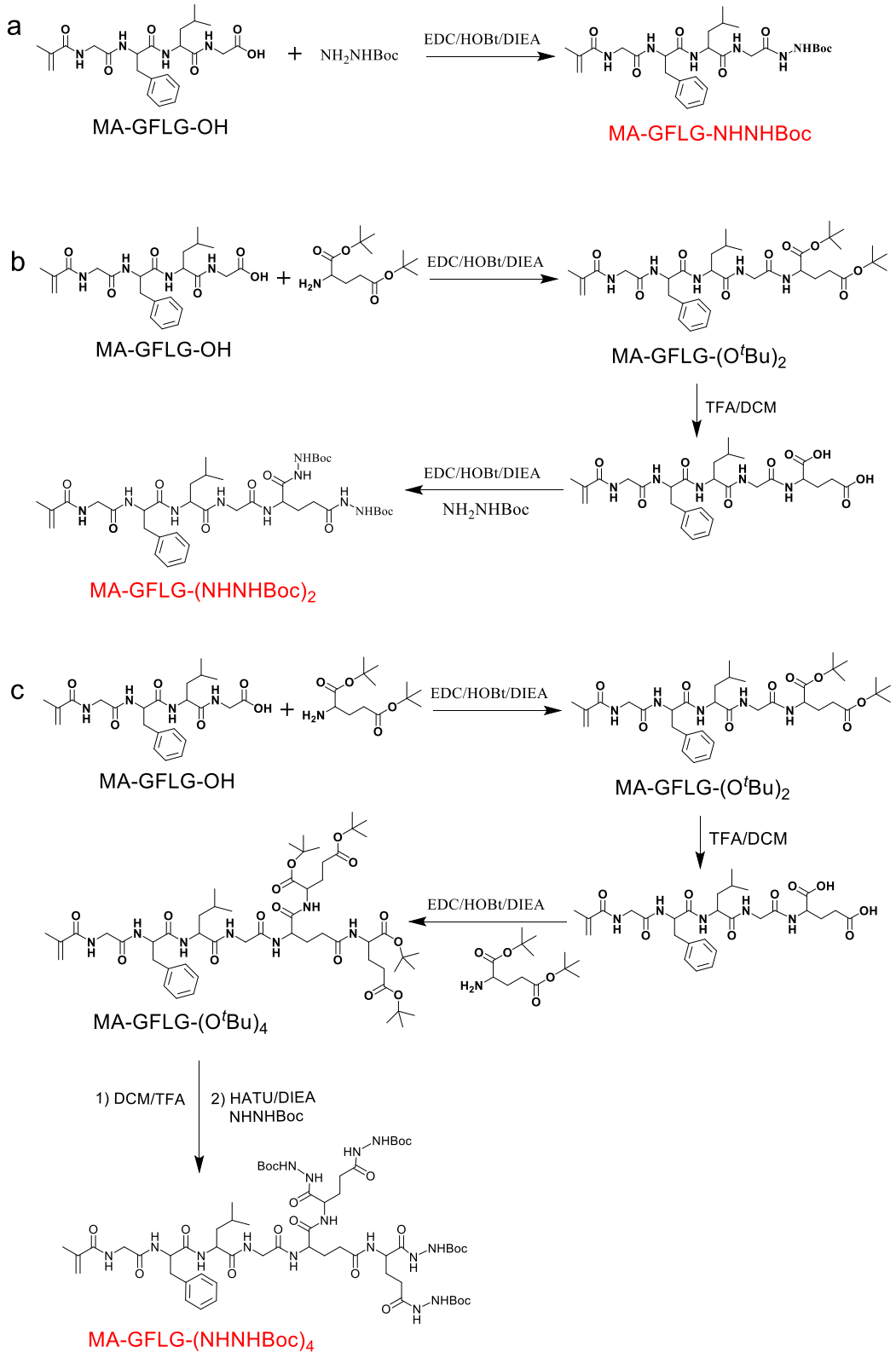
size, 150 μm. 3D images were reconstructed using an Analyze 12.0 software (PerkinElmer, US) to produce a visual representation of the results.[11] After the mice were sacrificed, the lungs were harvested and fixed with 4% paraformaldehyde. H&E staining analysis of lung lobe sections from mice and calculation of metastatic nodules on surface of lungs were carried out.

## 1.19. Statistical analysis

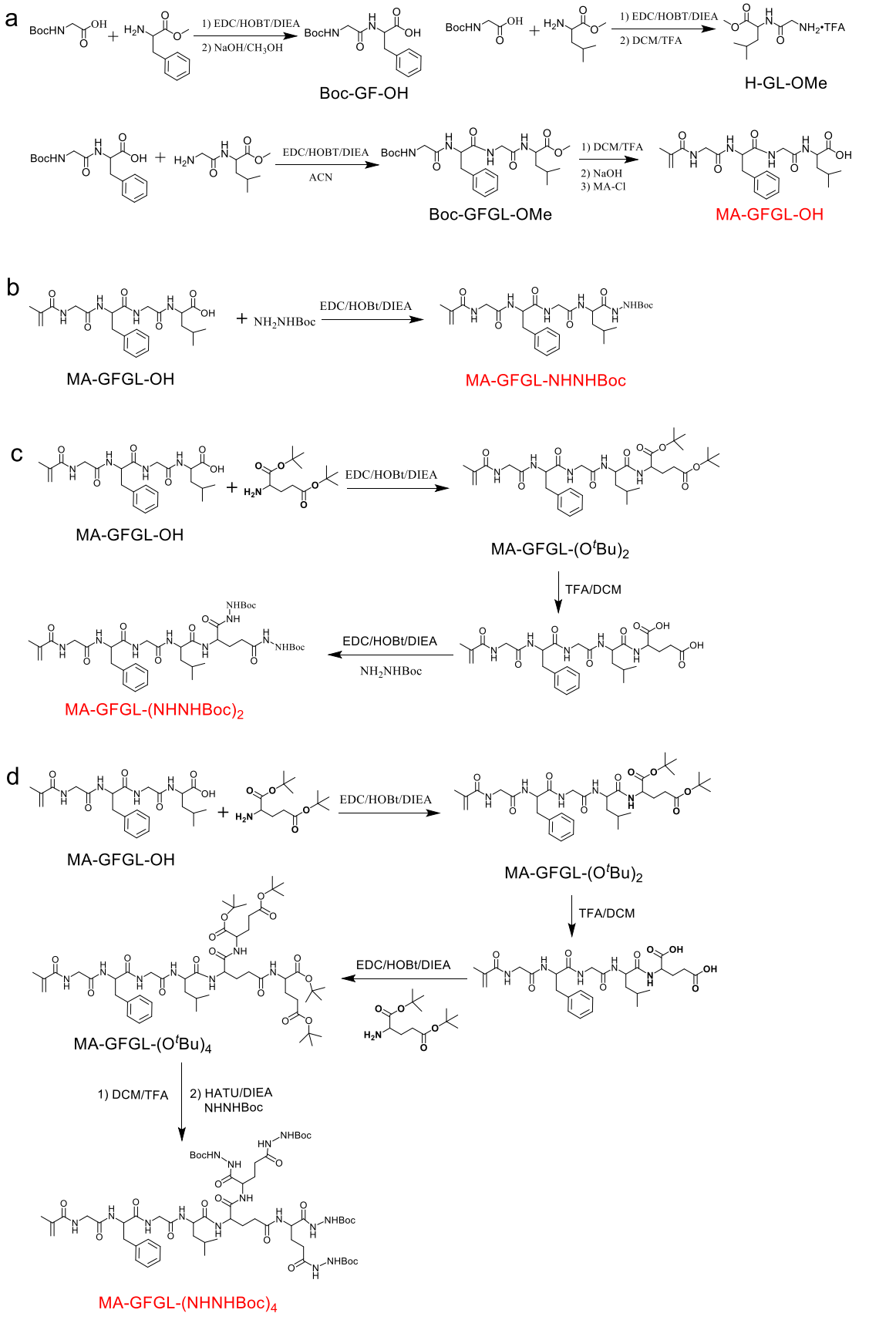
All numeric data are expressed as mean ± standard deviation (SD), unless otherwise indicated. Differences between groups were assessed using Student's t test. Statistical analysis was performed using GraphPad Prism 7.0. *P* values of less than 0.05 were considered significant; **P* < 0.05, ***P* < 0.01, ****P* < 0.001 and *****P* < 0.0001.

## 2. Supplementary results

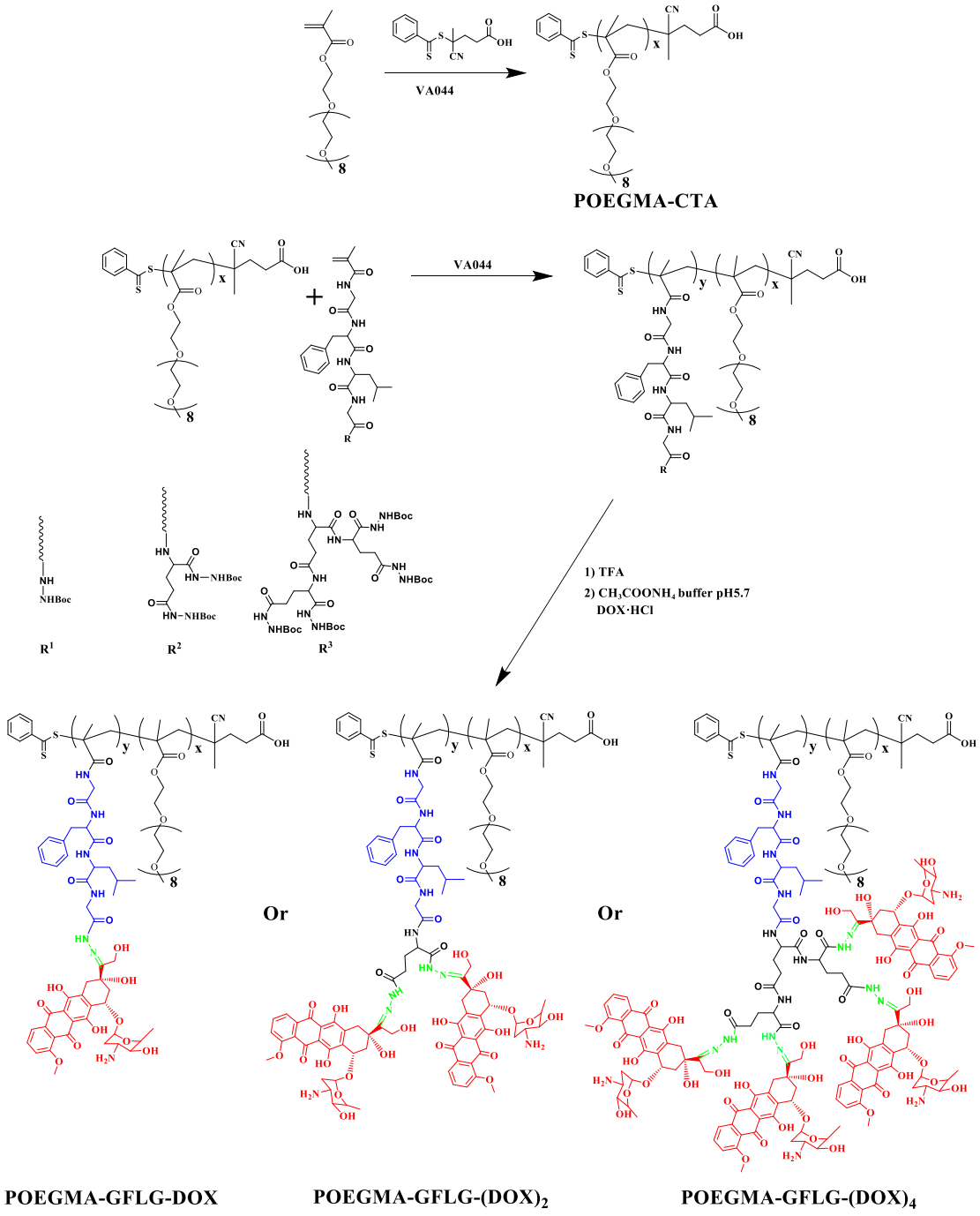
### 2.1. Schemes and figures



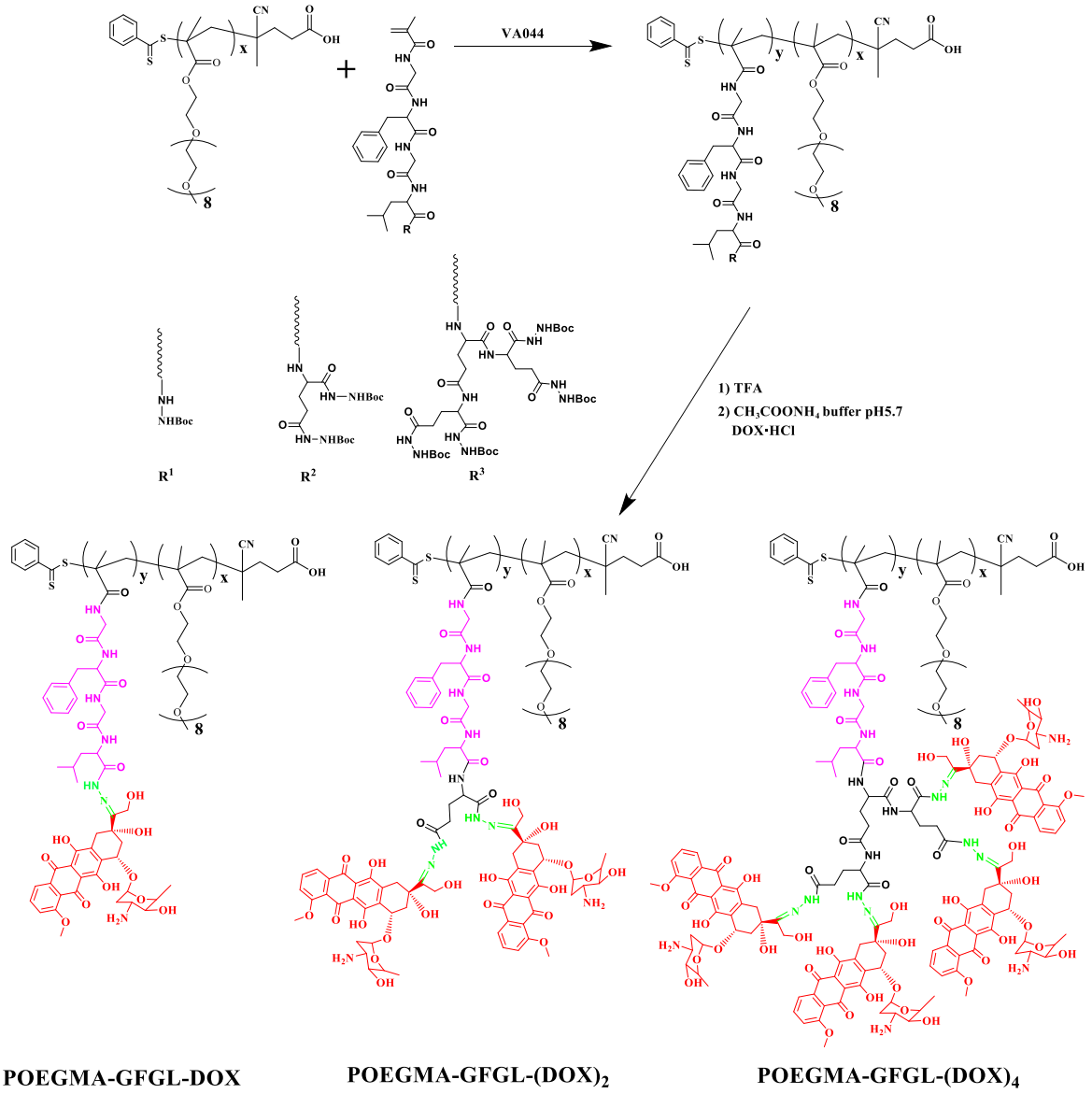

**Scheme S1.** Synthesis routes of monomers (a) MA-GFLG-NHNHBoc, (b) MA-GFLG-(NHNHBoc)$_2$ and (c) MA-GFLG-(NHNHBoc)$_4$.




**Scheme S2.** Synthesis routes of monomers (a) MA-GFGL-OH, (b) MA-GFGL-NHNHBoc, (c) MA-GFGL-(NHNHBoc)$_2$ and (d) MA-GFGL-(NHNHBoc)$_4$.




**Scheme S3.** Synthetic routes of amphiphilic linear-dendritic polymer prodrugs POEGMA-GFLG-DOX, POEGMA-GFLG-$(DOX)_2$ and POEGMA-GFLG-$(DOX)_4$.




**Scheme S4.** Synthetic routes of amphiphilic linear-dendritic polymer prodrugs POEGMA-GFGL-DOX, POEGMA-GFGL-$(DOX)_2$ and POEGMA-GFGL-$(DOX)_4$.

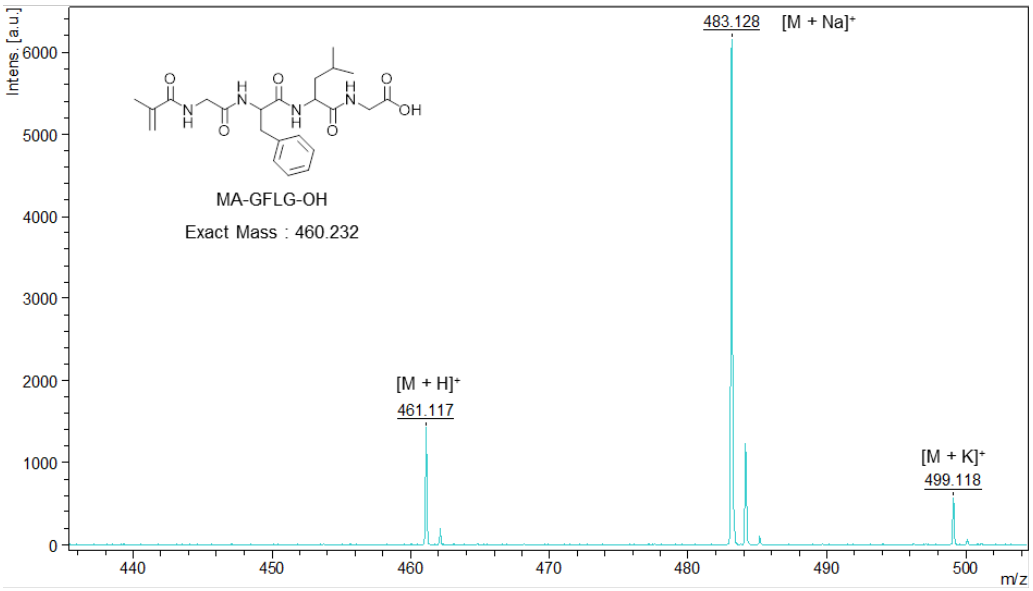



**Figure S1.** MALDI-TOF mass spectra of MA-GFLG-OH, $[M+H]^+$, at m/z = 461.117.

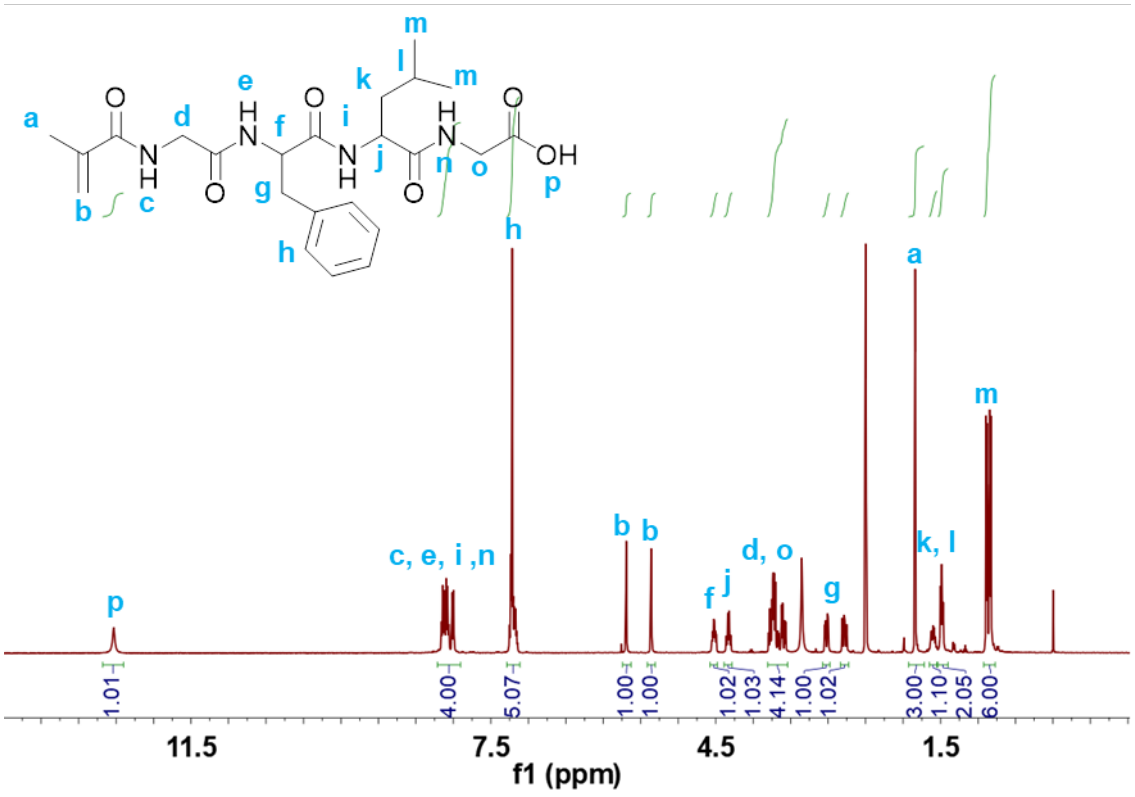



**Figure S2.** $^1$H NMR spectra of MA-GFLG-OH in DMSO-*d*$_6$. $^1$H NMR (400 MHz, DMSO-*d6*) δ 12.58 (s, 1H), 7.30 – 7.10 (m, 5H), 5.69 (s, 1H), 5.36 (s, 1H), 4.59 – 4.47 (m, 1H), 4.36 – 4.27 (m, 1H), 3.82 – 3.55 (m, 4H), 3.06 – 2.90 (m, 1H), 2.87 – 2.73 (m, 1H), 1.84 (s, 3H), 1.68 – 1.28 (m, 3H), 0.86 (dd, 6H).

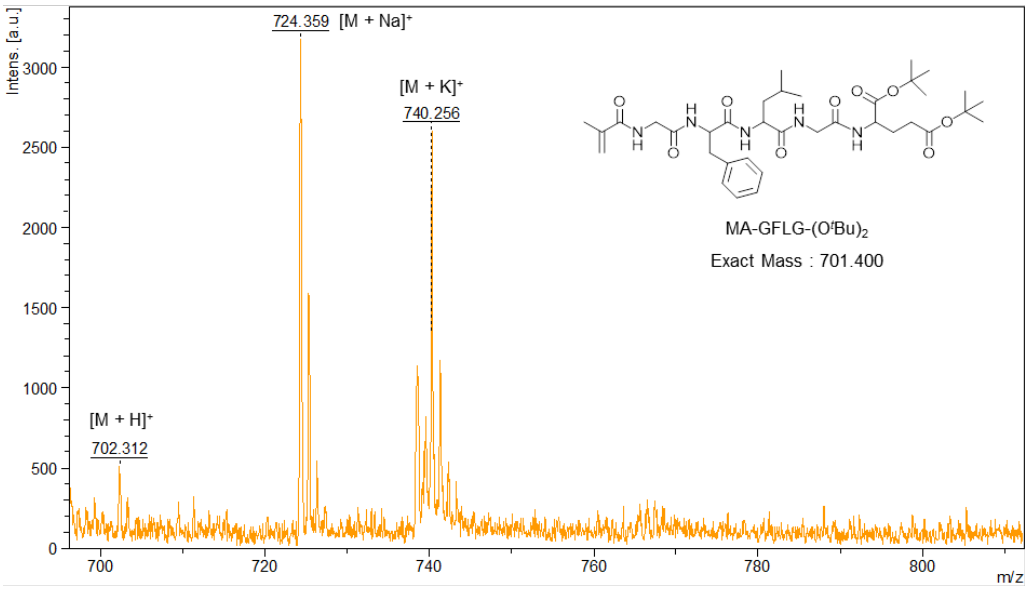



**Figure S3.** MALDI-TOF mass spectra of MA-GFLG-(O$^t$Bu)$_2$, $[M+H]^+$, at m/z = 702.312.

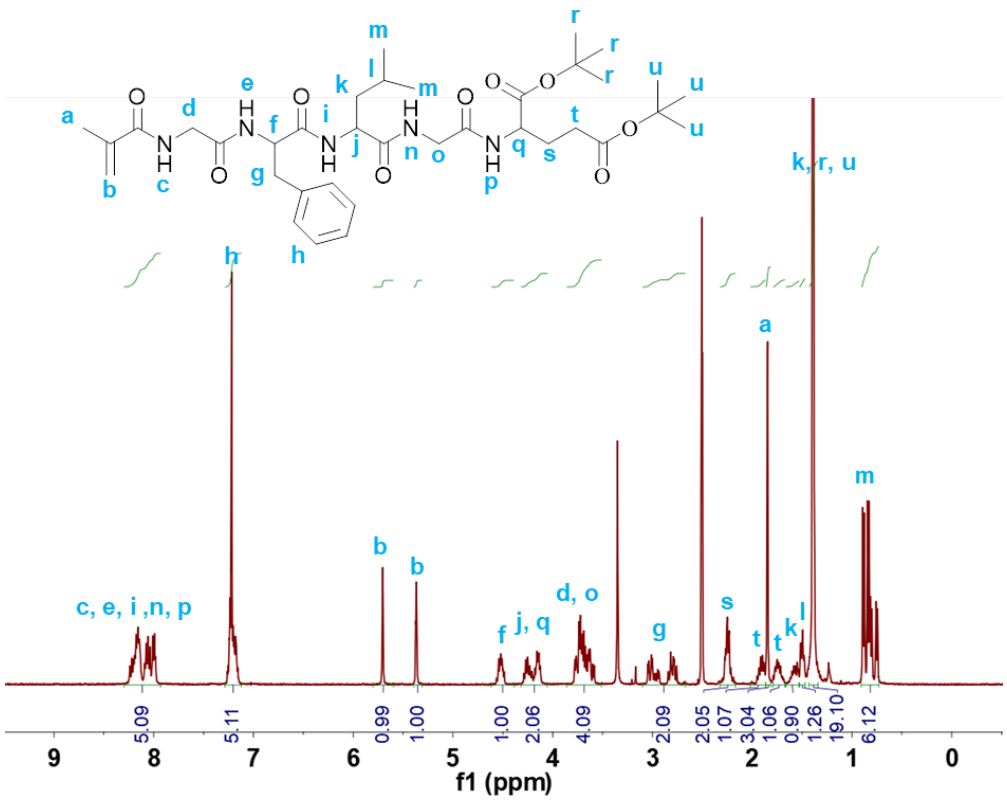



**Figure S4.** $^1$H NMR spectra of MA-GFLG-Glu-(OtBu)$_2$ in DMSO-*d*$_6$. $^1$H NMR (400 MHz, DMSO-*d6*) δ 7.41 – 6.96 (m, 5H), 5.70 (s, 1H), 5.37(s, 1H), 4.59 – 4.44 (m, 1H), 4.32 – 4.07 (m, 2H), 3.80 – 3.57 (m, 4H), 3.06 – 2.91 (m, 1H), 2.84 – 2.75 (m, 1H), 2.29 – 2.18 (m, 2H), 1.96 – 1.87 (m, 1H), 1.85 (s, 3H), 1.80 – 1.67 (m, 1H), 1.64 – 1.53 (m, 1H), 1.53 – 1.47 (m, 1H), 1.43 – 1.34 (m, 19H), 0.86 (dd, 6H).

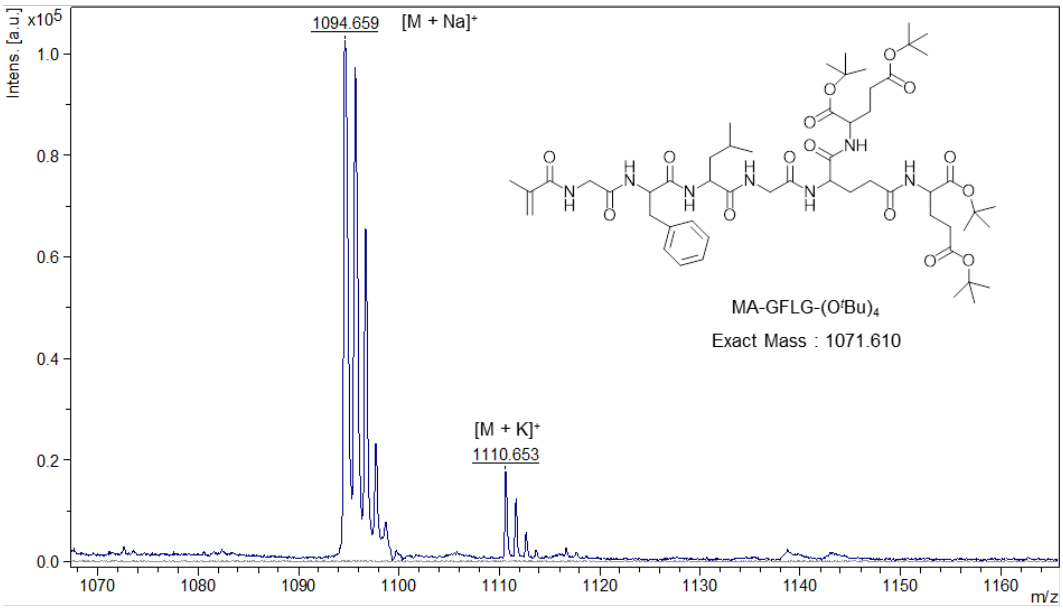



**Figure S5.** MALDI-TOF mass spectra of MA-GFLG-(O$^t$Bu)$_4$, $[M+Na]^+$, at m/z = 1094.659.

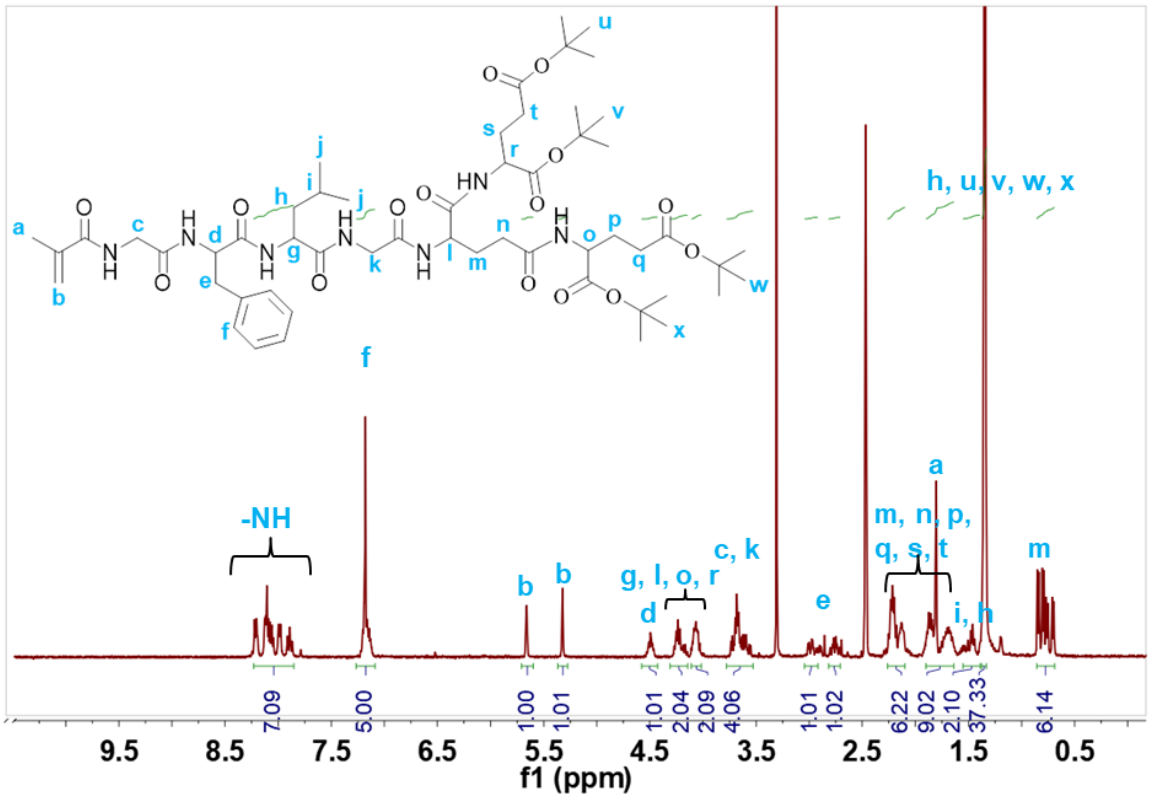



**Figure S6.** $^1$H NMR spectra of MA-GFLG-(O$^t$Bu)$_4$ in DMSO-*d*$_6$. $^1$H NMR (400 MHz, DMSO-*d6*) δ 7.25 – 7.09 (m, 5H), 5.66 (s, 1H), 5.32 (s, 1H), 4.54 – 4.44 (m, 1H), 4.29 – 4.01 (m, 4H), 3.79 – 3.52 (m, 4H), 3.02 – 2.92 (m, 1H), 2.82 – 2.71 (m, 1H), 2.31 – 2.09 (m, 6H), 1.90 – 1.64 (m, 9H), 1.55 – 1.41 (m, 2H), 1.38 – 1.32 (m, 37H), 0.86 (dd, 6H).

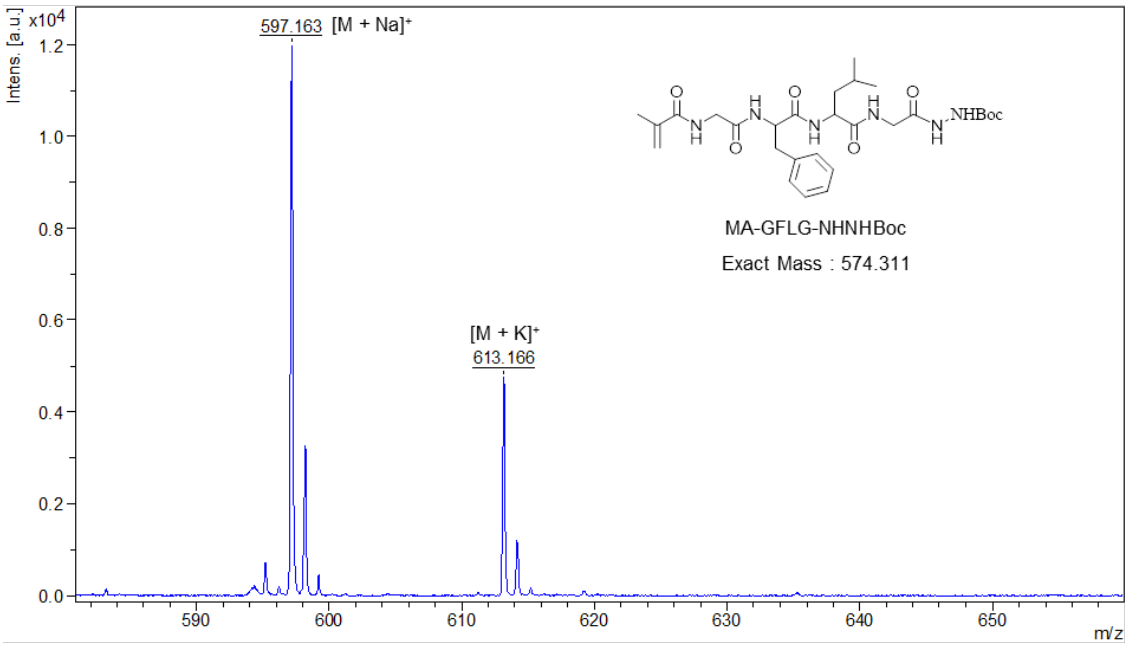



**Figure S7.** MALDI-TOF mass spectra of MA-GFLG- NHNHBoc, $[M+Na]^+$, at m/z = 597.163.

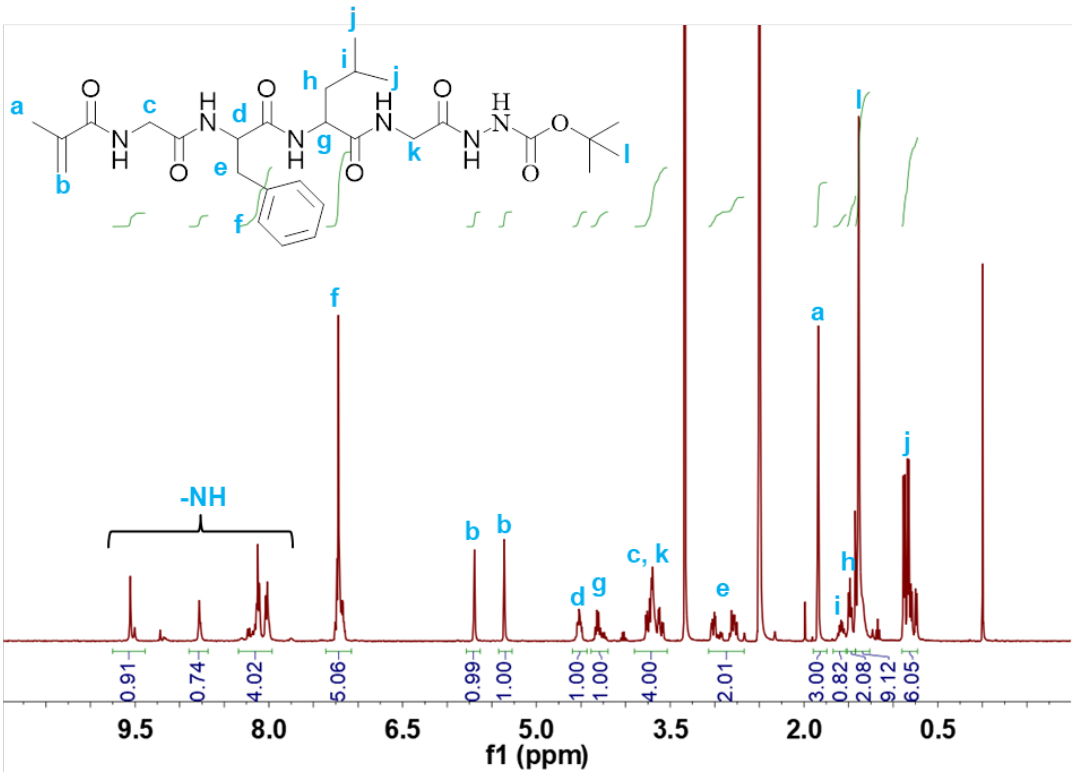



**Figure S8.** $^1$H NMR spectra of MA-GFLG- NHNHBoc in DMSO-$d_6$. $^1$H NMR (400 MHz, DMSO-*d6*) δ 7.32 – 7.11 (m, 5H), 5.69 (s, 1H), 5.36 (s, 1H), 4.59 – 4.47 (m, 1H), 4.38 – 4.20 (m, 1H), 3.79 – 3.56 (m, 4H), 3.05 – 2.68 (m, 2H), 1.84 (s, 3H), 1.68 – 1.53 (m, 1H), 1.52 – 1.45 (m, 2H), 1.39 (s, 9H), 0.85 (dd, 6H).

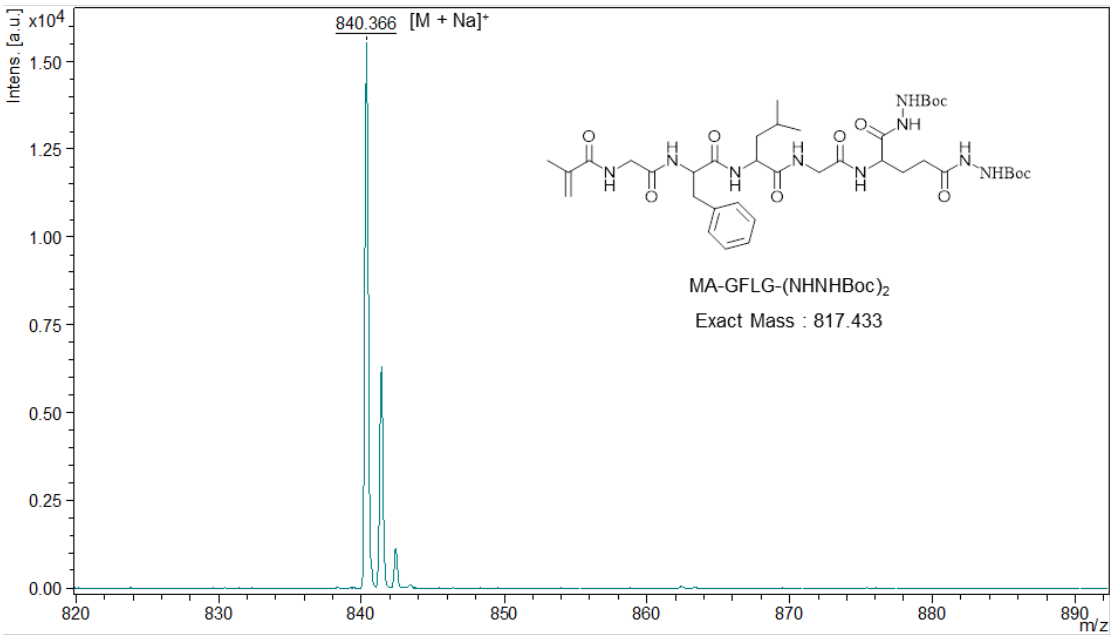



**Figure S9.** MALDI-TOF mass spectra of MA-GFLG- $(NHNHBoc)_2$, $[M+Na]^+$, at m/z = 840.366.

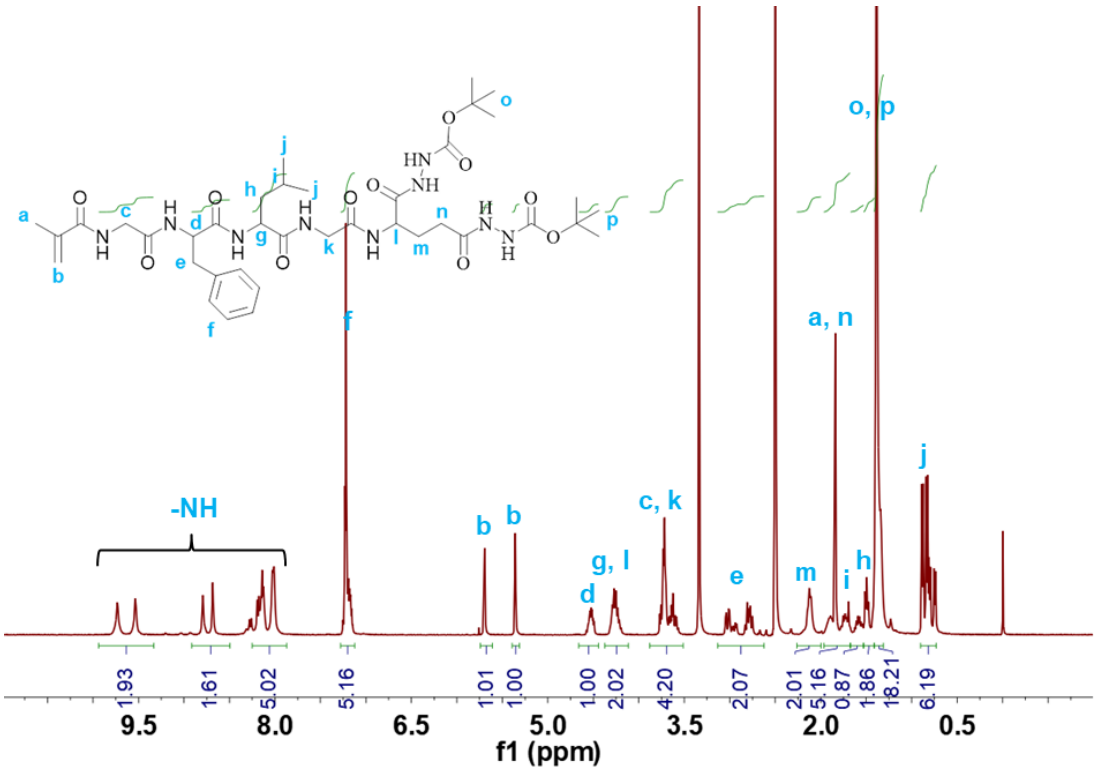



**Figure S10.** $^1H$ NMR spectra of MA-GFLG- $(NHNHBoc)_2$ in DMSO-$d_6$. $^1H$ NMR (400 MHz, DMSO-*d6*) δ 7.32 – 7.09 (m, 5H), 5.69 (s, 1H), 5.36 (s, 1H), 4.66 – 4.09 (m, 3H), 3.86 – 3.55 (m, 4H), 3.09 – 2.67 (m, 2H), 2.26 – 2.01 (m, 2H), 1.98 – 1.68 (m, 5H), 1.65 – 1.53 (m, 1H), 1.53 – 1.46 (m, 2H), 1.36 (s, 18H), 0.86 (dd, 6H).

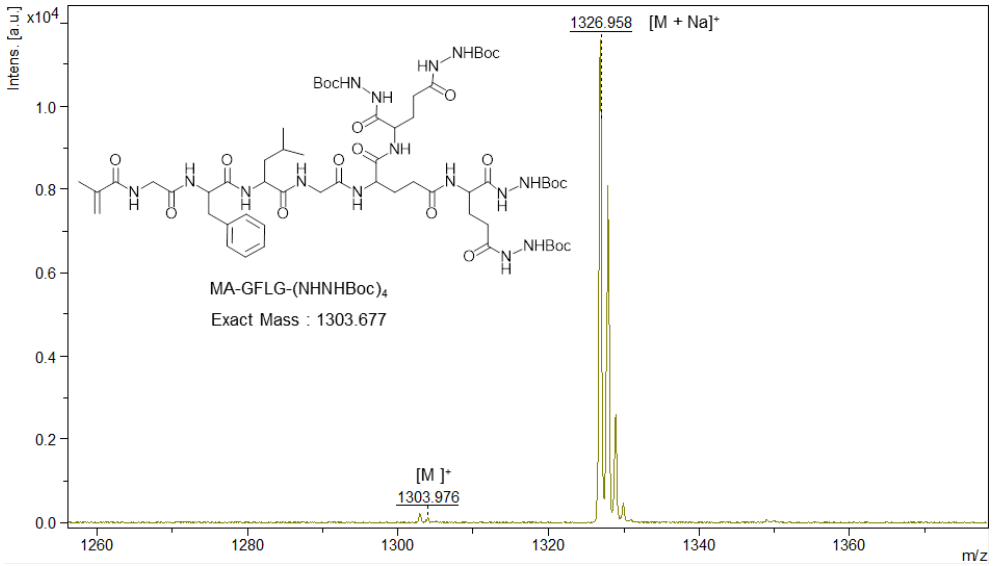



**Figure S11.** MALDI-TOF mass spectra of MA-GFLG-(NHNHBoc)$_4$, $[M+Na]^+$, at m/z = 1326.958.

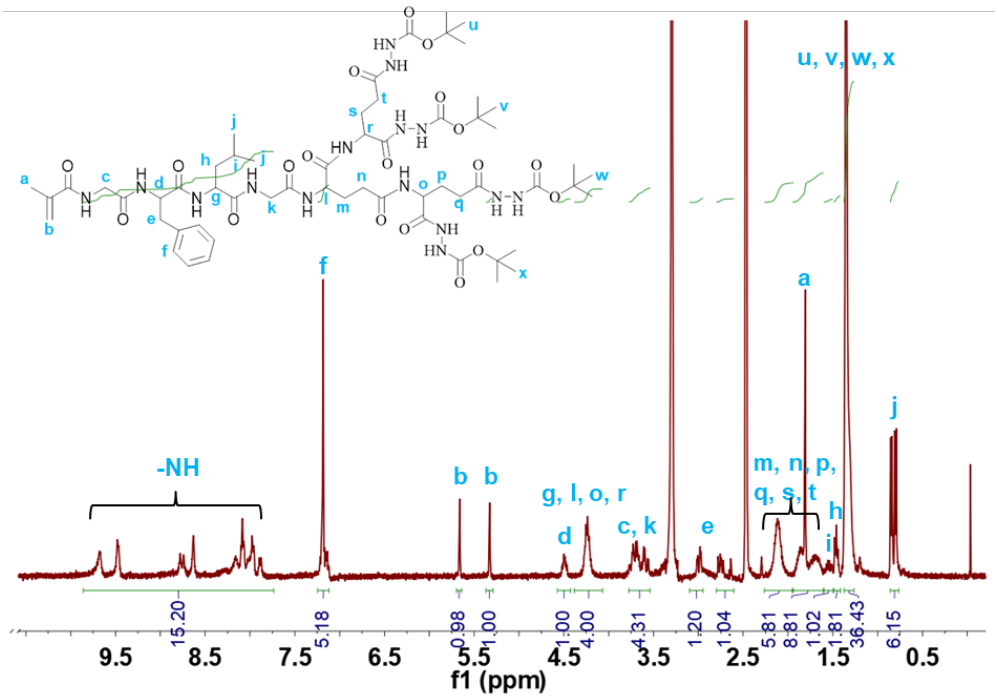



**Figure S12.** $^1$H NMR spectra of MA-GFLG-(NHNHBoc)$_4$ in DMSO-*d*$_6$. $^1$H NMR (400 MHz, DMSO-*d6*) δ 7.34 – 7.03 (m, 5H), 5.69 (s, 1H), 5.36 (s, 1H), 4.53 – 4.47 (m, 1H), 4.31 – 4.25 (m, 4H), 3.77 – 3.58 (m, 4H), 3.07 – 2.99 (m, 1H), 2.83 – 2.70 (m, 1H), 2.24 – 2.04 (m, 6H), 1.99 – 1.85 (m, 3H), 1.84 (s, 3H), 1.77 – 1.67 (m, 3H), 1.61 – 1.53 (m, 1H), 1.51 – 1.48 (m, 2H), 1.38 (s, 36H), 0.86 (m, 6H).

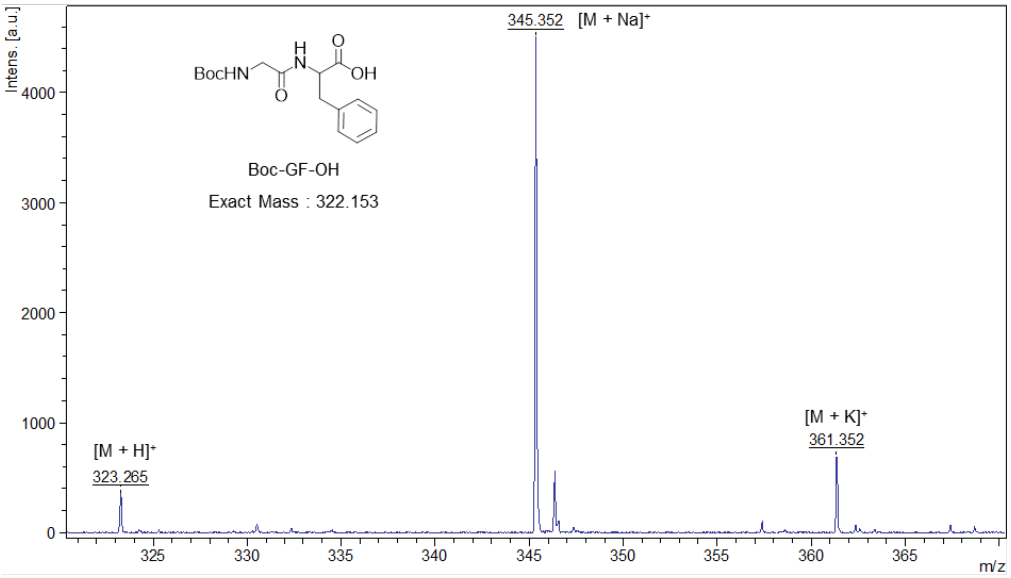



**Figure S13.** MALDI-TOF mass spectra of Boc-GF-OH, $[M+H]^+$, at m/z = 323.265.

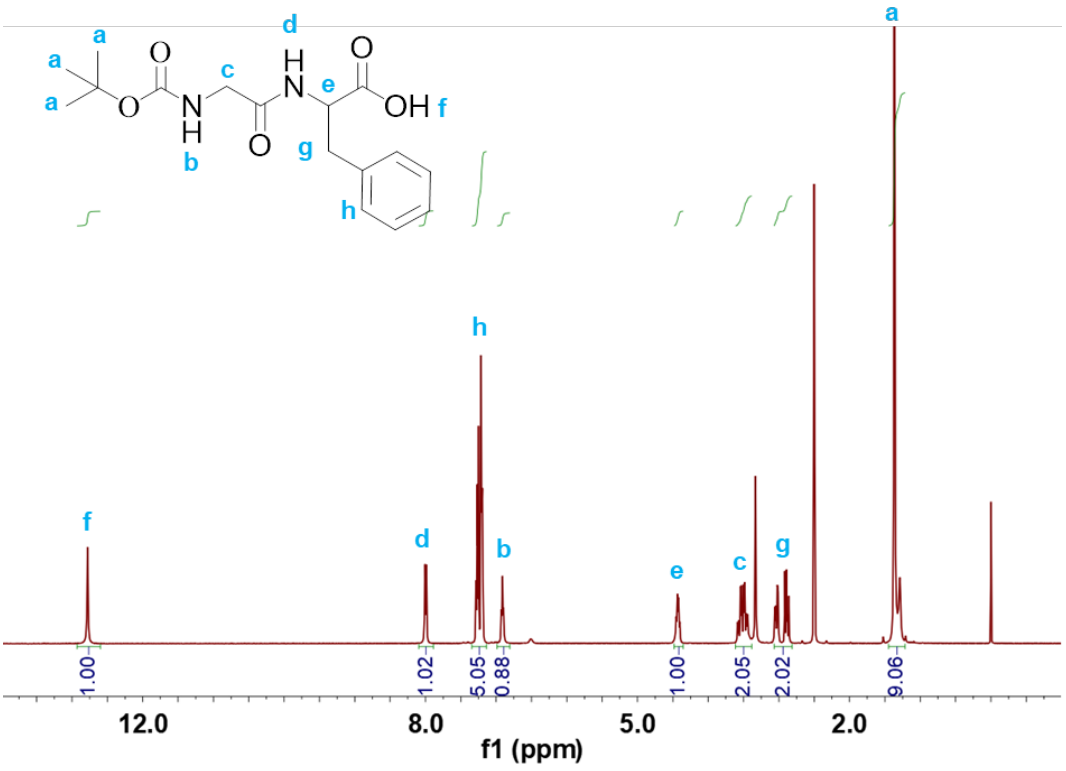



**Figure S14.** $^1$H NMR spectra of Boc-GF-OH in DMSO-*d*$_6$. $^1$H NMR (400 MHz, DMSO-*d6*) δ 12.78 (s, 1H), 8.00 (d, 1H), 7.35 – 7.12 (m, 5H), 6.91 (t, 1H), 4.45 – 4.43 (m, 1H), 3.60 – 3.37 (m, 2H), 3.05 – 2.86 (m, 2H), 1.37 (s, 9H).

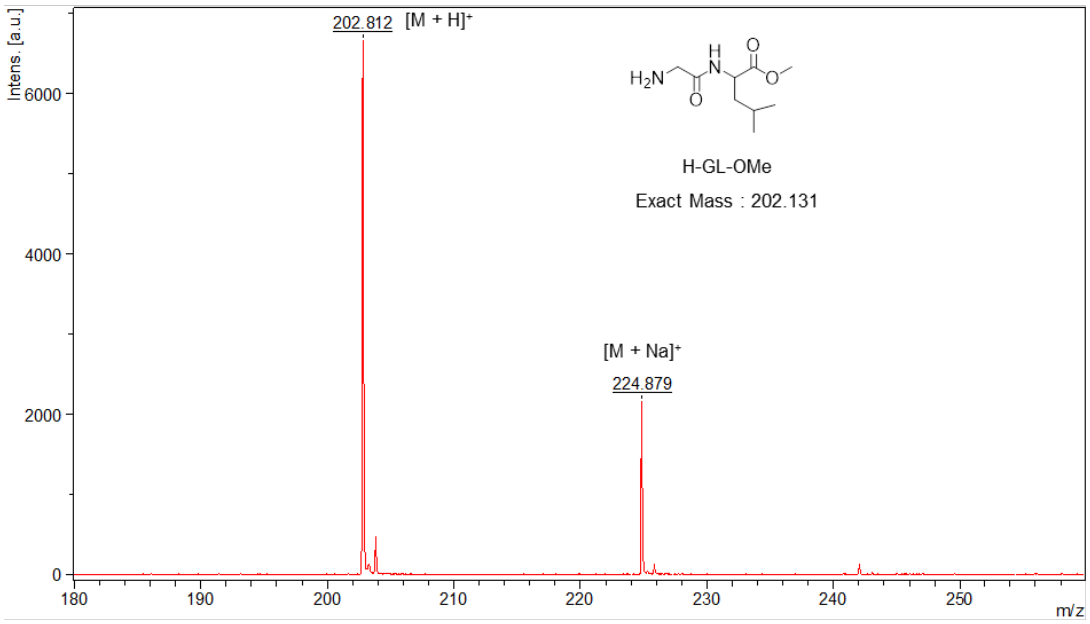



**Figure S15.** MALDI-TOF mass spectra of $NH_2$-GL-OMe, $[M+H]^+$, at m/z = 202.812.

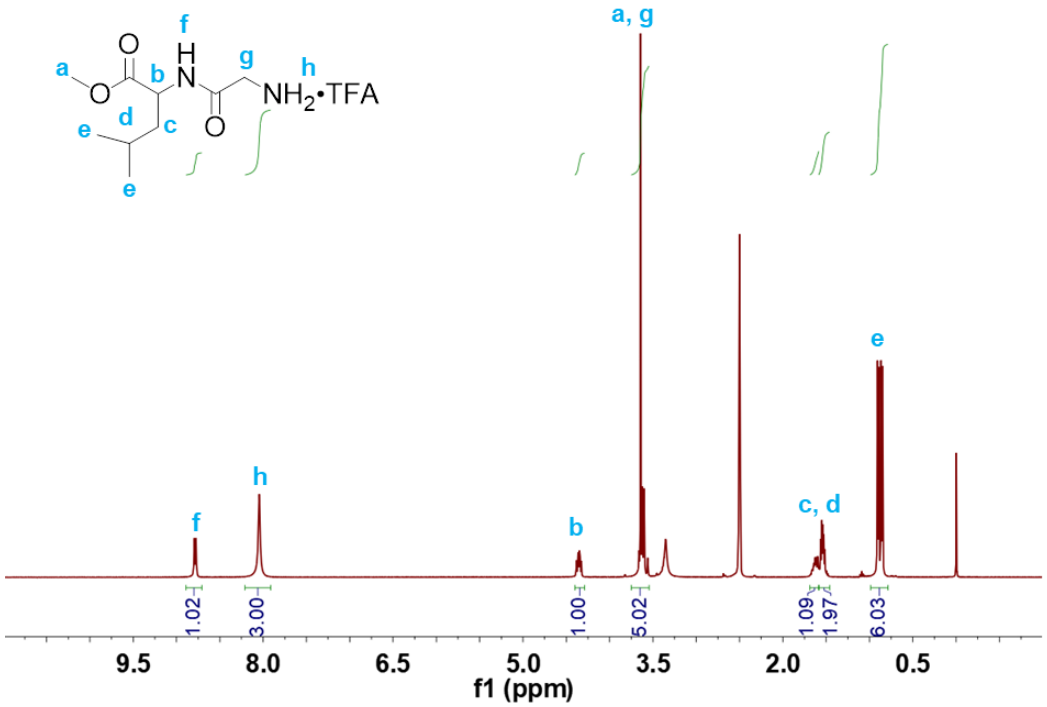



**Figure S16.** $^1$H NMR spectra of $NH_2$·TFA-GL-OMe in DMSO-*d6*. $^1$H NMR (400 MHz, DMSO-*d6*) δ 8.78 (d, 1H), 8.05 (s, 1H), 4.47 – 4.23 (m, 1H), 3.73 – 3.57 (m, 5H), 1.62 – 1.52 (m, 3H), 0.88 (dd, 6H).

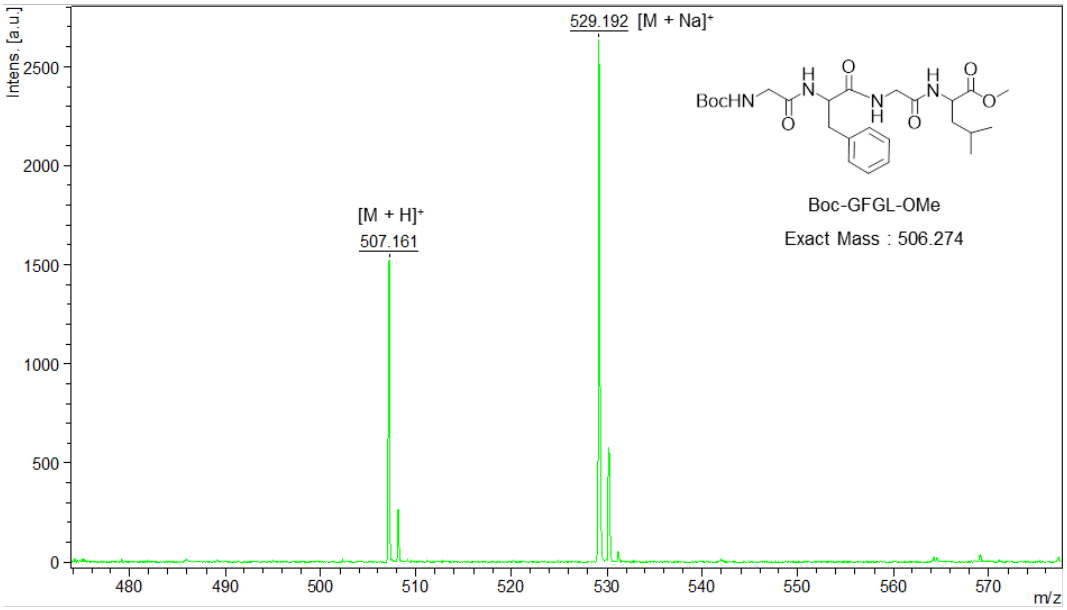



**Figure S17.** MALDI-TOF mass spectra of Boc-GFGL-OMe, $[M+H]^+$, at m/z = 507.161.

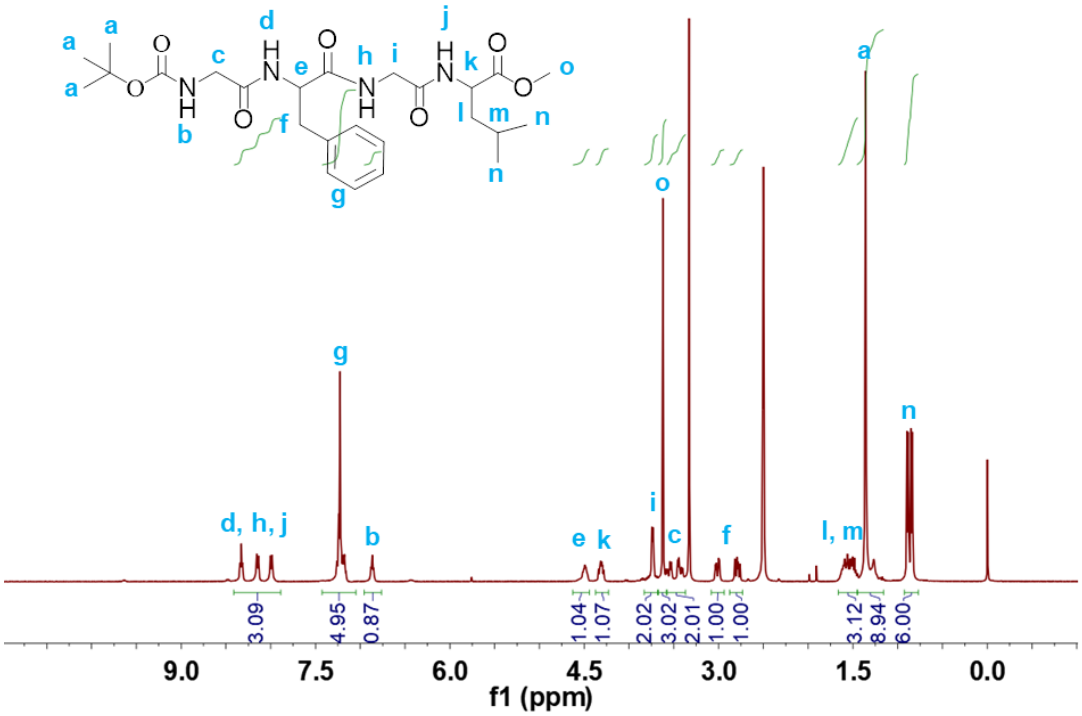



**Figure S18.** $^1$H NMR spectra of Boc-GFGL-OMe in DMSO-*d6*. $^1$H NMR (400 MHz, DMSO-*d6*) δ 7.27 – 7.16 (m, 5H), 4.54 – 4.45 (m, 1H), 4.34 – 4.28 (m, 1H), 3.77 – 3.70 (m, 2H), 3.62 (s, 3H), 3.58 – 3.40 (m, 2H), 3.01 – 2.97 (m, 1H), 2.84 – 2.74 (m, 1H), 1.66 – 1.45 (m, 3H), 1.40 – 1.31 (s, 9H), 0.87 (dd, 6H).

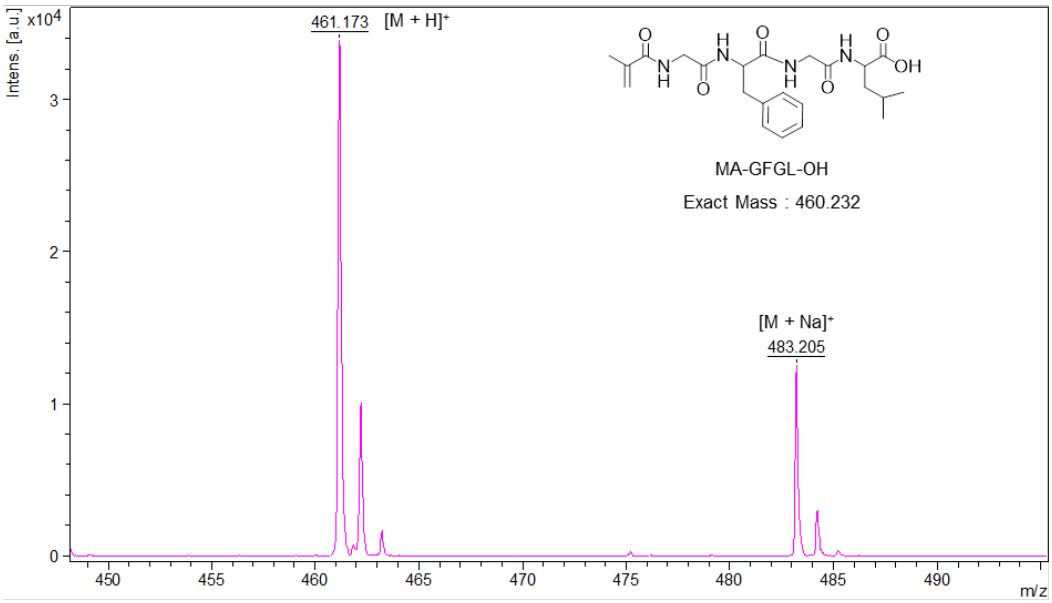



**Figure S19.** MALDI-TOF mass spectra of MA-GFGL-OH, $[M+H]^+$, at m/z = 461.173.

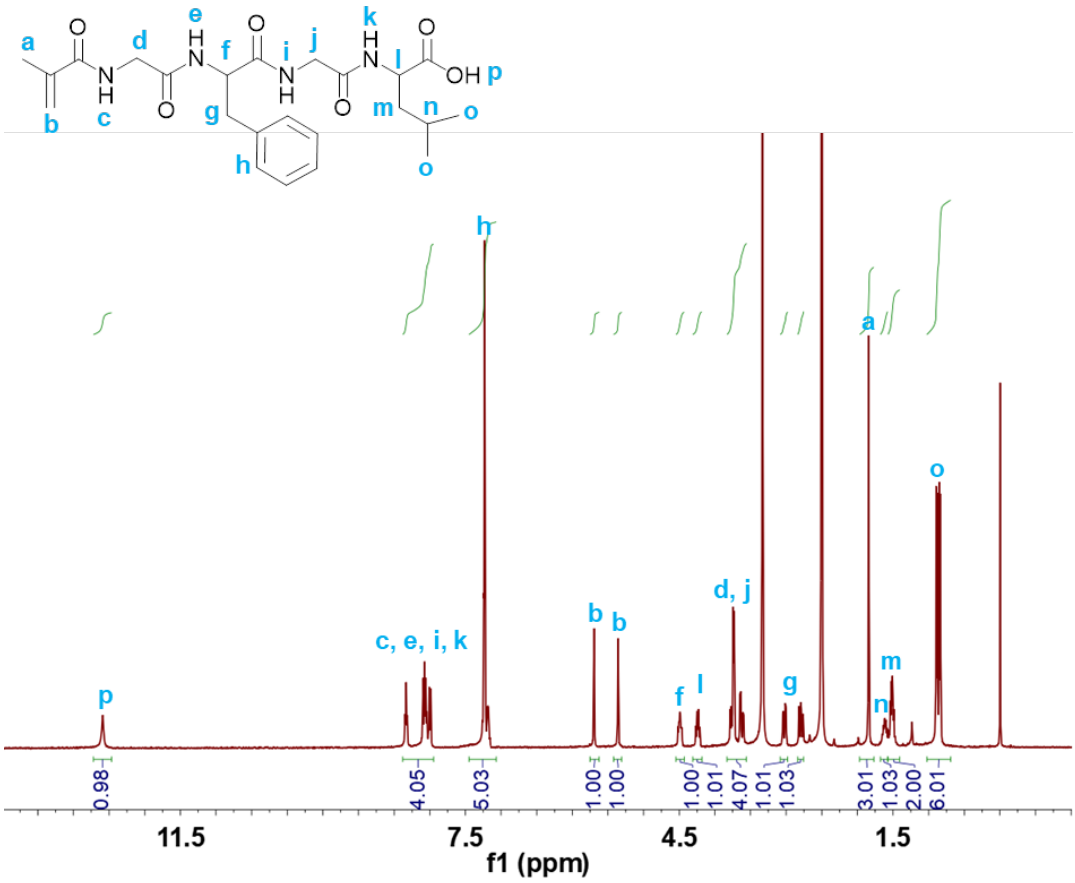



**Figure S20.** $^1$H NMR spectra of MA-GFGL-OH in DMSO-*d6*. $^1$H NMR (400 MHz, DMSO-*d6*) δ 7.39 – 7.07 (m, 5H), 5.73 (s, 1H), 36 (m, 1H), 4.54 – 4.44 (m, 1H), 4.29 – 4.19 (m, 1H), 3.82 – 3.58 (m, 4H), 3.07 – 2.97 (m, 1H), 2.84 – 3.74 (m, 1H), 1.84 (s, 3H), 1.69 – 1.59 (m, 1H), 1.57 – 1.46 (m, 2H), 0.86 (dd, 6H).

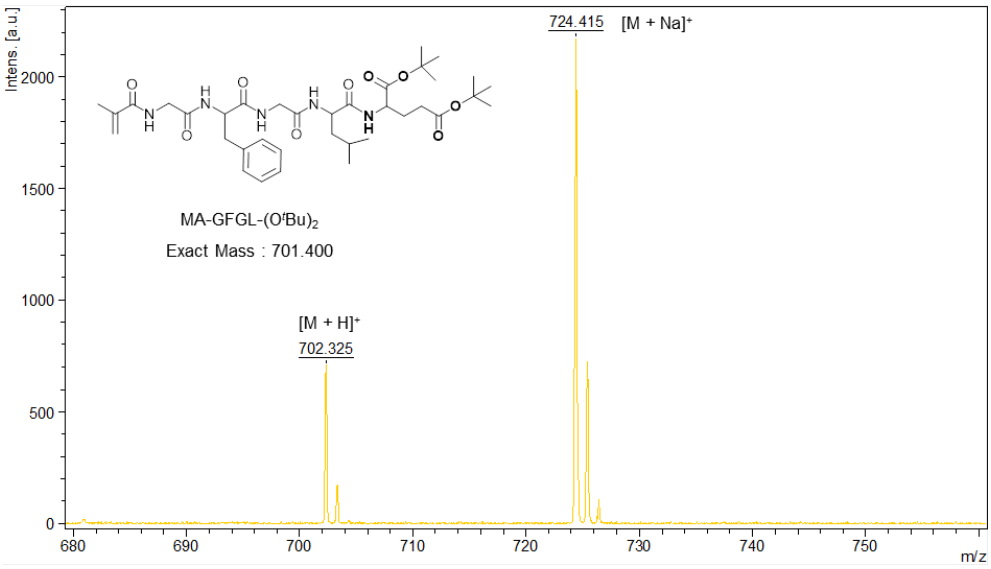



**Figure S21.** MALDI-TOF mass spectra of MA-GFGL-(O$^t$Bu)$_2$, $[M+H]^+$, at m/z = 702.325.

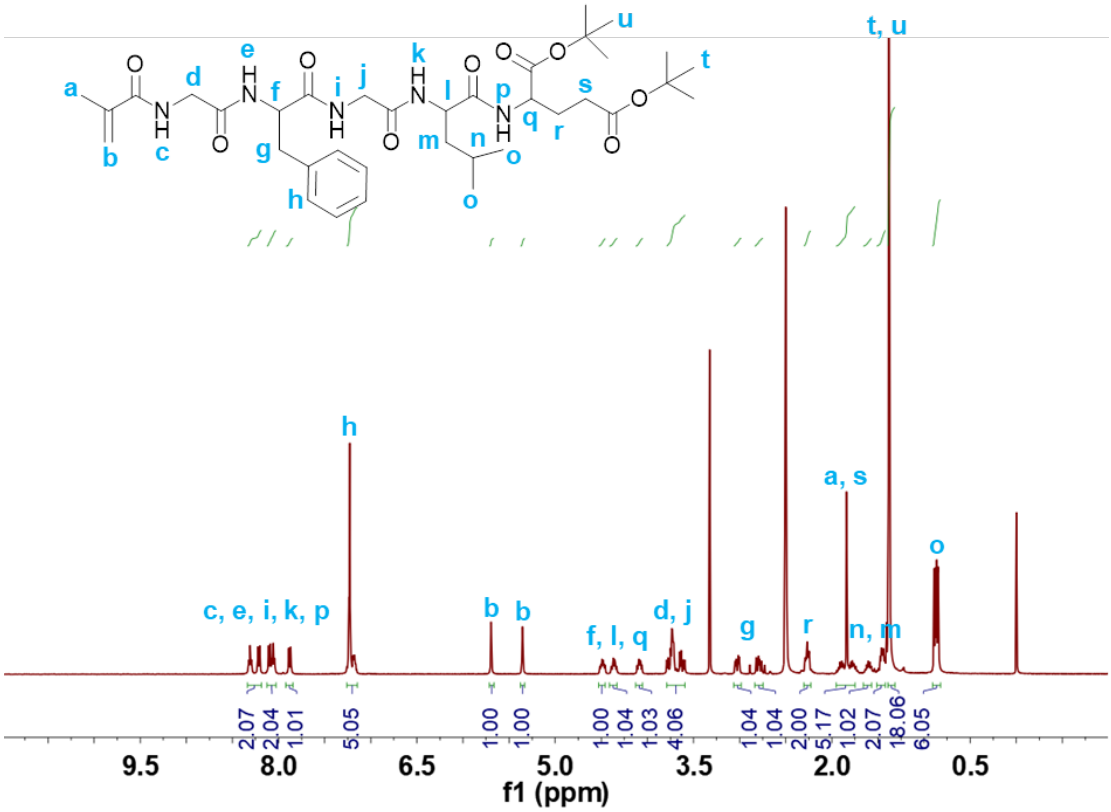



**Figure S22.** $^1$H NMR spectra of MA-GFGL-(O$^t$Bu)$_2$ in DMSO-*d*$_6$. $^1$H NMR (400 MHz, DMSO-*d6*) δ 7.33 – 7.11 (m, 5H), 5.70 (s, 1H), 5.35 (s, 1H), 4.53 – 4.46 (m, 1H), 4.42 – 4.32 (m, 1H), 4.13 – 4.05 (m, 1H), 3.81 – 3.57 (m, 4H), 3.06-2.98 (m, 1H), 2.84 – 2.75 (m, 1H), 2.30 – 2.21 (m, 2H), 1.96 – 1.74 (m, 5H), 1.66 – 1.56 (m, 1H), 1.52 – 1.42 (m, 2H), 1.38 (s, 18H), 0.87 (dd, 6H).

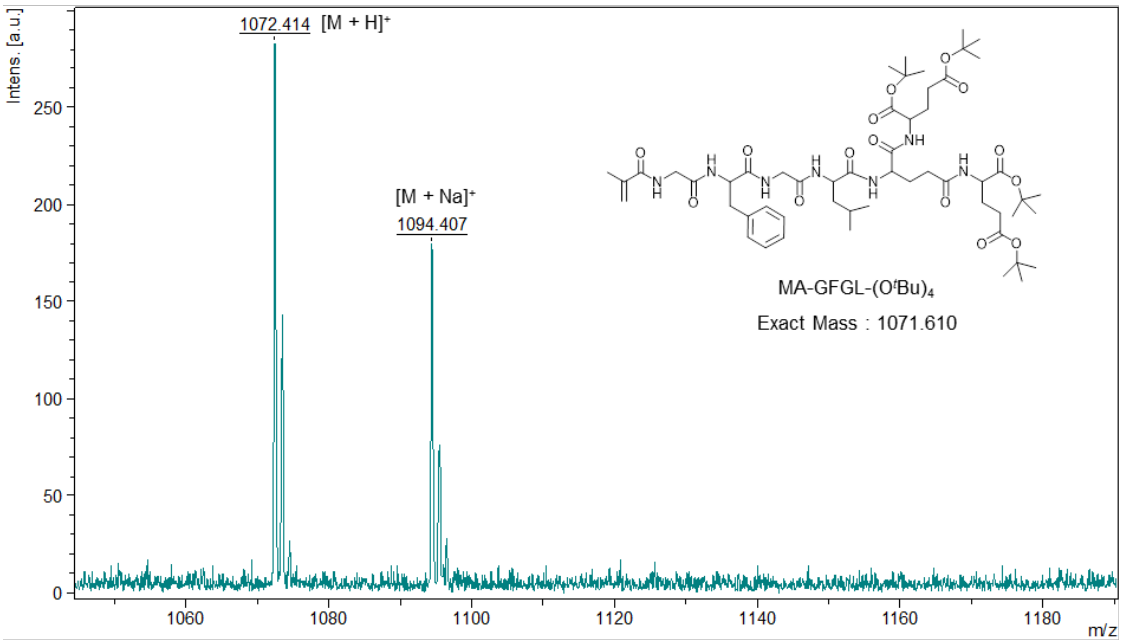



**Figure S23.** MALDI-TOF mass spectra of MA-GFGL-(O$^t$Bu)$_4$, $[M+H]^+$, at m/z = 1072.414.

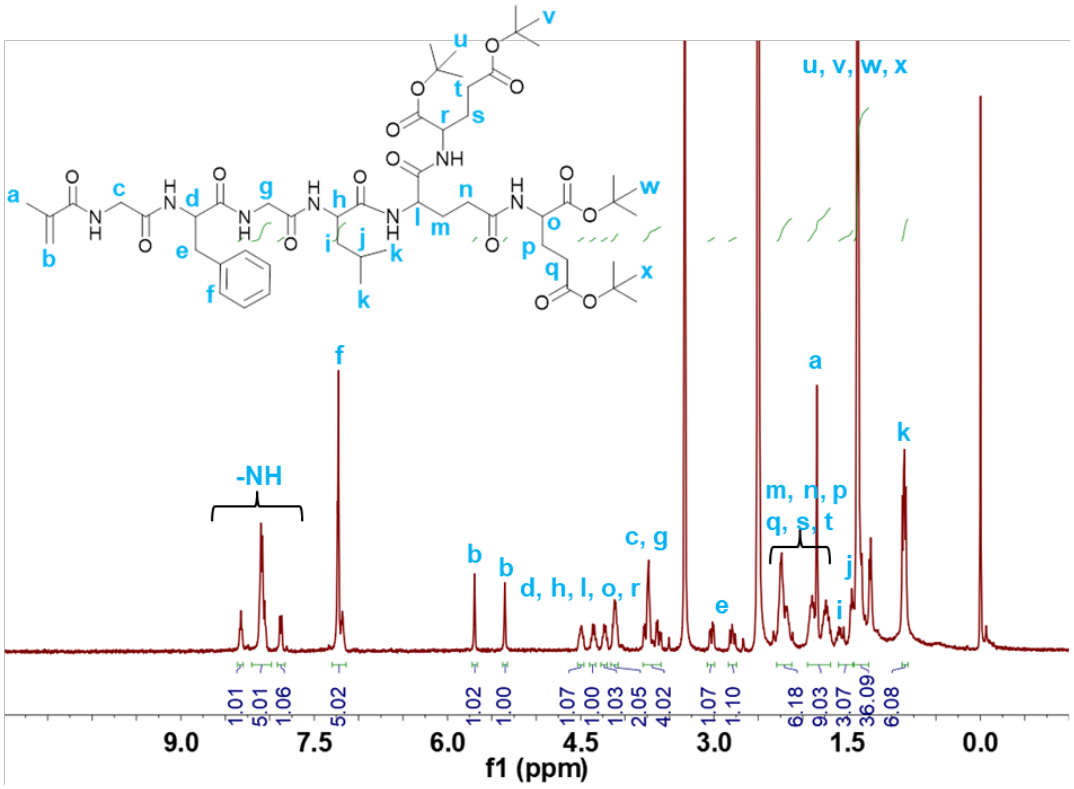



**Figure S24.** $^1$H NMR spectra of MA-GFGL-(O$^t$Bu)$_4$ in DMSO-$d_6$. $^1$H NMR (400 MHz, DMSO-*d6*) δ 7.30 – 7.10 (m, 5H), 5.70 (s, 1H), 5.36 (s, 1H), 4.56 – 4.08 (m, 5H), 3.83 – 3.58 (m, 4H), 3.09 – 2.98 (m, 1H), 2.86 – 2.74 (m, 1H), 2.35 – 2.14 (m, 6H), 1.94 – 1.69 (m, 9H), 1.64 – 1.35 (m, 3H), 1.39 (s, 36H), 0.86 (dd, 6H).

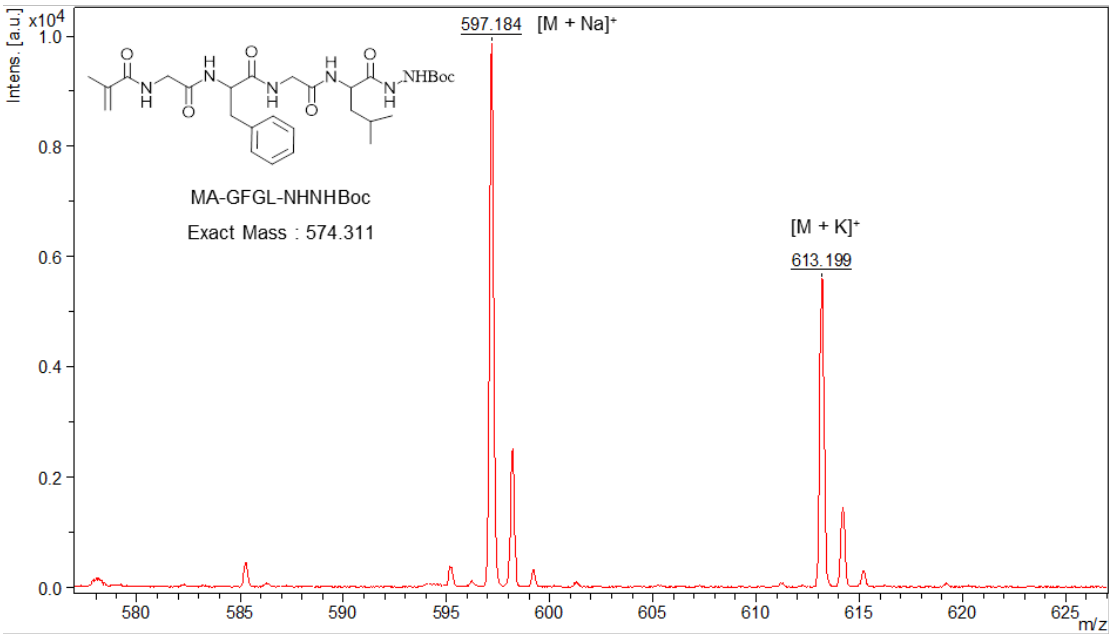



**Figure S25.** MALDI-TOF mass spectra of MA-GFGL-NHNHBoc, $[M+Na]^+$, at m/z = 597.184.

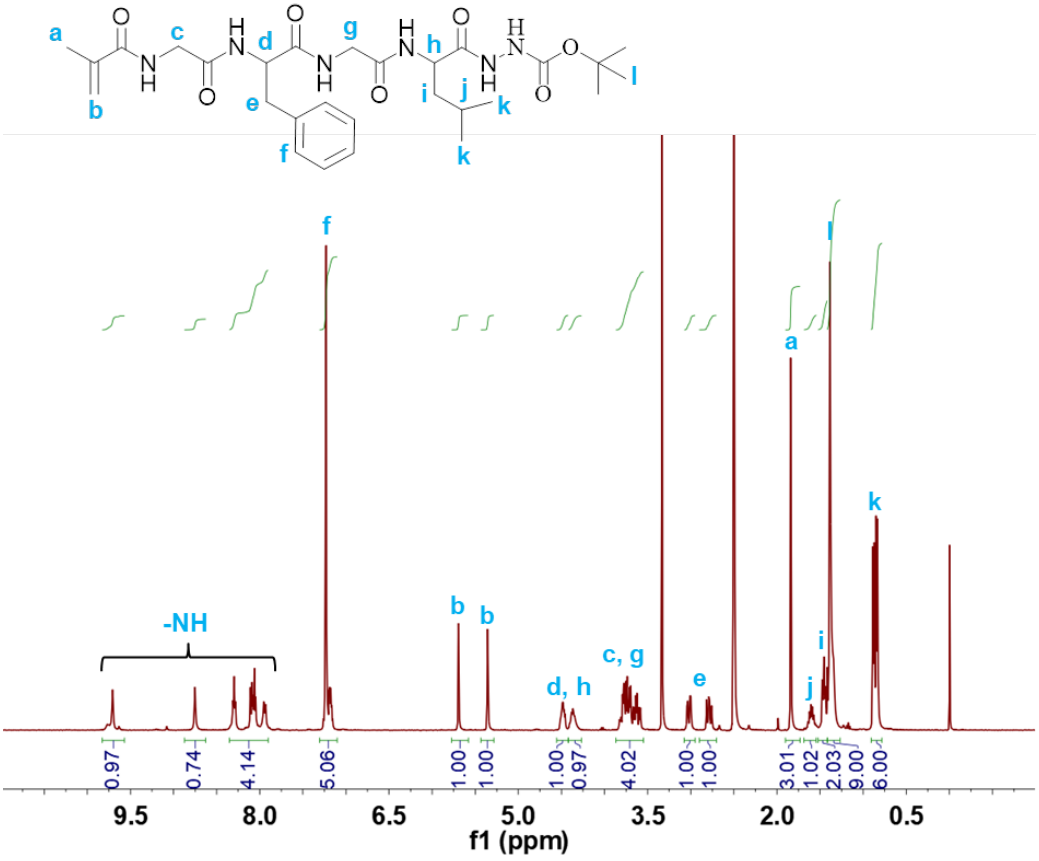



**Figure S26.** $^1$H NMR spectra of MA-GFGL-NHNHBoc in DMSO-$d_6$. $^1$H NMR (400 MHz, DMSO-*d6*) δ 7.32 – 7.09 (m, 5H), 5.70 (s, 1H), 5.36 (s, 1H), 4.52 – 4.29 (m, 2H), 3.89 – 3.53 (m, 4H), 3.06 – 2.73 (m, 2H), 1.84 (s, 3H), 1.69 – 1.54 (m, 1H), 1.52 – 1.42 (m, 2H), 1.38 (s, 9H), 0.86 (dd, 6H).

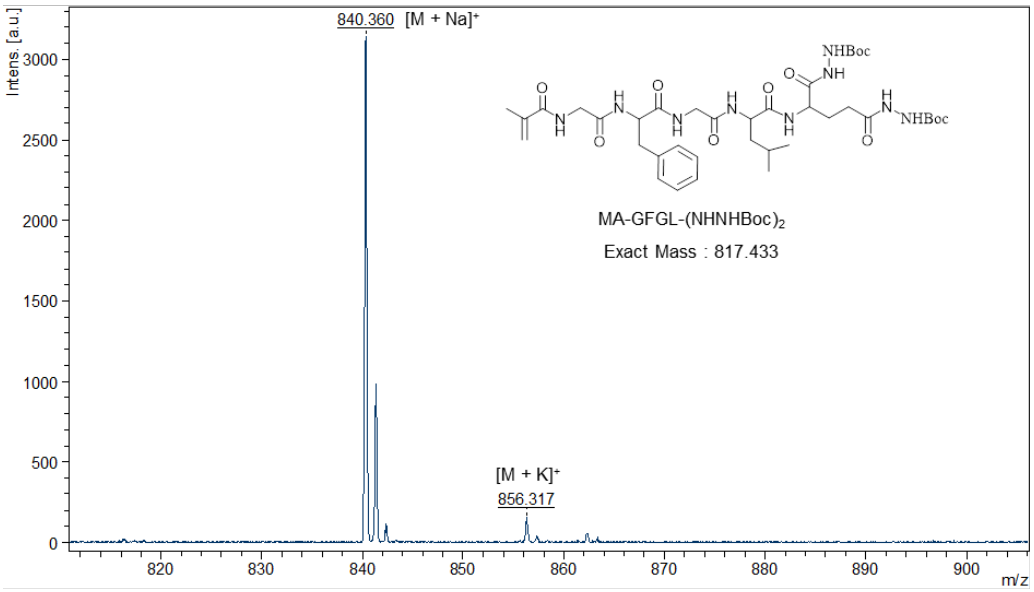



**Figure S27.** MALDI-TOF mass spectra of MA-GFGL-(NHNHBoc)$_2$, $[M+Na]^+$, at m/z = 840.360.

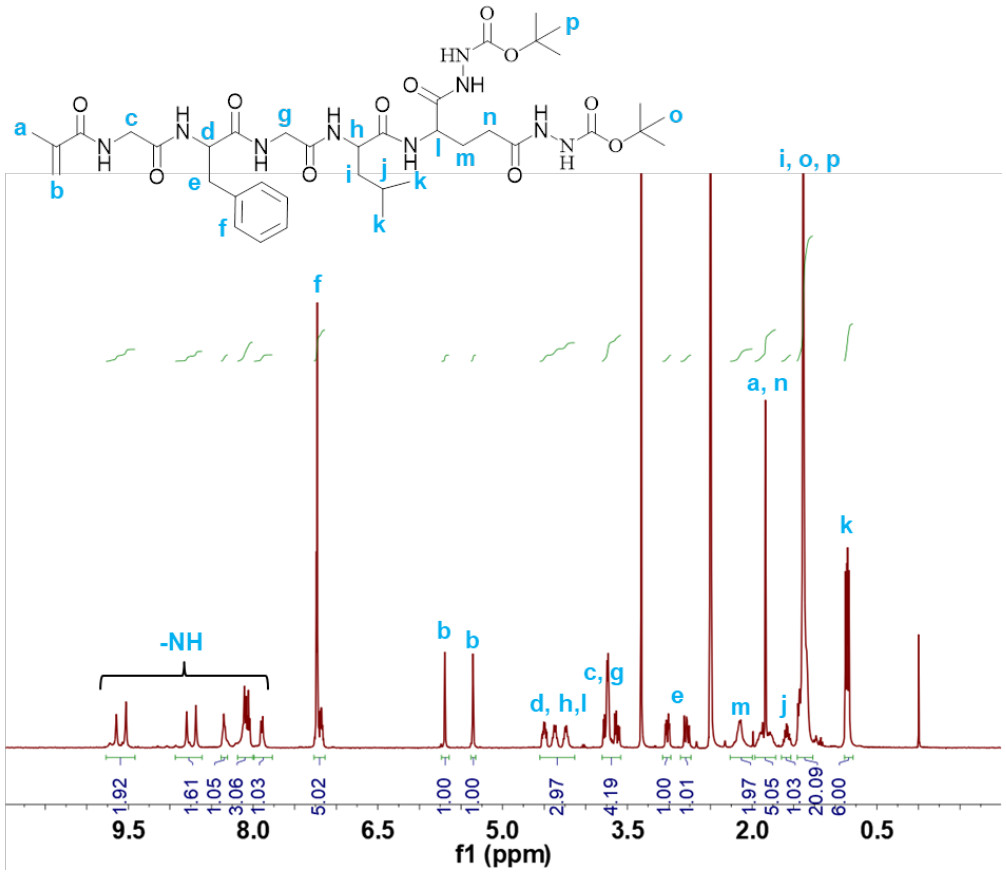



**Figure S28.** $^1$H NMR spectra of MA-GFGL-(NHNHBoc)$_2$ in DMSO-$d_6$. $^1$H NMR (400 MHz, DMSO-*d6*) δ 7.32 – 7.14 (m, 5H), 5.70 (s, 1H), 5.36 (s, 1H), 4.59 – 4.13 (m, 3H), 3.87 – 3.53 (m, 4H), 3.06 – 2.98 (m, 1H), 2.83 – 2.73 (m, 1H), 2.26 – 2.00 (m, 2H), 1.97 – 1.71 (m, 5H), 1.64 – 1.53 (m, 1H), 1.48 – 1.26 (m, 20H), 0.86 (dd, 6H).

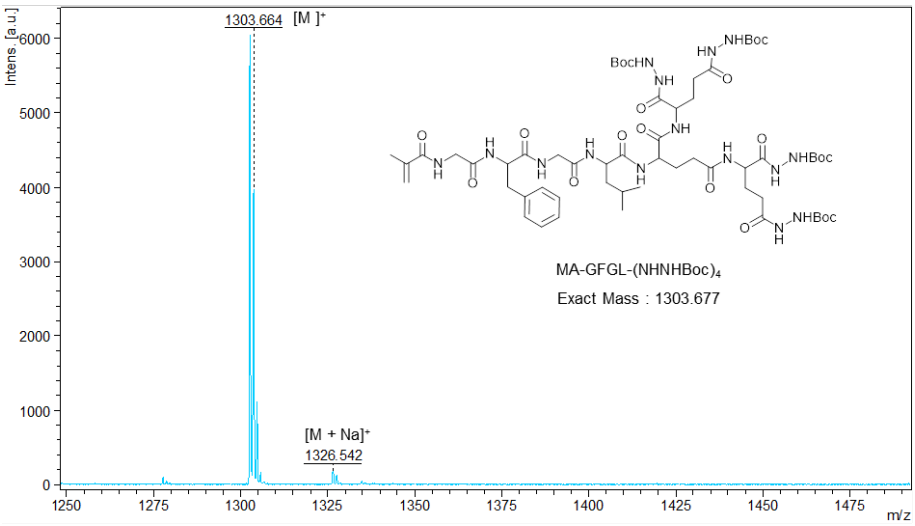



**Figure S29.** MALDI-TOF mass spectra of MA-GFGL-(NHNHBoc)$_4$, $[M+Na]^+$, at m/z = 1326.542.

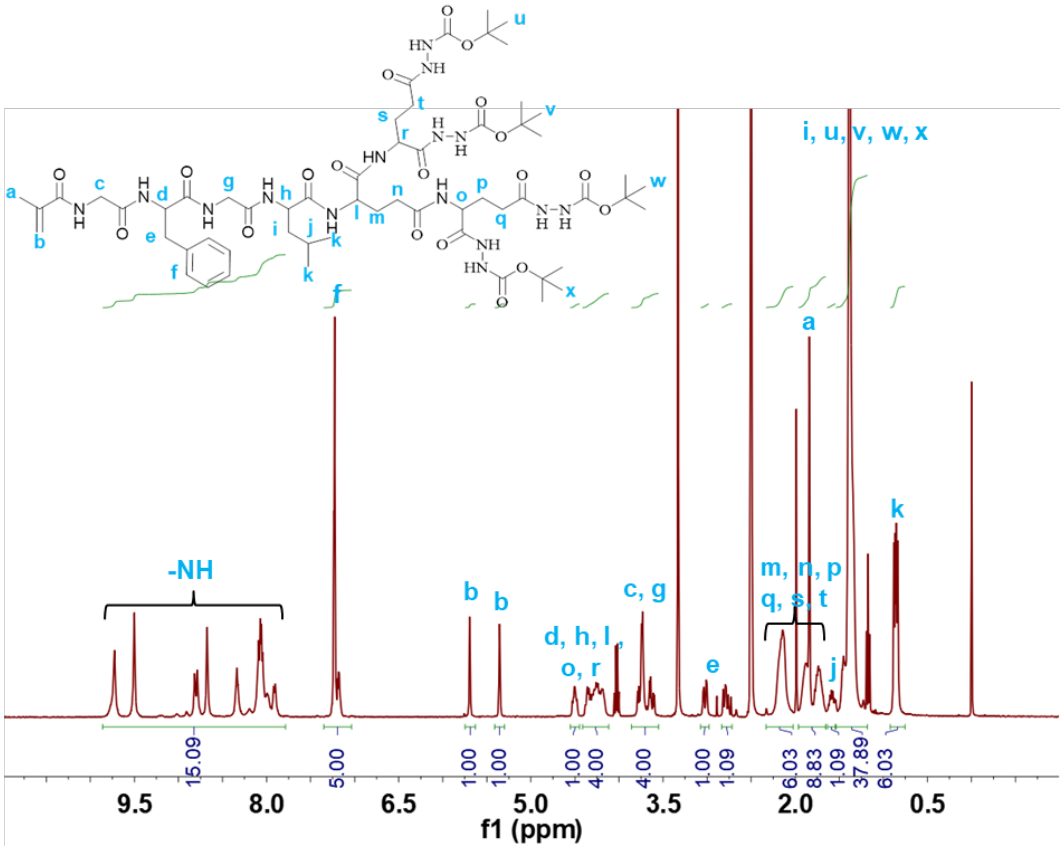



**Figure S30.** $^1$H NMR spectra of MA-GFGL-(NHNHBoc)$_4$ in DMSO-$d_6$. $^1$H NMR (400 MHz, DMSO-*d6*) δ 7.32 – 7.09 (m, 5H), 5.70 (s, 1H), 5.36 (s, 1H), 4.59 – 4.09 (m, 5H), 3.85 – 3.52 (m, 4H), 3.10 – 2.70 (m, 2H), 2.26 – 2.04 (m, 6H), 1.96 – 1.64 (m, 9H), 1.64 – 1.53 (m, 1H), 1.49 – 1.20 (m, 38H), 0.86 (dd, 6H).

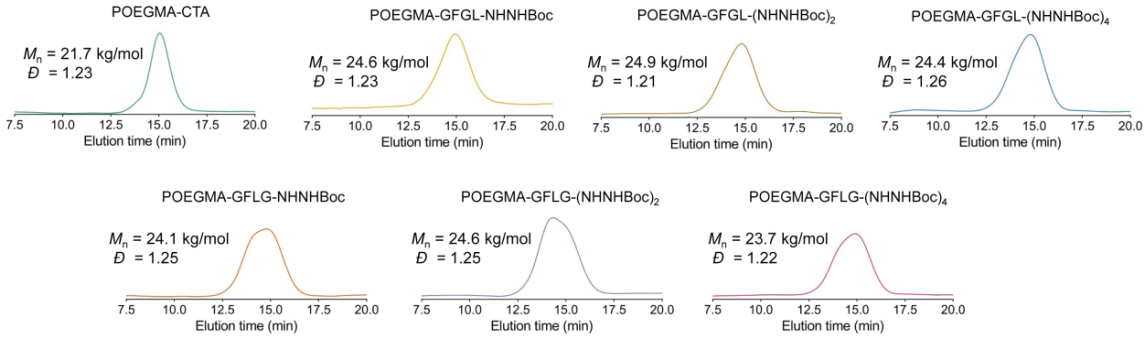



**Figure S31.** Experimental MWD of POEGMA-CTA, POEGMA-GFLG-(NHNHBoc)$_x$ and POEGMA-GFGL-(NHNHBoc)$_x$ (x = 1, 2 or 4).

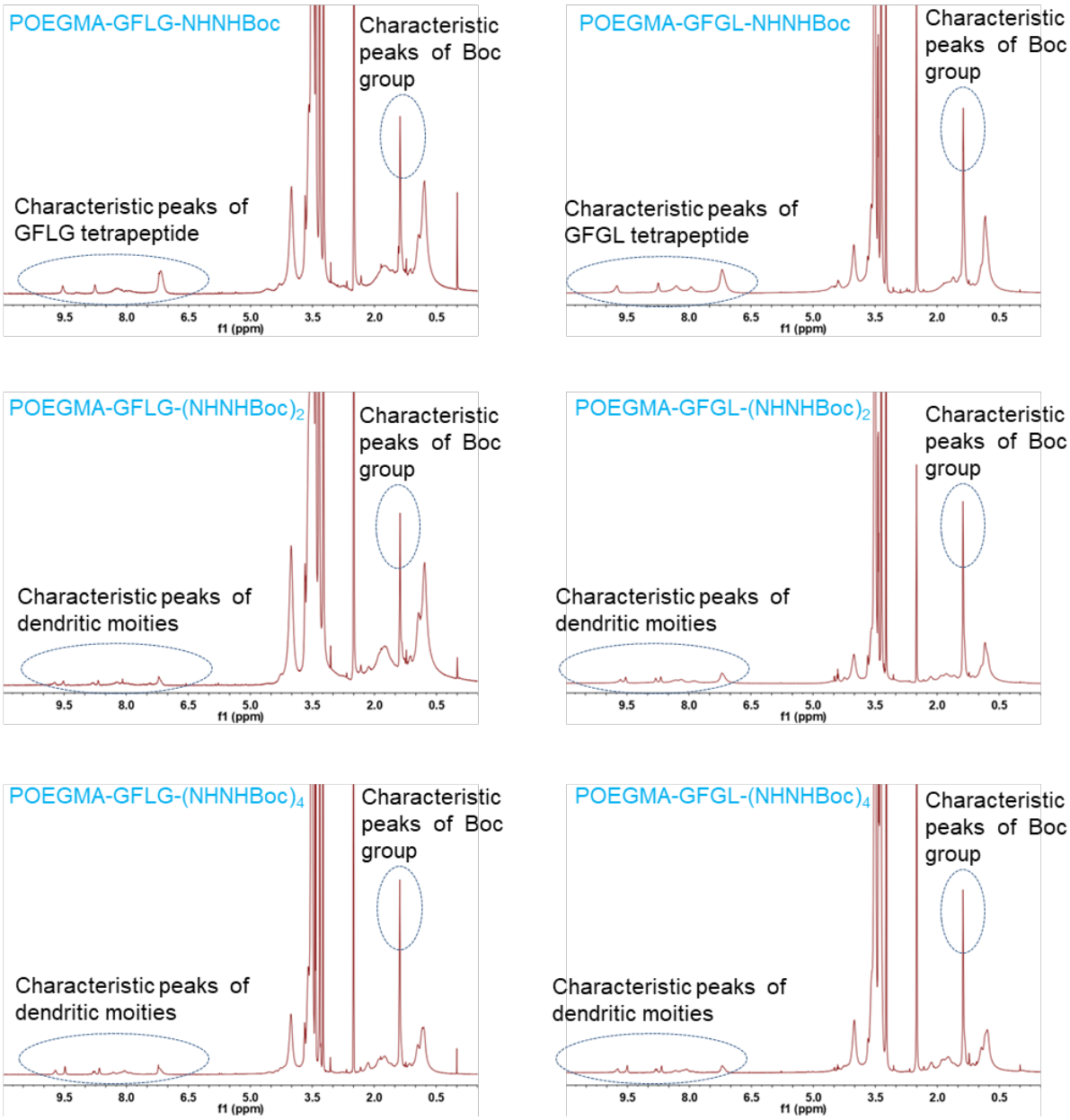



**Figure S32.** $^1$H NMR spectra of POEGMA-GFLG-(NHNHBoc)$_x$ and POEGMA- GFGL-(NHNHBoc)$_x$ (x = 1, 2 or 4) in DMSO-*d*$_6$.

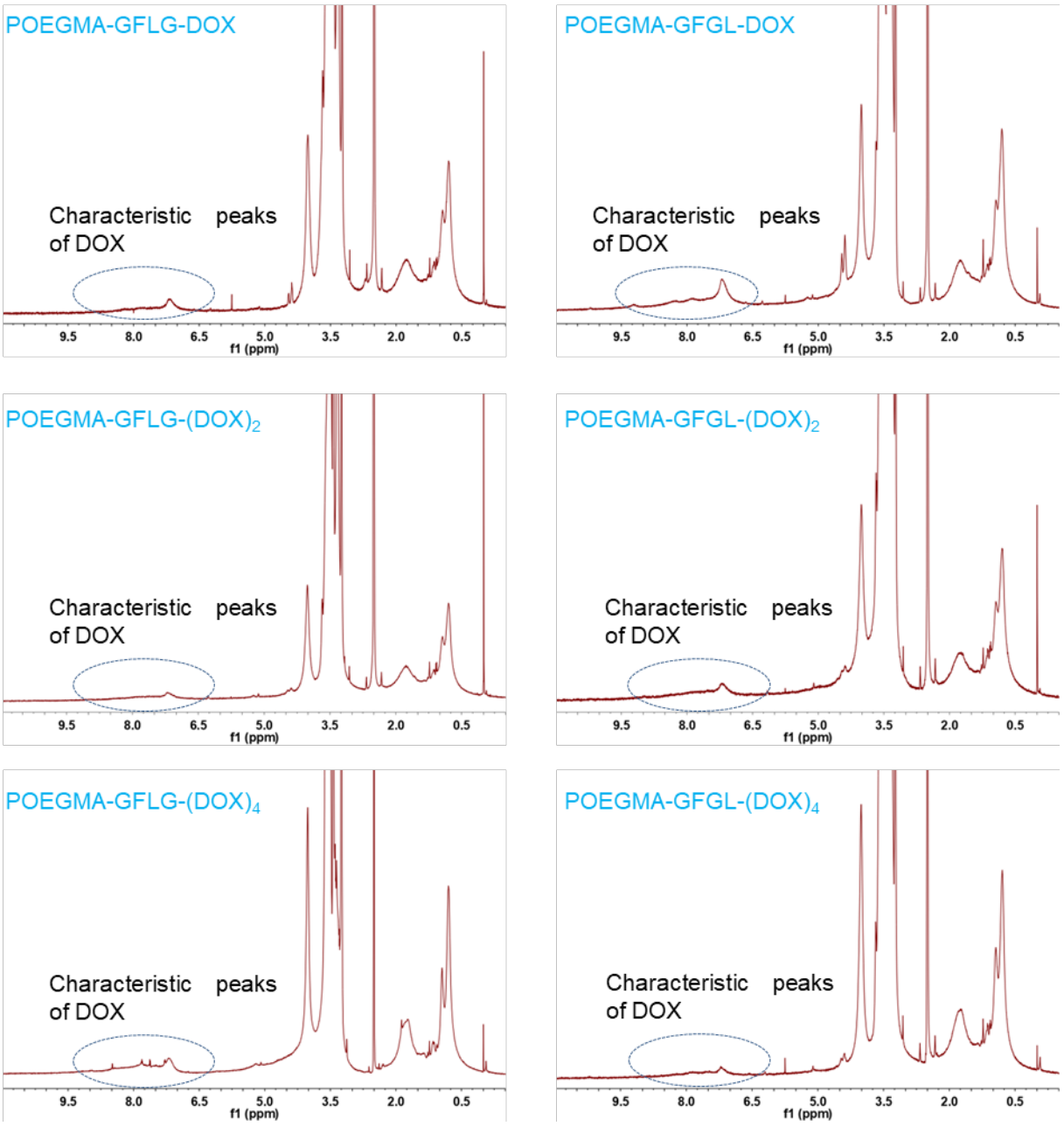



**Figure S33.** $^{1}$H NMR spectra of POEGMA-GFLG-$(DOX)_x$ and POEGMA- GFGL-$(DOX)_x$ (x = 1, 2 or 4) (x = 1, 2 or 4) in DMSO-$d_6$.

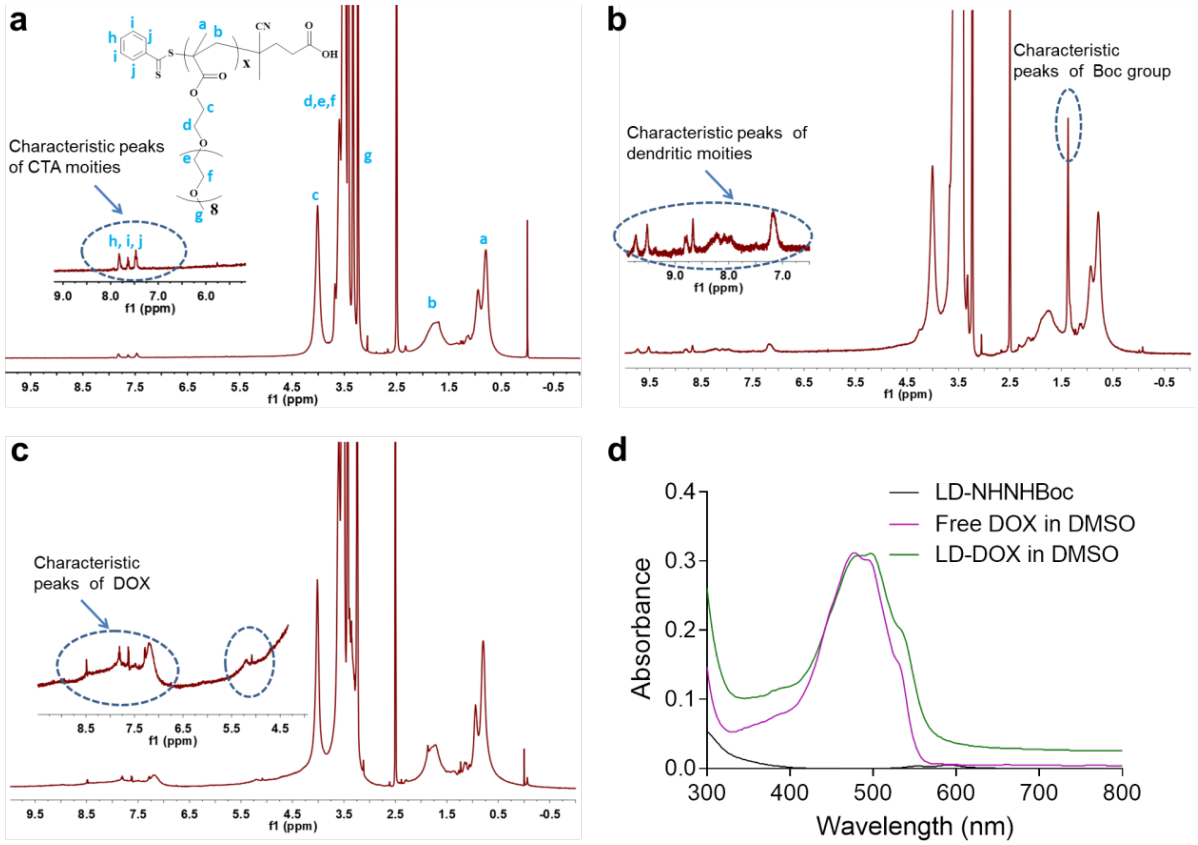



**Figure S34.** $^{1}$H NMR spectra of (a) POEGMA-CTA, (b) POEGMA-GFLG-(NHNHBoc)$_4$ and (c) POEGMA-GFLG-(DOX)$_4$ (LD-DOX) in DMSO-$d_6$. (d) UV-Vis absorption spectra of free DOX and LD-DOX in DMSO. The LD-NHNHBoc was used as a control.

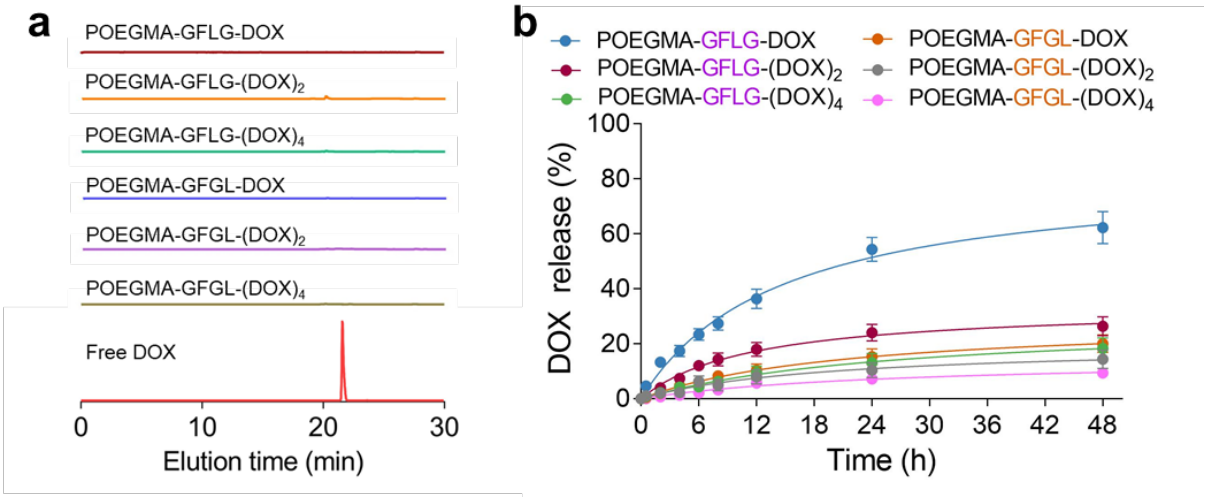



**Figure S35.** (a) HPLC chromatograms of prodrugs dissolved in methanol. Free DOX at an equivalent DOX concentration of 10 μg mL$^{-1}$ as a control. Gradient elution from 5 to 95% of Buffer B within 30 min; flow rate:1.0 mL/min; wavelength: 480 nm; Buffer A: deionized water with 0.1% TFA; Buffer B: methyl alcohol. (b) DOX release profiles from POEGMA-GFLG-(DOX)$_x$ and POEGMA-GFGL-(DOX)$_x$ in the presence of cathepsin B at pH 7.4 (x = 1, 2 or 4).

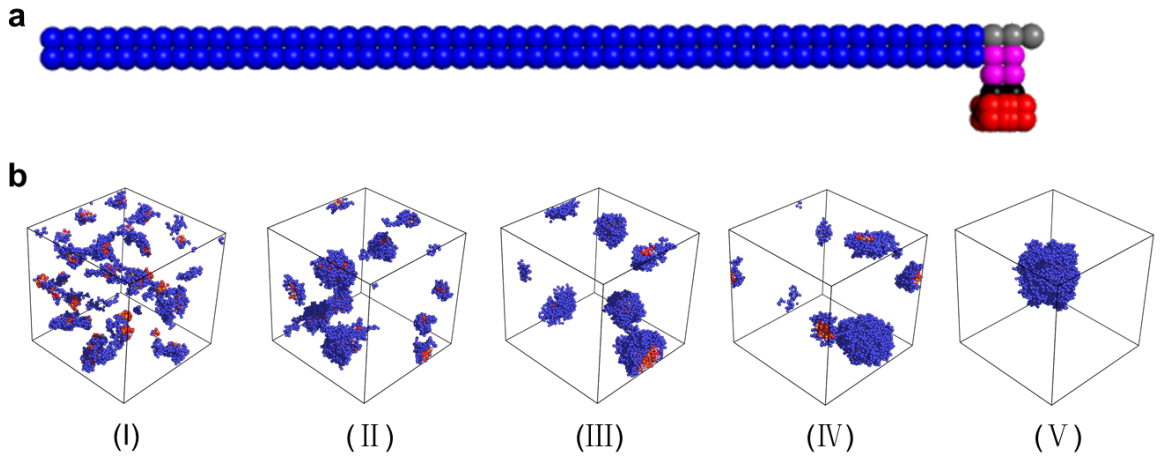



**Figure S36.** (a) Coarse-grained model of POEGMA-GFLG-$(DOX)_4$. (b) The modelling process of nanoparticle (NP) formation by POEGMA-GFLG-$(DOX)_4$ in a neutral solvent. The DPD simulations were performed for 200, 000 time steps with an integration time step of 0.02.

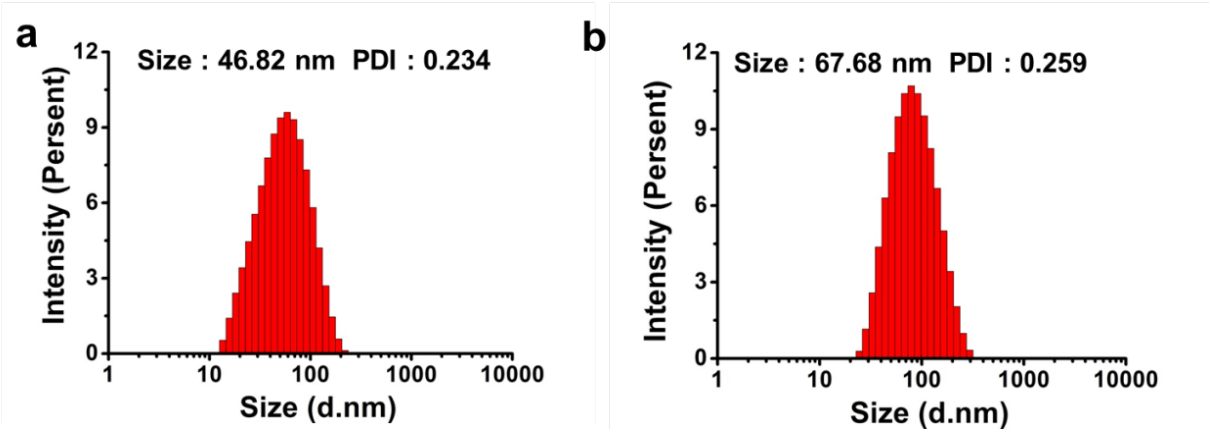



**Figure S37.** Size distribution and morphology of LD-DOX/Ce6 NPs by DLS.

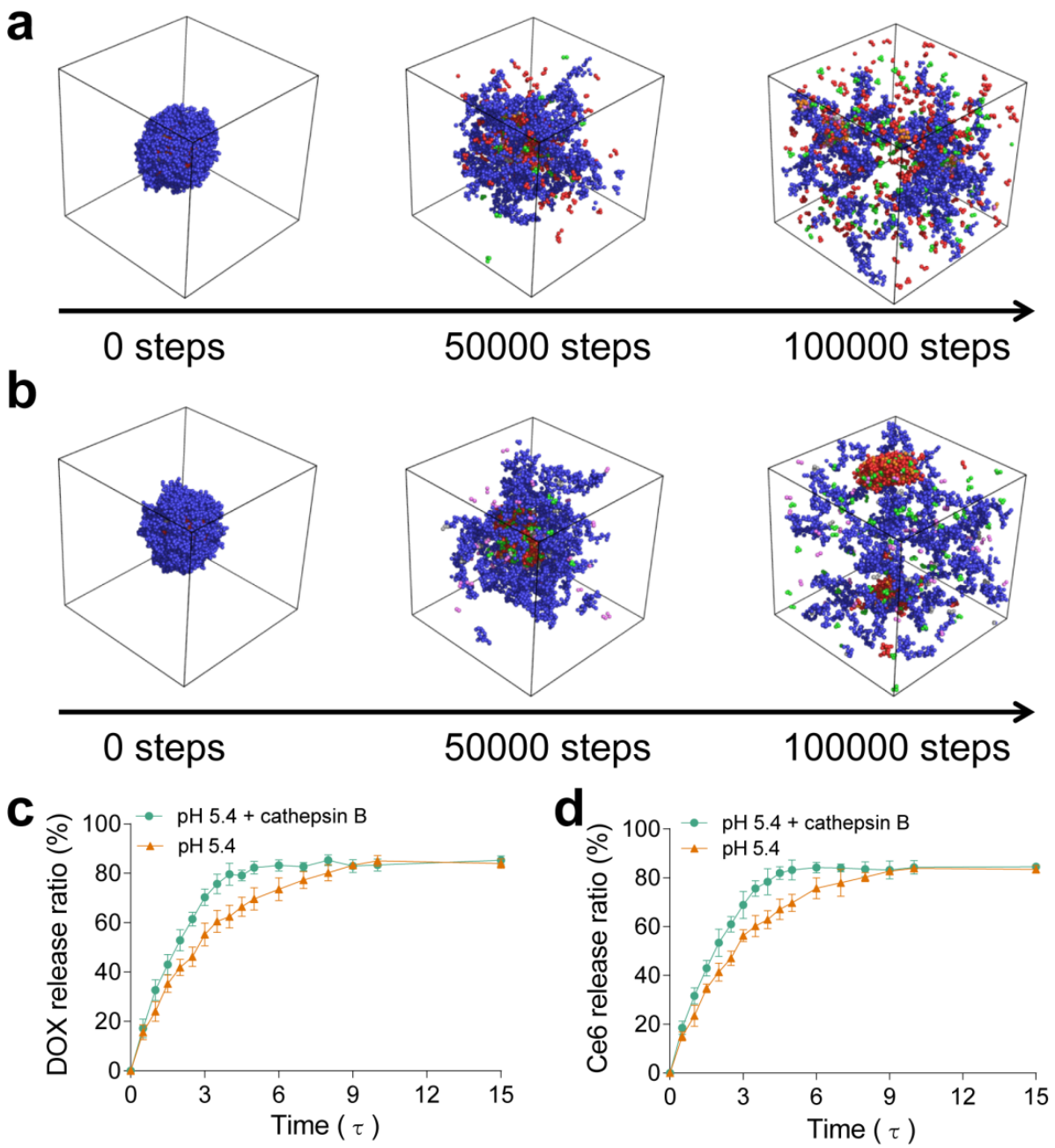



**Figure S38.** Dynamic drug release process from LD-DOX/Ce6 upon breakage of the (a) hydrazone bond (acid environment, pH5.4) or (b) GFLG (in presence of cathepsin B). The DPD simulations were performed for 100, 000 time steps to analyze the drug release process in protonation conditions. Drug release curves of (c) DOX and (d) Ce6 obtained by the DPD simulations of under different conditions. The release curves for drugs are obtained by counting the number of drug beads in the micelle at different times.

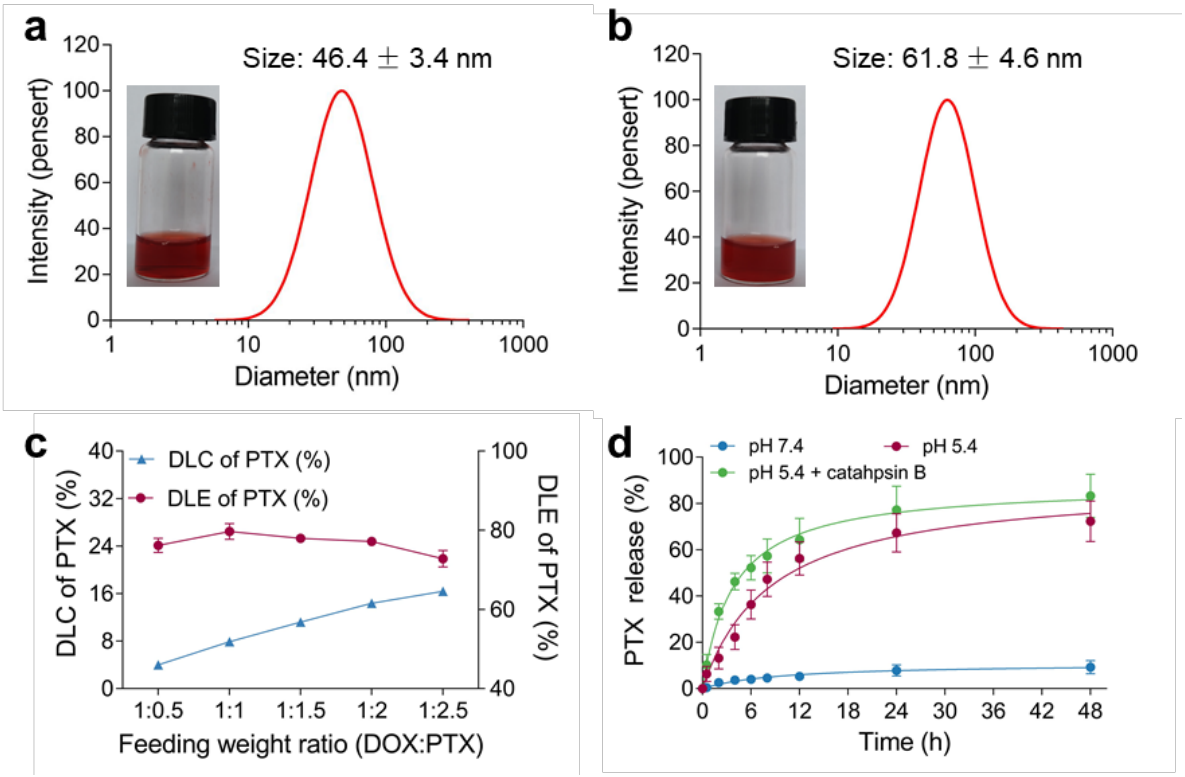



**Figure S39.** Encapsulation of PTX into LD-DOX as a versatile nano-platform. Size distribution of LD-DOX before (a) and after (b) encapsulation of PTX into LD-DOX as measured by dynamic light scattering (DLS). (c) Drug loading content (DLC) and drug loading efficiency (DLE) of PTX-loaded LD-DOX NPs with different feeding weight ratios of DOX to PTX. PTX-release profiles in the presence or absence of cathapsin B at different pH values.

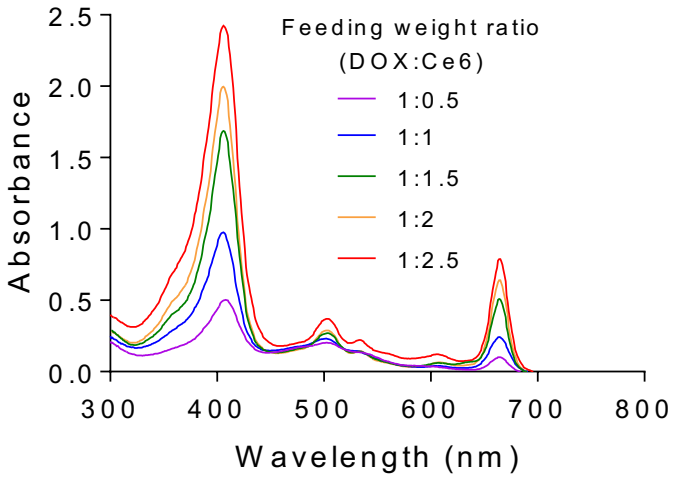



**Figure S40.** UV-Vis spectra of Ce6-loaded LD-DOX NPs with different feeding weight ratio of DOX to Ce6 in DMSO.

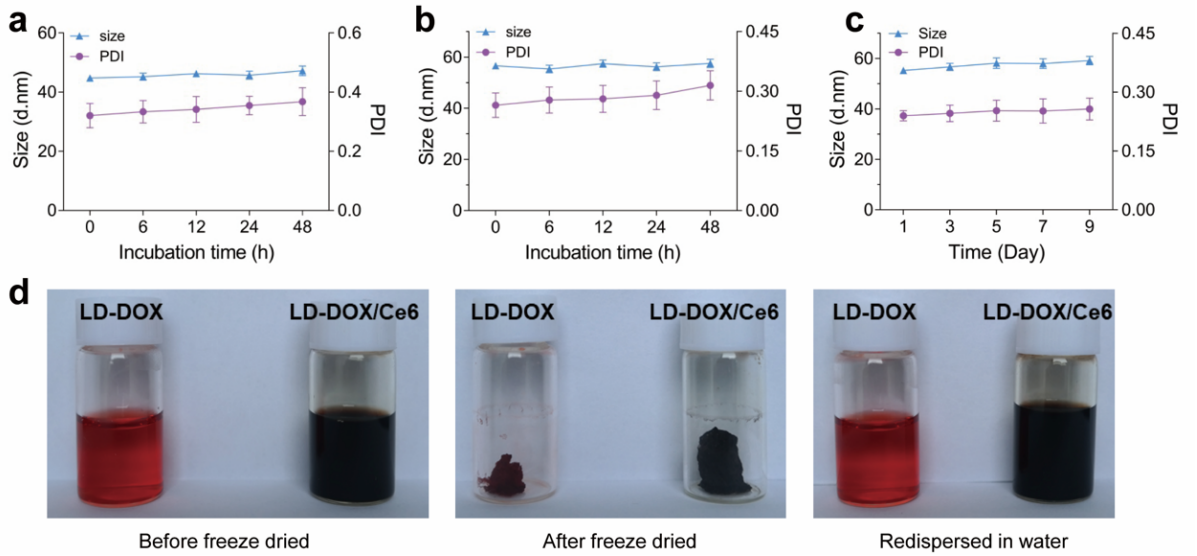



**Figure S41.** Stability of LD-DOX/Ce6 NPs in (a) PBS containing 10% FBS for 48 h in a shaker at 37 °C, (b) the cell culture medium for 48 h in a shaker at 37 °C and (c) in PBS (pH 7.4) for 9 days at 4 °C. (d) Photographs of LD-DOX and LD-DOX/Ce6 prepared by the thin film method before and after freeze drying and re-dispersion of them in water at an equivalent LD-DOX concentration of 3 mg $mL^{-1}$.

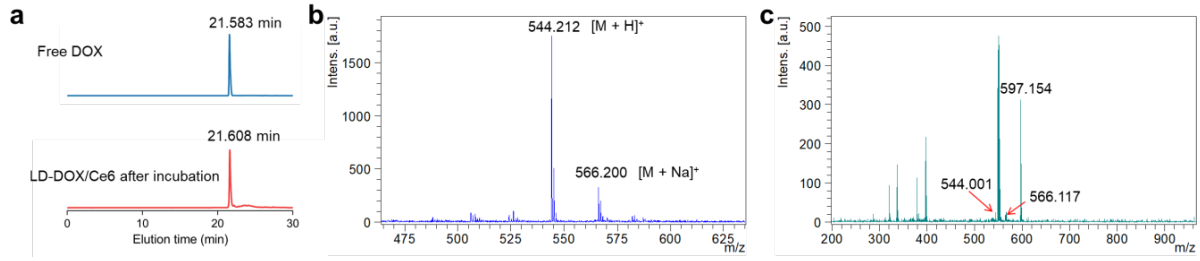



**Figure S42.** (a) HPLC chromagram for LD-DOX after incubation in the presence of cathepsin B at pH 5.4 for 24 h. Free DOX as a control. (b) MALDI-TOF MS spectrum for the elution sample at 21.150 min from HPLC analysis. The observed mass was 544.212, which was the characteristic peak of DOX ($[M + H]^+$). (c) MALDI-TOF MS spectrum of LD-DOX/Ce6 incubated with cathepsin B at pH 5.4. The peak at m/z = 566.117 was the characteristic peak of DOX ($[M + Na]^+$), and the peak at m/z = 597.154 was the characteristic peak of Ce6 ($[M + H]^+$).

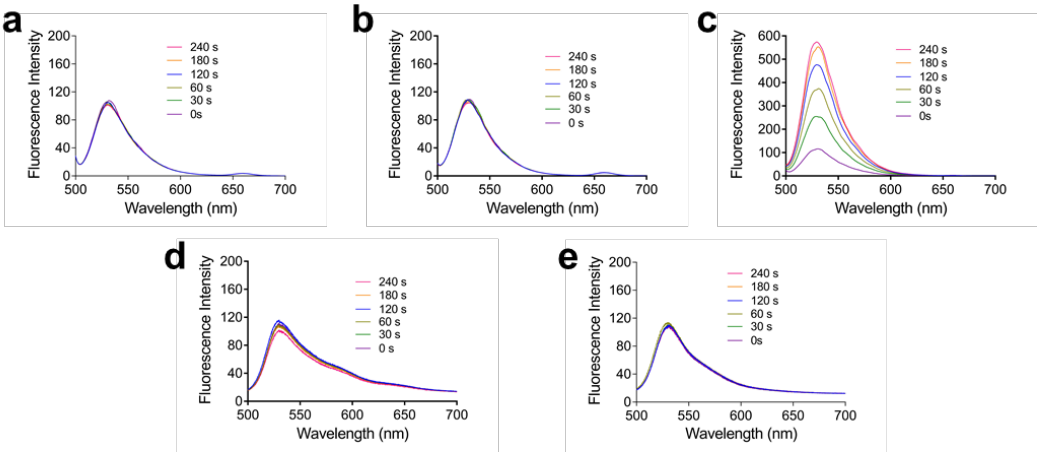



**Figure S43.** Fluorescence emission spectra of singlet oxygen sensor green (SOSG) generated from 0 to 240 s in (a) free Ce6 and (b) LD-DOX/Ce6 NPs without laser irradiation. Singlet oxygen generation by (c) free Ce6, (d) free DOX and (e) LD-DOX under laser irradiation at different time points.

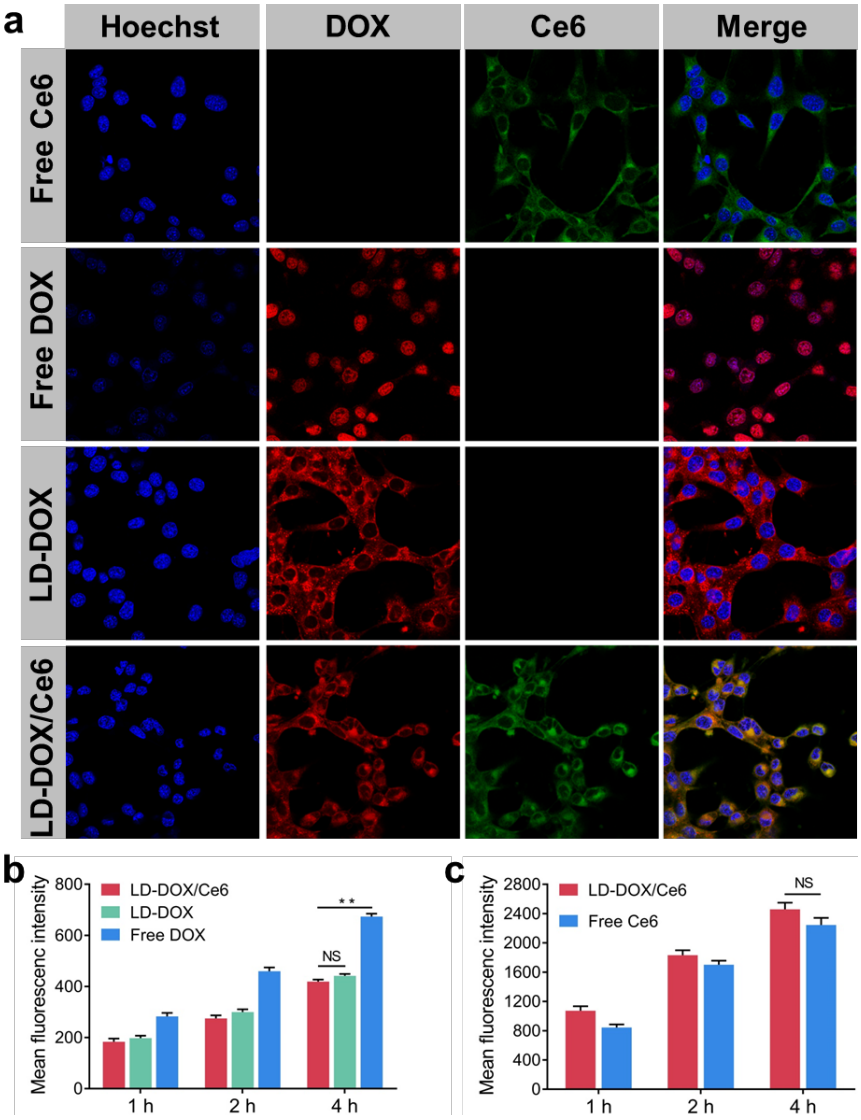



**Figure S44.** (a) Confocal microscopic images of 4T1 cells incubated with free Ce6, free DOX, LD-DOX and LD-DOX/Ce6 for 4 h (scale bars, 50 μm). Quantitative analysis of the mean fluorescence intensity of (b) DOX and (c) Ce6 in 4T1 cells for 1 h, 2 h and 4 h.

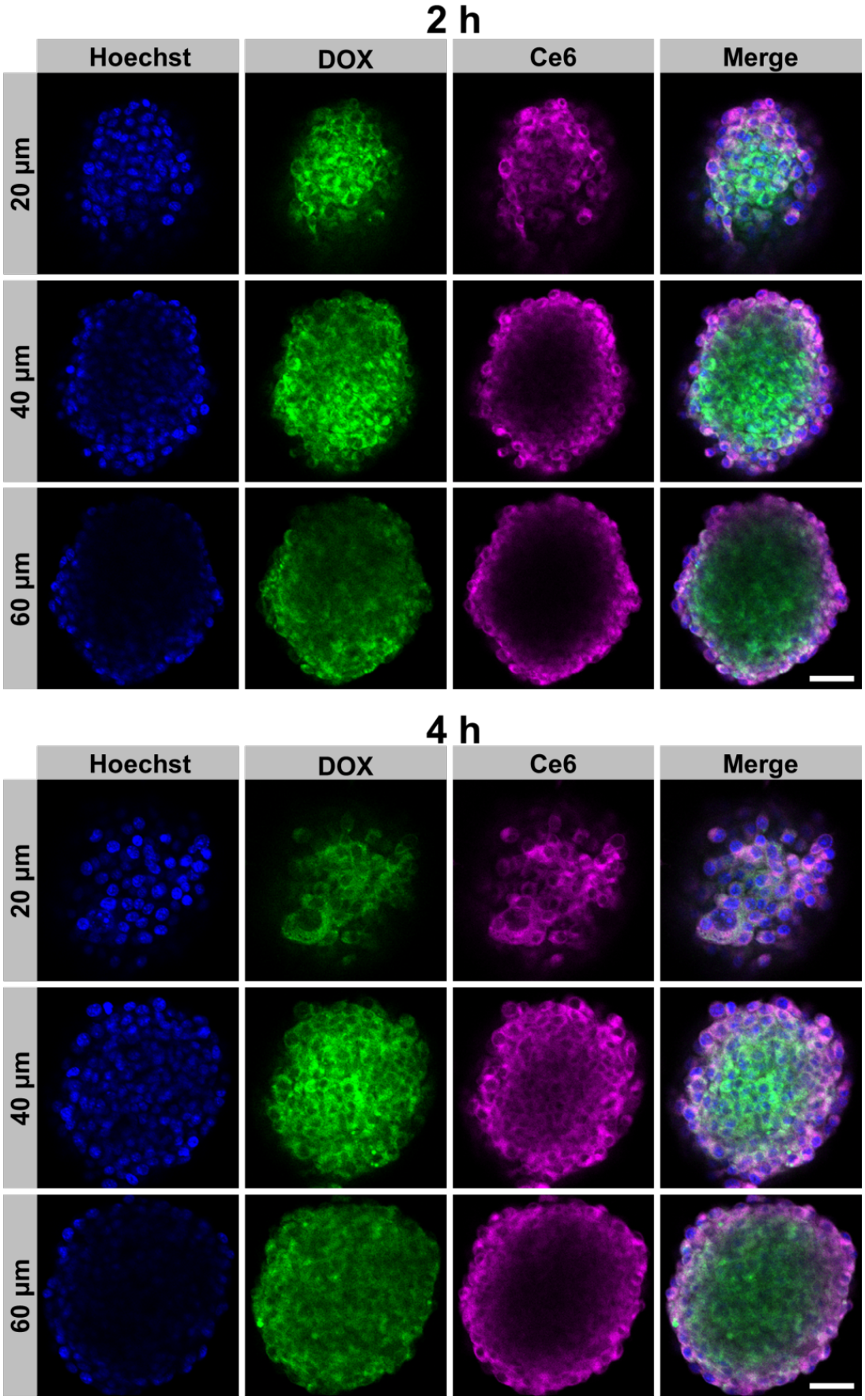



**Figure S45.** CLSM images of 4T1 tumor spheroids after treatment with LD-DOX/Ce6 for 2 h and 4 h, respectively (scale bars, 50 μm).

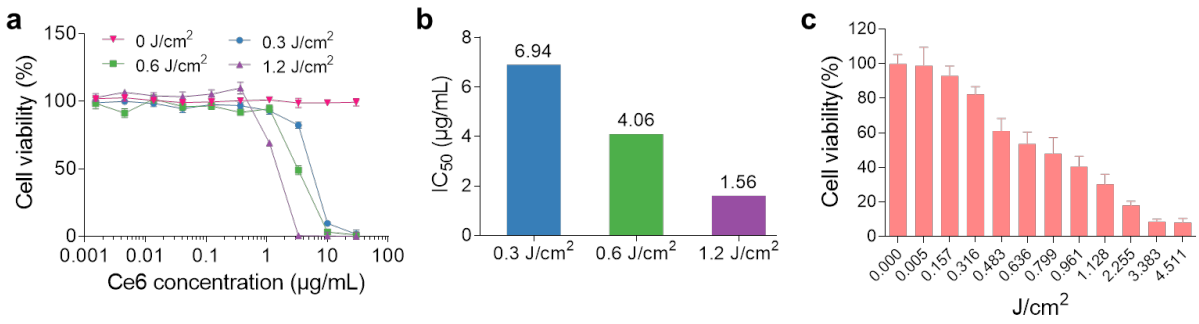



**Figure S46.** (a) Cytotoxicity and (b) $IC_{50}$ values of free Ce6 toward 4T1 cells under different laser intensities. (c) Cytotoxicity of Ce6 (3 μg $mL^{-1}$) toward 4T1 cells under the same laser intensity but different illumination time points.

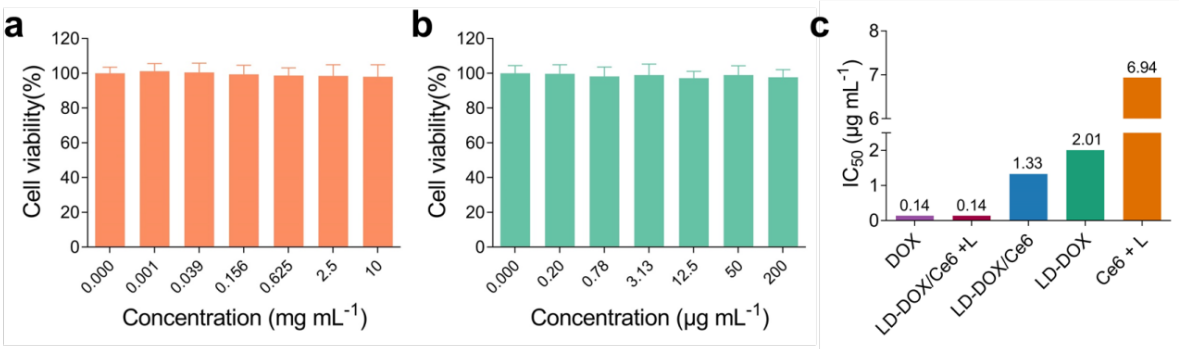



**Figure S47.** Cytotoxicity of (a) POEGMA-CTA and (b) MA-GFLG-$(NHNH_2)_4$ against 4T1 cells after incubation for 24 h at different concentrations. (c) $IC_{50}$ values for different formulations against 4T1 cells without laser radiation (DOX, LD-DOX, and LD-DOX/Ce6) and with laser radiation (LD-DOX/Ce6 + L, Ce6 + L).

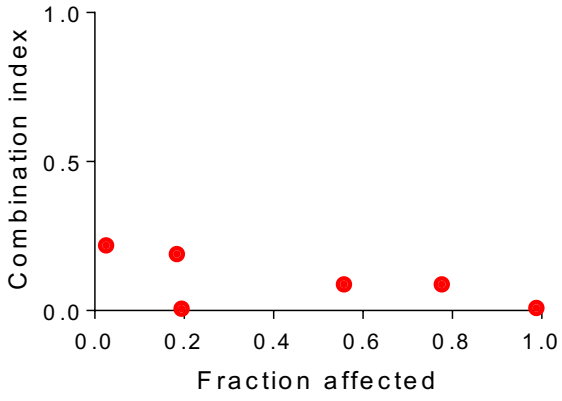



**Figure S48.** Combination indexes (CI) of LD-DOX prodrug and Ce6 with laser radiation.

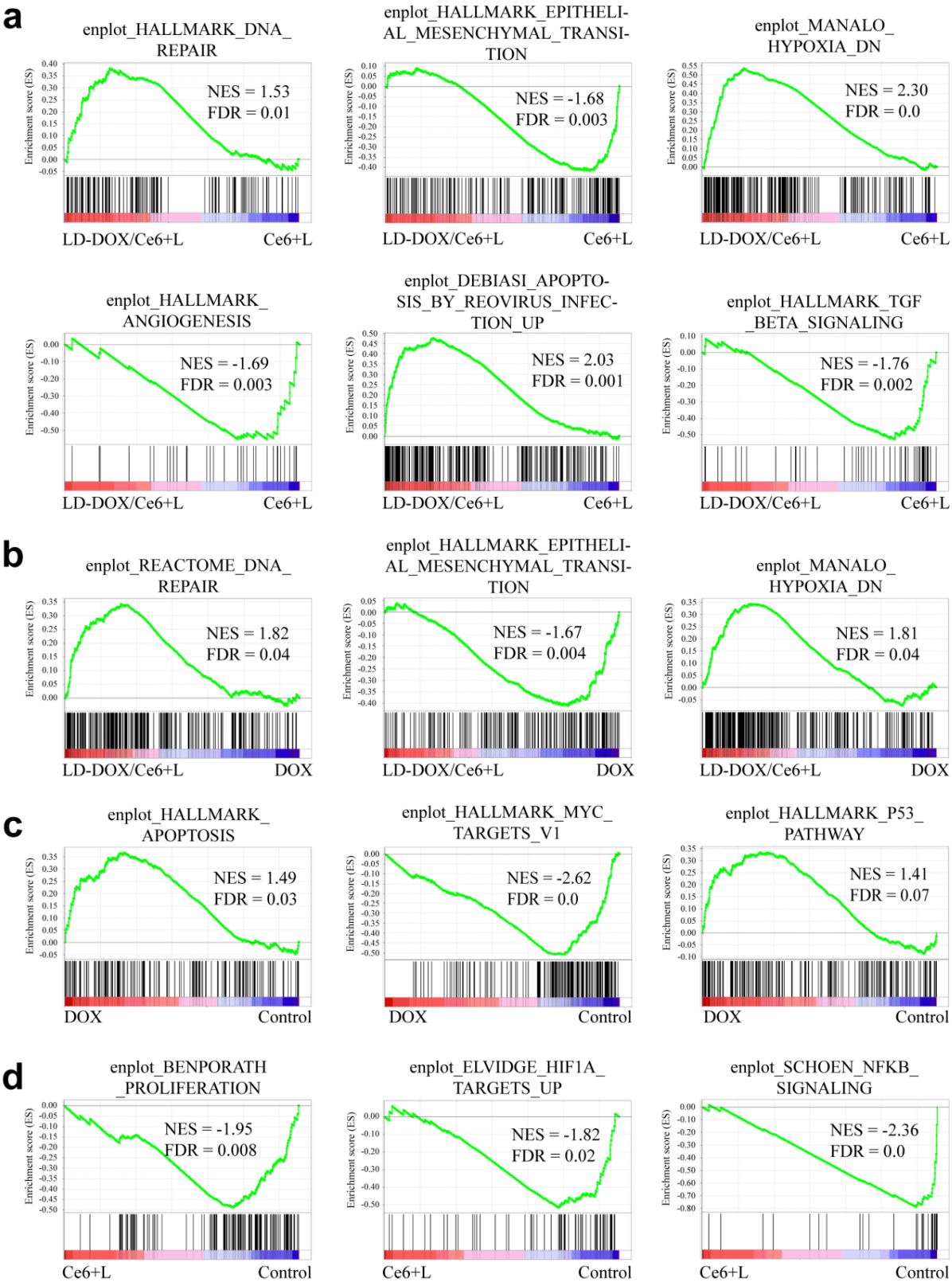



**Figure S49.** Gene Set Enrichment Analysis (GSEA) showing the pathways enriched in (a) LD-DOX/Ce6 + L vs Ce6 + L, (b) LD-DOX/Ce6 + L vs DOX (b), (c) DOX vs Control, and (d) Ce6 + L vs Control (d).

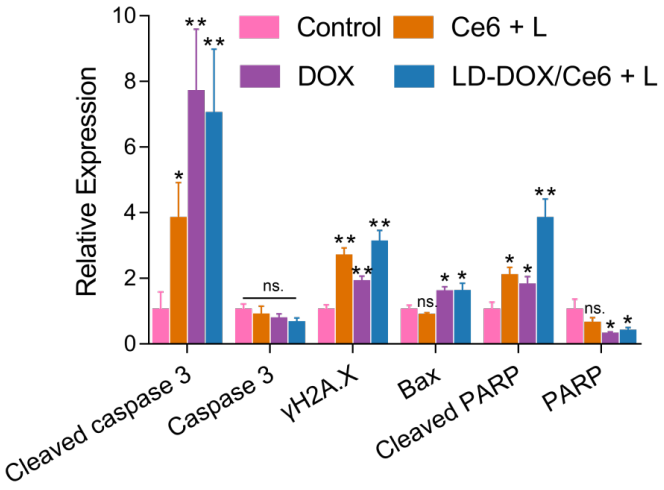



**Figure S50.** Semi-quantitative determination of the protein expression levels of cleaved Caspase 3, Caspase 3, γH2A.X, Bax, cleaved PARP, and PARP using the Western blotting after Control, Ce6 + L, DOX, or LD-DOX/Ce6 + L treatment. The bar graphs depict the relative protein expression levels normalized to GAPDH expression in three independent experiments. The bars correspond to the standard deviations of the mean of 3 replicates. *$p < 0.05$; **$p < 0.01$; ns., not significant.

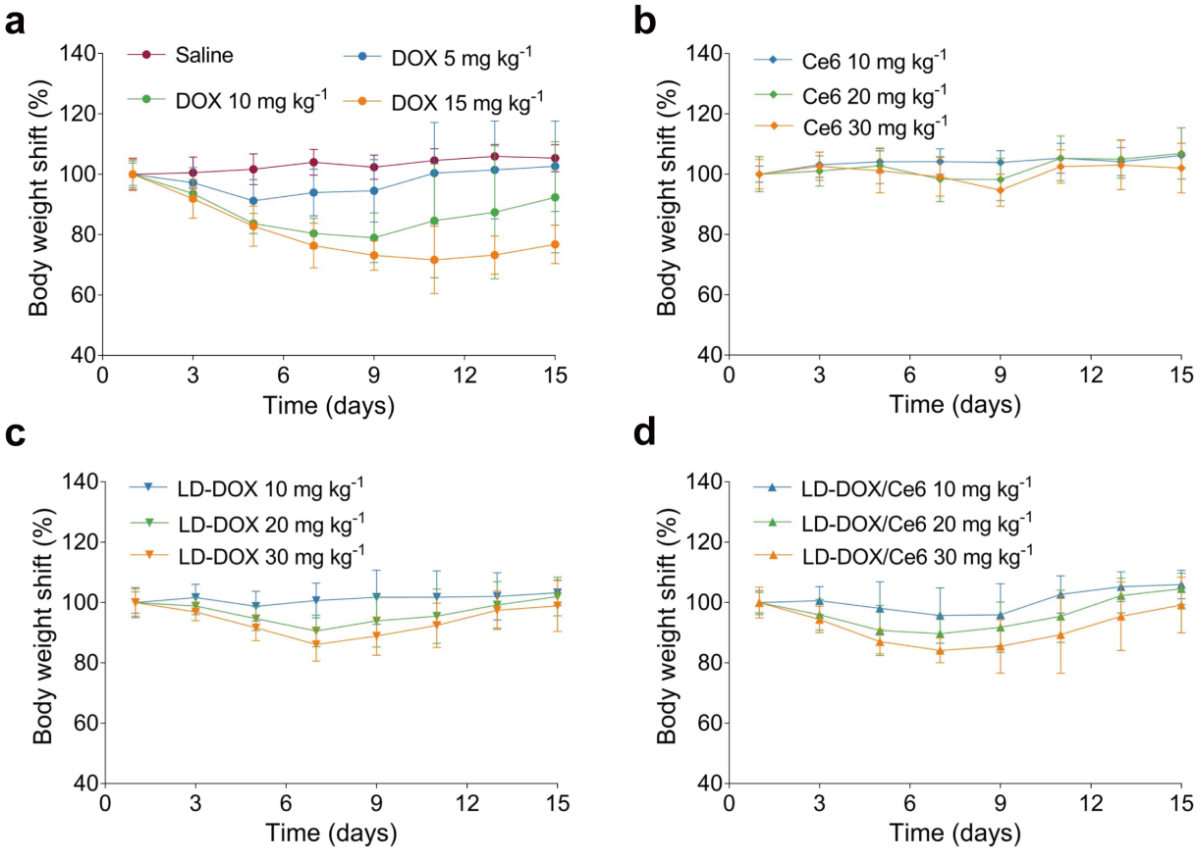



**Figure S51.** Body weight changes of normal mice treated by saline, free DOX, free Ce6，LD-DOX and LD-DOX/Ce6. For the DOX-treated group, one mouse died on day 13 at the DOX dose of 10 mg $kg^{-1}$; 2 mice died on day 9, and 2 on day 11 at a DOX dose of 15 mg $kg^{-1}$. Mice in other groups survived during the treatment period.

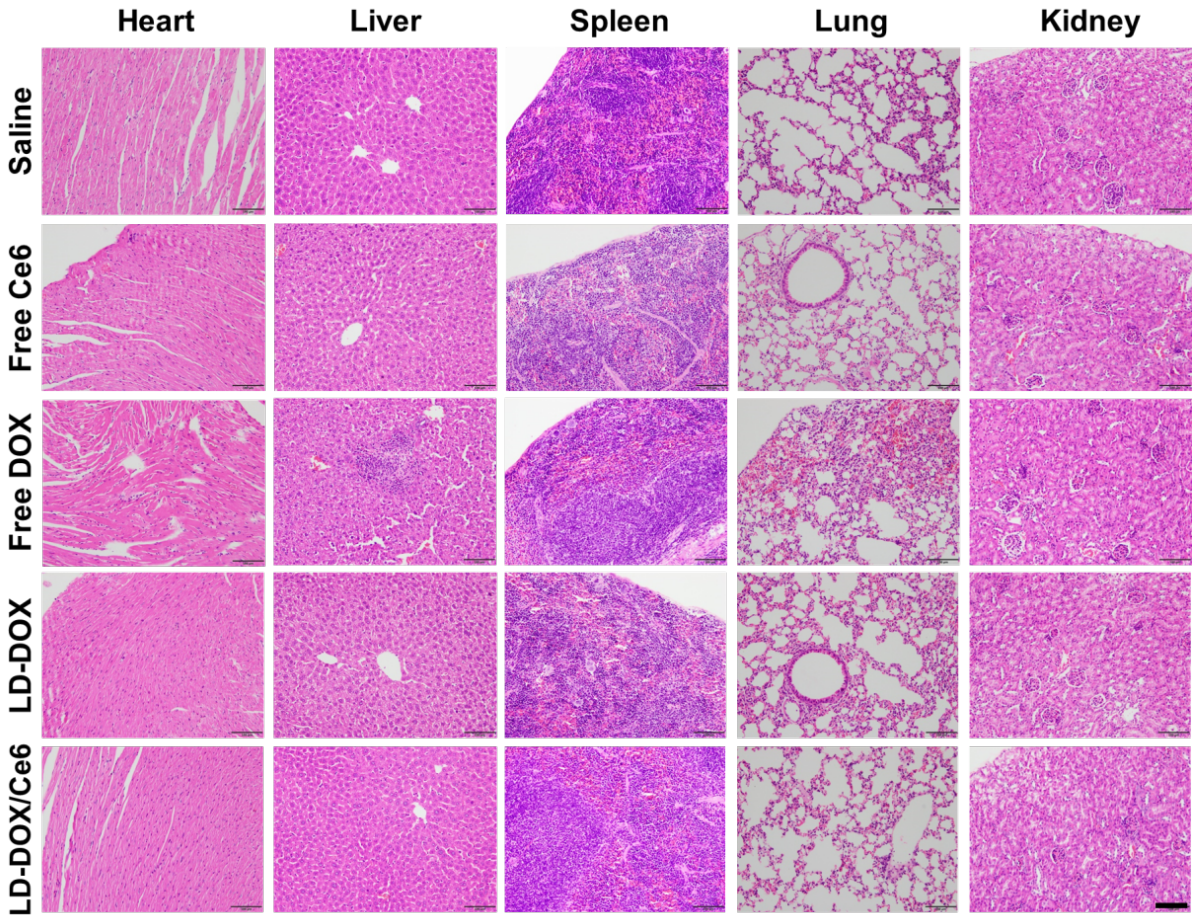



**Figure S52.** H&E staining tissue sections from major organs (heart, liver, spleen, lung and kidney) of normal 4T1 mice after treatment with saline, free DOX (10 mg $kg^{-1}$), free Ce6 (10 mg $kg^{-1}$), LD-DOX (equivalent DOX of 10 mg $kg^{-1}$) and LD-DOX/Ce6 (equivalent DOX of 10 mg $kg^{-1}$ and Ce6 of 11.1 mg $kg^{-1}$). In the DOX treatment group, the structure of myocardial cells was disordered, and the liver was infiltrated with inflammatory cells. No obvious abnormalities were observed in other experimental groups.

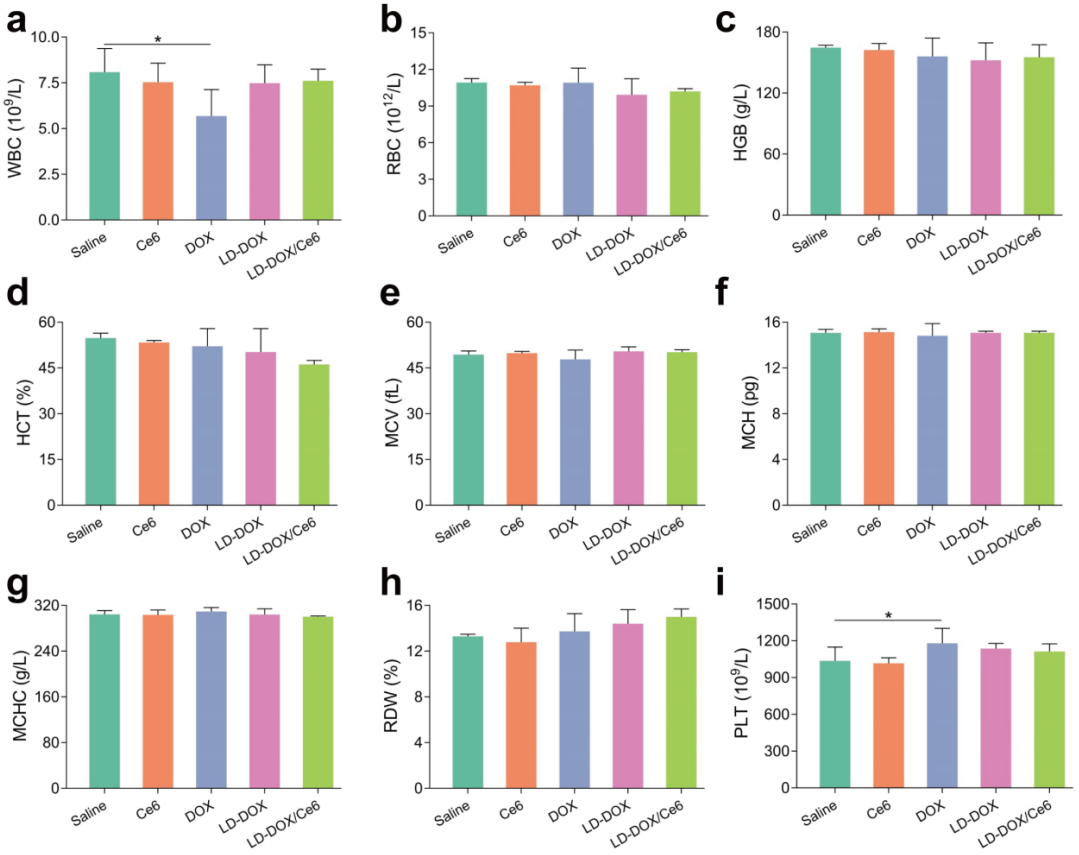



**Figure S53.** In vivo biosafety assessment of mice treated with free DOX (10 mg $kg^{-1}$), free Ce6 (10 mg $kg^{-1}$), LD-DOX (equivalent DOX of 10 mg $kg^{-1}$) and LD-DOX/Ce6 (equivalent DOX of 10 mg $kg^{-1}$ and Ce6 of 11.1 mg $kg^{-1}$). Mice treated with saline were used as a control. Routine blood analysis: (a)WBC, (b) RBC, (c) HGB, (d) HCT, (e) MCV, (f) MCH, (g) CHC, (h) RDW, and (i) PLT (mean ± SD, n = 4, **P* < 0.05).

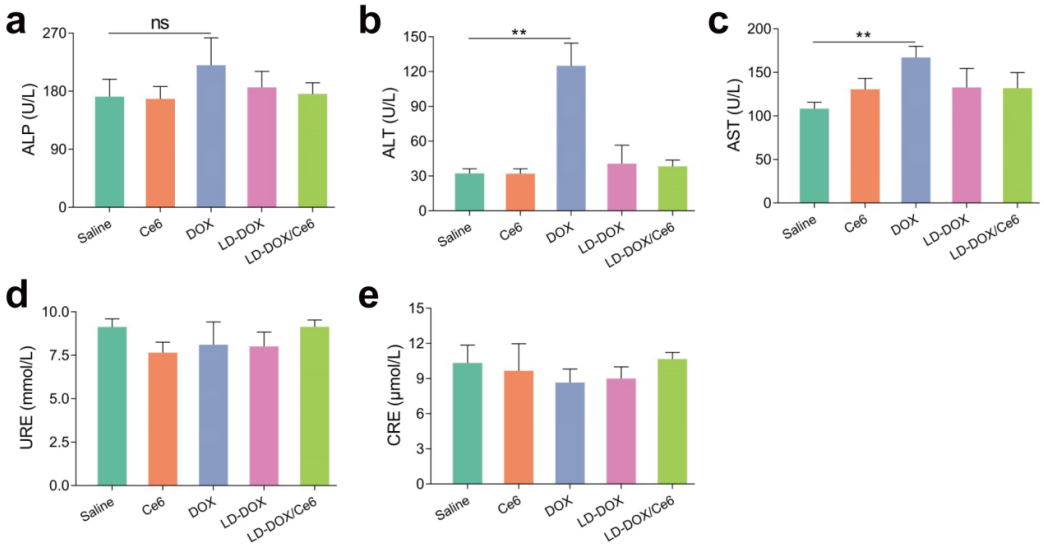



**Figure S54.** *In vivo* biosafety assessment of mice treated with free DOX (10 mg $kg^{-1}$), free Ce6 (10 mg $kg^{-1}$), LD-DOX (equivalent DOX of 10 mg $kg^{-1}$) and LD-DOX/Ce6 (equivalent DOX of 10 mg $kg^{-1}$ and Ce6 11.1 mg $kg^{-1}$). Mice treated with saline were used as a control. Blood biochemistry tests: (a) ALP, (b) ALT, (c) AST, (d) URE, and (e) CRE. Mean ± SD, n = 5, ***P* < 0.01, ns for no significant difference.

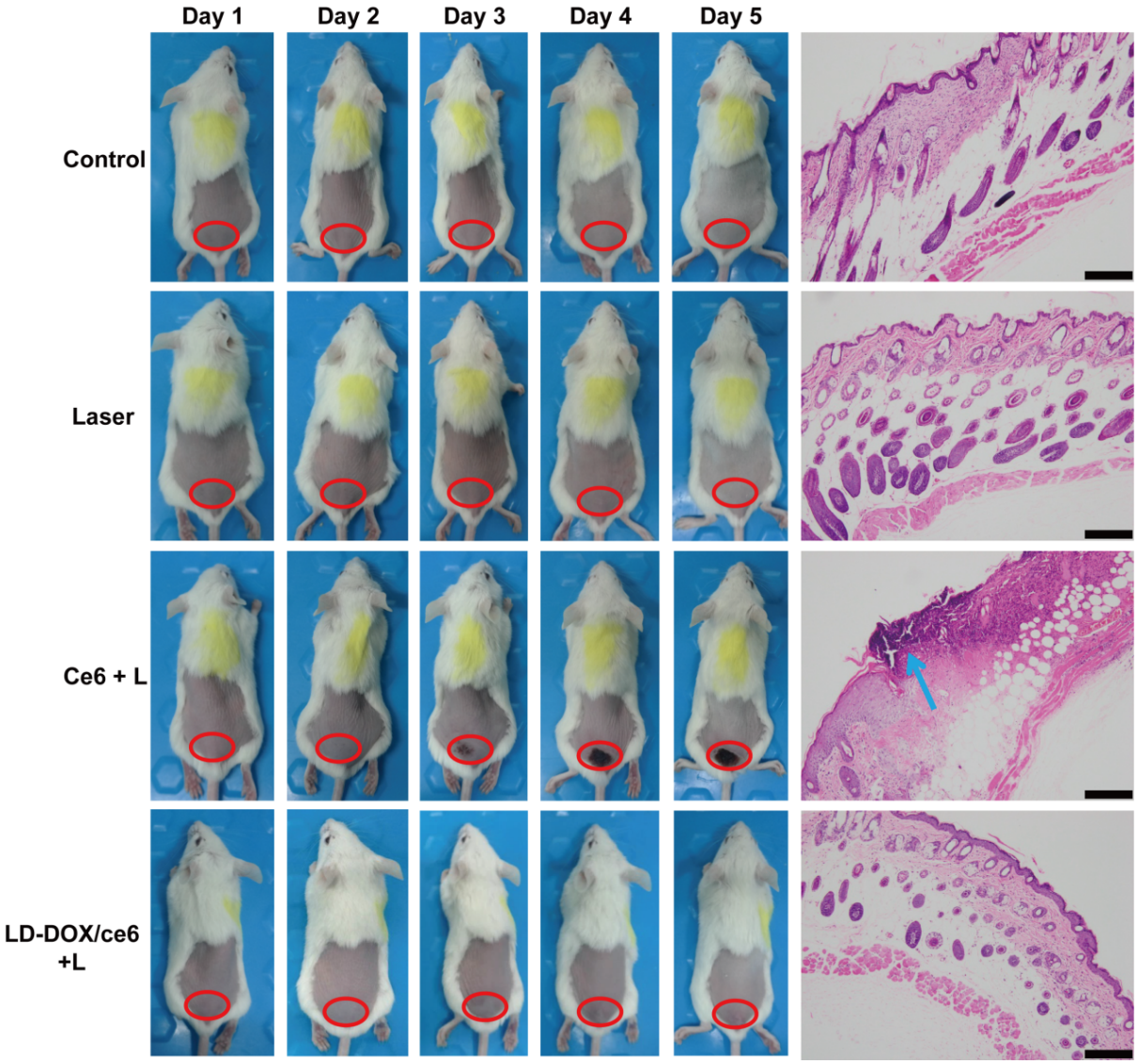



**Figure S55.** Representative skin phototoxicity photographs and H&E staining images of pathological changes on the shaved back of mice receiving iv. injection of free Ce6 or LD-DOX/Ce6 under irradiation of a 660 nm laser. Red circles for the regions exposed to laser light, and the blue arrow pointing to necrosis of the skin tissue (scale bar, 200 μm).

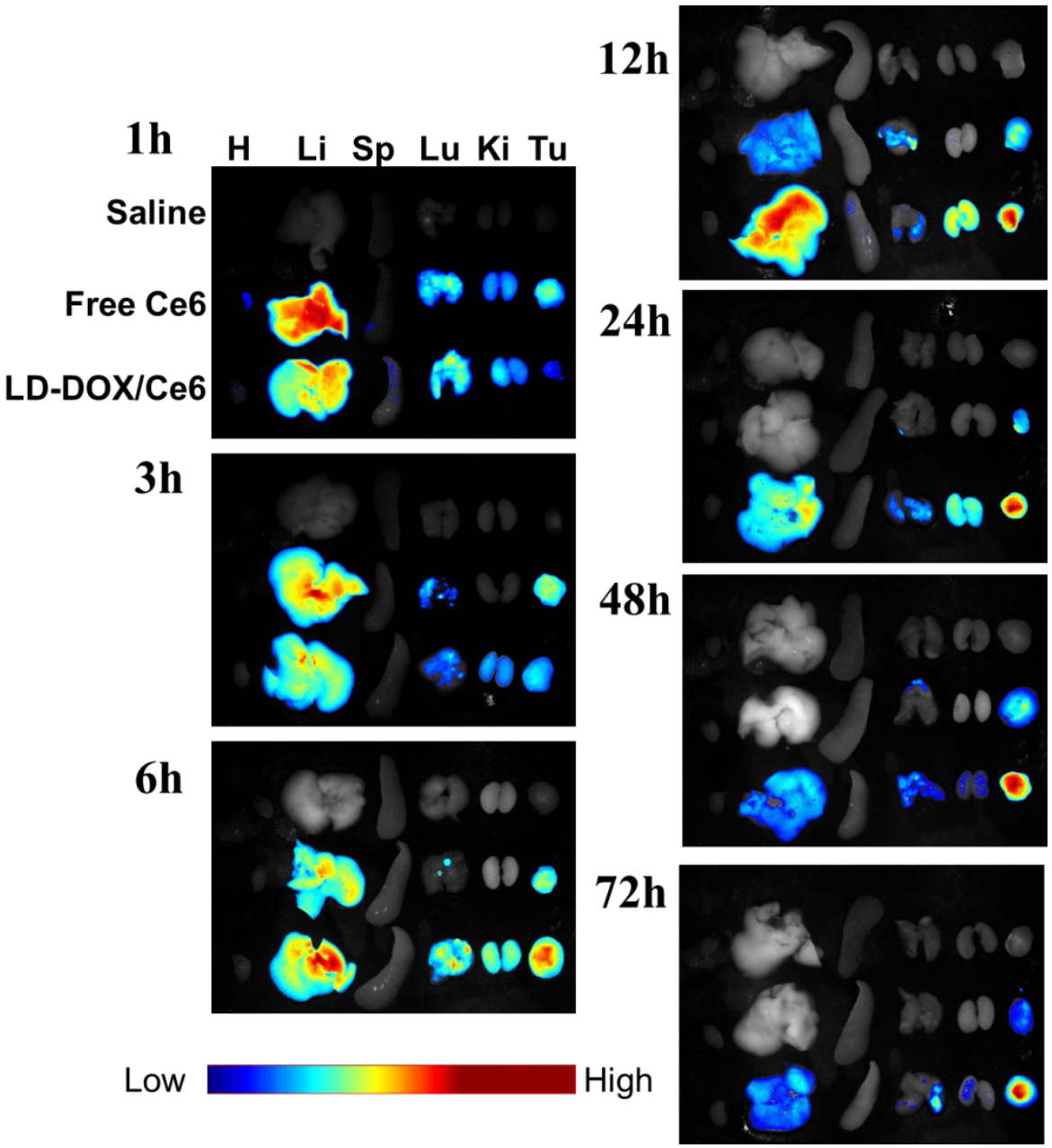



**Figure S56.** Fluorescence imaging of BALB/c mice bearing 4T1 tumors after injection of saline (top row), free Ce6 (second row) or LD-DOX/Ce6 (bottom row) at different time points in different organs and tumor (H: heart; Li: liver; Sp: spleen; Lu: lung; Ki: kidney; Tu: Tumor).

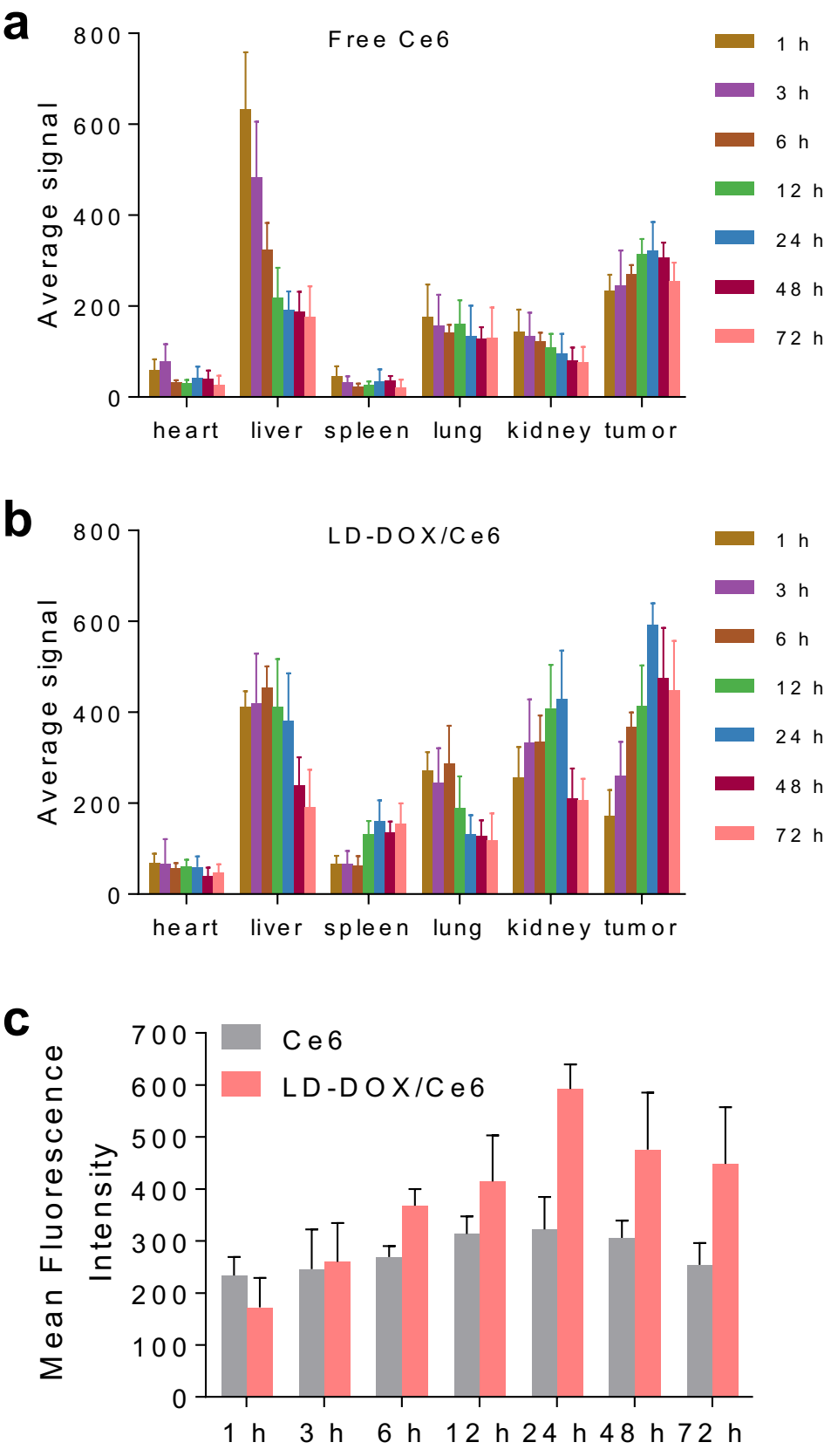



**Figure S57.** Semi-quantitative mean fluorescence intensity of (a) Ce6 and (b) LD-DOX/Ce6 NPs in major organs and tumors. (c) Temporal changes in the fluorescence signal of LD-DOX/Ce6 and Ce6 at the tumor site.

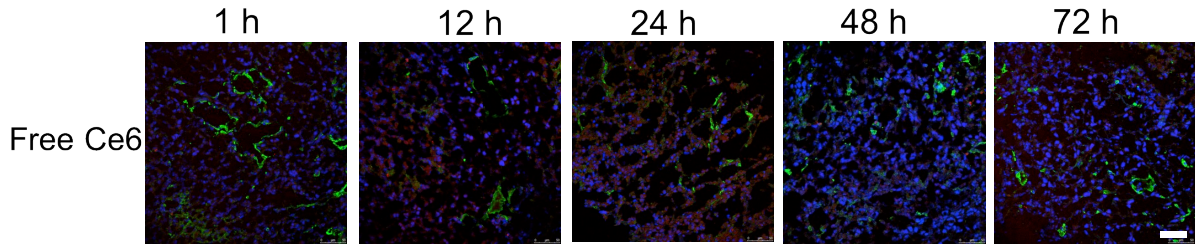



**Figure S58.** Frozen sections of the tumor under a CLSM at various time points after administration of Ce6 (× 400, scale bars = 50 μm). Green fluorescence was from anti-CD31 labeled blood vessels, red fluorescence from Ce6 and blue fluorescence from DAPI-stained nuclei.

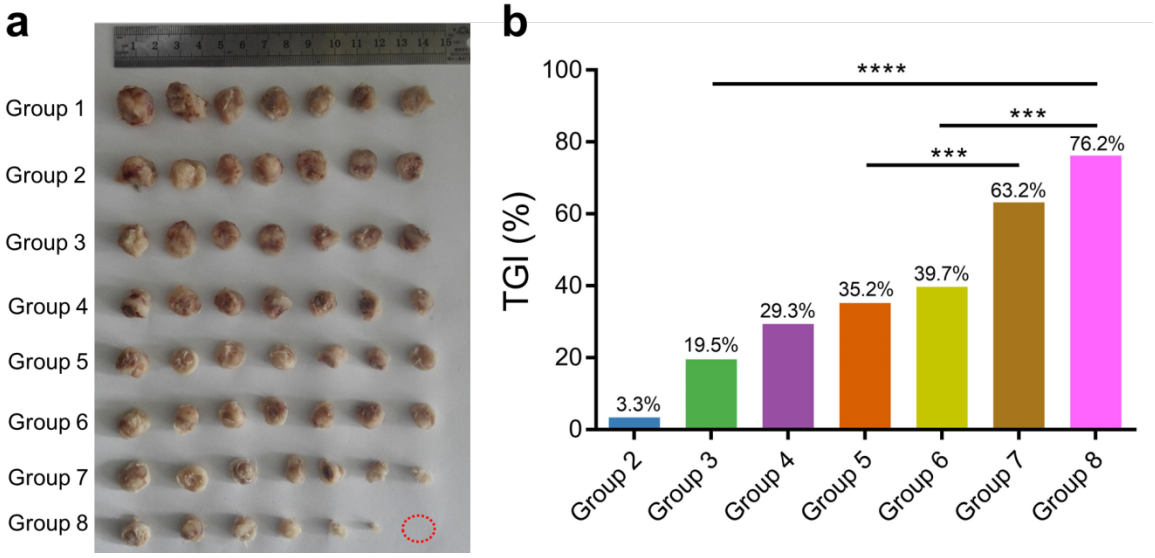



**Figure S59.** (a) Photographs of tumors from each treatment group collected at the end of treatment (Day 21), the red circle indicates that the mouse tumor completely disappeared. (b) Tumor growth inhibition (TGI) of mice in each treatment group. ***$P < 0.001$ and ****$P < 0.0001$. Group 1: saline; Group 2: laser alone; Group 3: free Ce6 + L (8.9 mg Ce6 $kg^{-1}$); Group 4: free DOX (4 mg DOX $kg^{-1}$); Group 5: LD-DOX/Ce6 without radiation (4 mg DOX $kg^{-1}$, 4.4 mg Ce6 $kg^{-1}$); Group 6: LD-DOX/Ce6 without laser irradiation (8 mg DOX $kg^{-1}$, 8.9 mg Ce6 $kg^{-1}$); Group 7: LD-DOX/Ce6 + L (4 mg DOX $kg^{-1}$, 4.4 mg Ce6 $kg^{-1}$); Group 8: LD-DOX/Ce6 + L (8 mg DOX $kg^{-1}$, 8.9 mg Ce6 $kg^{-1}$).

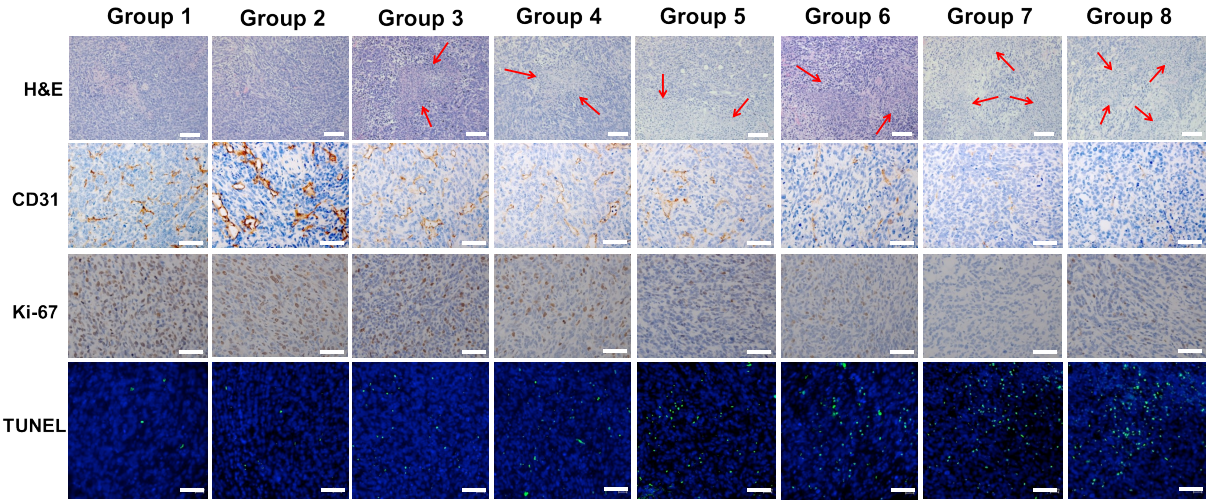



**Figure S60.** H&E stained tumors (× 200, red arrows point to the areas of tumor necrosis, scale bar = 100 μm) and histological analysis of tumor slices (× 400, scale bars = 50 μm) by CD 31 staining, Ki-67 staining and TUNEL staining after various treatments. Group 1: saline; Group 2: laser alone; Group 3: free Ce6 + L (8.9 mg Ce6 $kg^{-1}$); Group 4: free DOX (4 mg DOX $kg^{-1}$); Group 5: LD-DOX/Ce6 without radiation (4 mg DOX $kg^{-1}$, 4.4 mg Ce6 $kg^{-1}$); Group 6: LD-DOX/Ce6 without laser irradiation (8 mg DOX $kg^{-1}$, 8.9 mg Ce6 $kg^{-1}$); Group 7: LD-DOX/Ce6 + L (4 mg DOX $kg^{-1}$, 4.4 mg Ce6 $kg^{-1}$); Group 8: LD-DOX/Ce6 + L (8 mg DOX $kg^{-1}$, 8.9 mg Ce6 $kg^{-1}$).

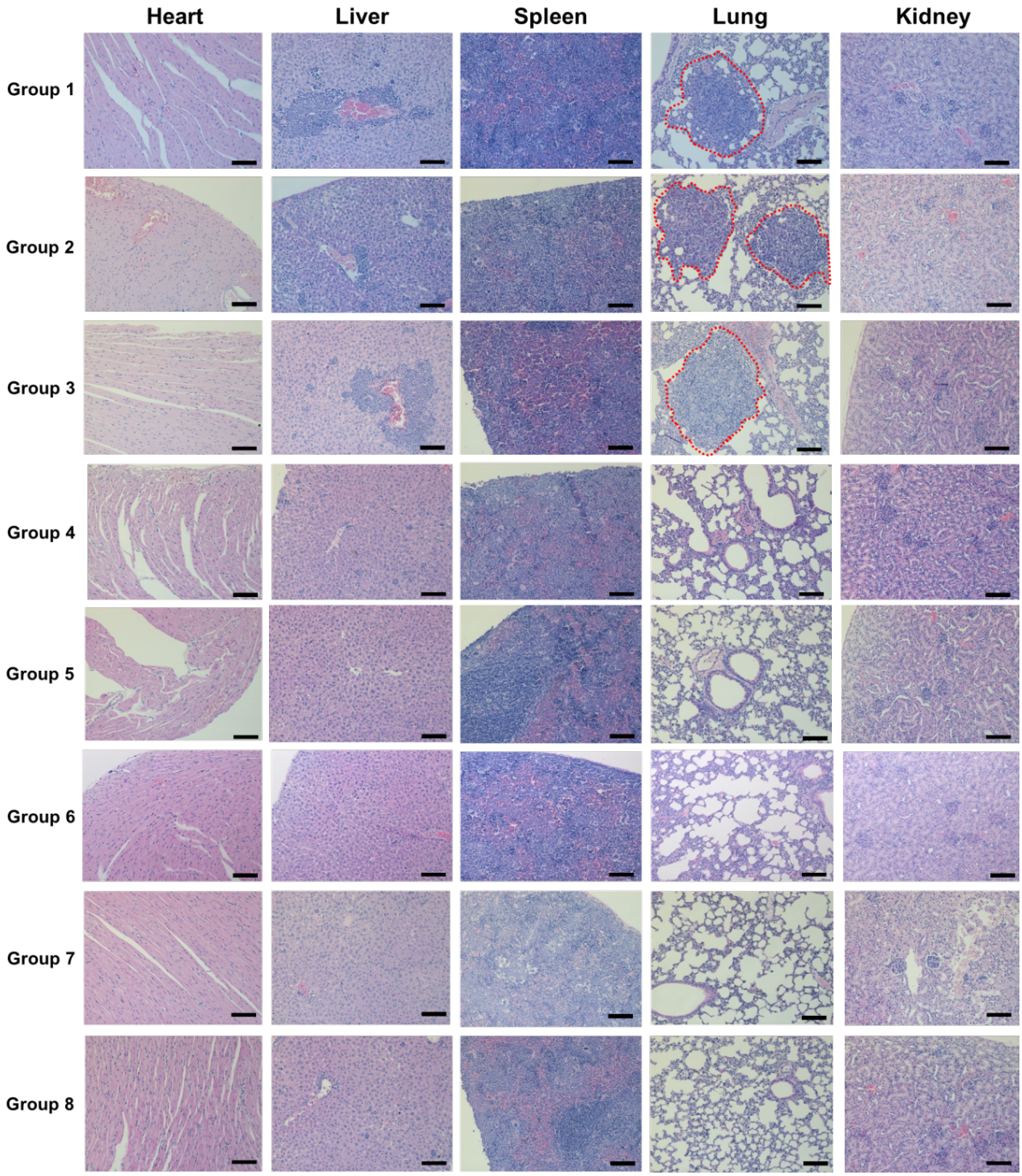



**Figure S61.** H&E stained tissue sections from the major organs (heart, liver, spleen, lung and kidney) of 4T1 tumor-bearing mice after 21 days post-treatment of chemo-photodynamic combination therapy (red circles indicated the pulmonary metastases. Scale bars, 100 μm). Group 1: saline; Group 2: laser alone; Group 3: free Ce6 + L (8.9 mg Ce6 $kg^{-1}$); Group 4: free DOX (4 mg DOX $kg^{-1}$); Group 5: LD-DOX/Ce6 without radiation (4 mg DOX $kg^{-1}$, 4.4 mg Ce6 $kg^{-1}$); Group 6: LD-DOX/Ce6 without laser irradiation (8 mg DOX $kg^{-1}$, 8.9 mg Ce6 $kg^{-1}$); Group 7: LD-DOX/Ce6 + L (4 mg DOX $kg^{-1}$, 4.4 mg Ce6 $kg^{-1}$); Group 8: LD-DOX/Ce6 + L (8 mg DOX $kg^{-1}$, 8.9 mg Ce6 $kg^{-1}$).

## 2.2. Tables

**Table S1.** Statistical parameters of molecular weight distribution (MWD) for POEGMA-CTA, POEGMA-GFLG-$(NHNHBoc)_x$ and POEGMA-GFGL-$(NHNHBoc)_x$ (x = 1, 2 or 4).

| Copolymer | $M_n$ (kgmol$^{-1}$) | $M_w$ (kg mol$^{-1}$) | Dispersity ($Đ$) |
|---|---|---|---|
| POEGMA-CTA | 21.7 | 26.7 | 1.23 |
| POEGMA-GFGL-NHNHBoc | 24.6 | 30.2 | 1.23 |
| POEGMA-GFGL-$(NHNHBoc)_2$ | 24.9 | 30.1 | 1.21 |
| POEGMA-GFGL-$(NHNHBoc)_4$ | 24.4 | 30.7 | 1.26 |
| POEGMA-GFLG-NHNHBoc | 24.1 | 30.1 | 1.25 |
| POEGMA-GFLG-$(NHNHBoc)_2$ | 24.6 | 30.7 | 1.25 |
| POEGMA-GFLG-$(NHNHBoc)_4$ | 23.7 | 28.9 | 1.22 |

**Table S2.** Drug loading content (DLC), critical micelle concentration (CMC) and self-assembled particle size of POEGMA-GFLG-$(DOX)_x$ and POEGMA-GFGL-$(DOX)_x$ (x = 1, 2 or 4).

| Copolymer prodrug | DLC of DOX (wt%) | CMC (μg mL$^{-1}$) | Size (nm) |
|---|---|---|---|
| POEGMA-GFGL-DOX | 8.7 | 107.98 | 45.9 ± 2.2 |
| POEGMA-GFGL-$(DOX)_2$ | 9.6 | 60.62 | 51.8 ± 1.9 |
| POEGMA-GFGL-$(DOX)_4$ | 11.3 | 7.83 | 55.2 ± 3.1 |
| POEGMA-GFLG-DOX | 8.1 | 77.45 | 39.5 ± 1.7 |
| POEGMA-GFLG-$(DOX)_2$ | 9.7 | 48.92 | 51.4 ± 2.6 |
| POEGMA-GFLG-$(DOX)_4$ | 10.8 | 2.22 | 46.8 ± 2.4 |

**Table S3.** Pharmacokinetic parameters, which were acquired by fitting the data to a non-compartment model using PKSolver 2.0 software, of Balb/c female mice after intravenous administration of free DOX, POEGMA-GFLG-DOX, POEGMA-GFLG-$(DOX)_2$ and POEGMA-GFLG-$(DOX)_4$ at an equivalent DOX dose of 5 mg kg$^{-1}$.

| Parameter | DOX | POEGMA-GFLG-DOX | POEGMA-GFLG-$(DOX)_2$ | POEGMA-GFLG-$(DOX)_4$ |
|---|---|---|---|---|
| AUC(0-∞) ( μg mL$^{-1}$ min) | 558.9 | 5076.0 | 6697.4 | 10887.1 |
| $T_{1/2}$ (h) | 3.7 | 13.5 | 17.0 | 24.0 |
| Cl ((μg mL$^{-1}$) min$^{-1}$) | 0.179 | 0.020 | 0.015 | 0.009 |
| MRT (0–∞) (h) | 4.8 | 19.6 | 24.7 | 34.4 |

**Table S4.** Characterization of Ce6-loaded NPs at different feeding weight ratios (DLC: drug loading content; DLE: drug loading efficiency). The DLC of DOX in POEGMA-GFLG-$(DOX)_4$ was 10.8 wt%.

| Sample | Feeding Weight ratio (Ce6 : DOX) | DLC of Ce6 | DLE of Ce6 | Zeta potential (mV) | Size (nm) | PDI |
|---|---|---|---|---|---|---|
| 1 | 0.5:1 | 3.8% ± 0.3 | 61.0% ± 2.3 | 0.19 ± 0.03 | 52.0 ± 0.4 | 0.229 ± 0.018 |
| 2 | 1:1 | 5.6% ± 0.2 | 67.9% ± 4.1 | 0.08 ± 0.02 | 61.7 ± 2.3 | 0.235 ± 0.021 |
| 3 | 1.5:1 | 10.0% ± 0.8 | 74.3% ± 2.7 | -0.21 ± 0.04 | 68.8 ± 4.2 | 0.257 ± 0.026 |
| 4 | 2:1 | 11.3% ± 1.4 | 71.5% ± 3.6 | -0.25 ± 0.03 | 74.4 ± 3.8 | 0.260 ± 0.023 |
| 5 | 2.5:1 | 14.0% ± 1.3 | 70.2% ± 2.8 | -0.33 ± 0.04 | 78.1 ± 3.6 | 0.283 ± 0.027 |

**Table S5.** Characterization of PTX-loaded NPs at different feeding weight ratios (DLC: drug loading content; DLE: drug loading efficiency). The DLC of DOX in POEGMA-GFLG-$(DOX)_4$ was 10.8 wt%.

| Sample | Feeding Weight ratio (PTX : DOX) | DLC of PTX | DLE of PTX | Zeta potential (mV) | Size (nm) | PDI |
|---|---|---|---|---|---|---|
| 1 | 0.5:1 | 4.0% ± 0.1 | 76.2% ± 1.8 | 0.49 ± 0.10 | 50.1 ± 1.7 | 0.285 ± 0.011 |
| 2 | 1:1 | 7.9% ± 0.2 | 79.7% ± 2.0 | 0.53 ± 0.05 | 56.4 ± 2.6 | 0.285 ± 0.010 |
| 3 | 1.5:1 | 11.2% ± 0.1 | 78.0% ± 1.0 | 0.57 ± 0.09 | 61.8 ± 4.6 | 0.240 ± 0.015 |
| 4 | 2:1 | 14.4% ± 0.2 | 77.2% ± 1.0 | 0.53 ± 0.05 | 66.6 ± 6.2 | 0.272 ± 0.018 |
| 5 | 2.5:1 | 16.4% ± 0.4 | 72.8% ± 2.1 | 0.56 ± 0.09 | 67.5 ± 6.0 | 0.280 ± 0.031 |

**Table S6.** Pharmacokinetic parameters, acquired by fitting the data to a non-compartment model using PKSolver 2.0 software, of Balb/c female mice after intravenous administration of Ce6 and LD-DOX/Ce6 NPs at an equivalent Ce6 dose of 5 mg $kg^{-1}$.

| Parameter | Ce6 | LD-DOX/Ce6 |
|---|---|---|
| AUC(0-∞) ( μg $mL^{-1}$ min) | 493.0 | 4184.2 |
| $T_{1/2}$ (h) | 1.6 | 13.6 |
| Cl ((μg $mL^{-1}$) $min^{-1}$) | 0.203 | 0.024 |
| MRT (0–∞) (h) | 1.5 | 18.4 |

## 3. References


[1] R. Zhang, K. Luo, J. Yang, M. Sima, Y. Sun, M. M. Janat-Amsbury, J. Kopecek, *J. Control. Release* **2013**, *166*, 66.

[2] M. B. Liu, G. R. Liu, L. W. Zhou, J. Z. Chang, *Arch. Comput. Method. E.* **2014**, *22*, 529.

[3] a) J. R. Spaeth, I. G. Kevrekidis, A. Z. Panagiotopoulos, *J. Chem. Phys.* **2011**, *135*, 184903; b) T. Chen, W. Liu, S. Xiong, D. Li, S. Fang, Z. Wu, Q. Wang, X. Chen, *ACS Appl. Mater. Interfaces* **2019**, *11*, 45276; c) S. Y. Nie, W. J. Lin, N. Yao, X. D. Guo, L. J. Zhang, *ACS Appl. Mater. Interfaces* **2014**, *6*, 17668.

[4] H. Zhang, *Methods Mol. Biol.* **2017**, *1522*, 17.

[5] T. C. Chou, *Pharmacol. Rev.* **2006**, *58*, 621.

[6] A. Dobin, C. A. Davis, F. Schlesinger, J. Drenkow, C. Zaleski, S. Jha, P. Batut, M. Chaisson, T. R. Gingeras, *Bioinformatics* **2013**, *29*, 15.

[7] M. I. Love, W. Huber, S. Anders, *Genome Biol.* **2014**, *15*, 550.

[8] G. Yu, L. G. Wang, Y. Han, Q. Y. He, *Omics.* **2012**, *16*, 284.

[9] A. Subramanian, P. Tamayo, V. K. Mootha, S. Mukherjee, B. L. Ebert, M. A. Gillette, A. Paulovich, S. L. Pomeroy, T. R. Golub, E. S. Lander, J. P. Mesirov, *P. Natl. Acad. Sci. USA.* **2005**, *102*, 15545.

[10] H. Cai, X. Dai, X. Wang, P. Tan, L. Gu, Q. Luo, X. Zheng, Z. Li, H. Zhu, H. Zhang, Z. Gu, Q. Gong, K. Luo, *Adv. Sci.* **2020**, *7*, 1903243.

[11] L. Quan, Y. Zhang, B. J. Crielaard, A. Dusad, S. M. Lele, C. J. F. Rijcken, J. M. Metselaar, H. Kostkova, T. Etrych, K. Ulbrich, F. Kiessling, T. R. Mikuls, W. E. Hennink, G. Storm, T. Lammers, D. Wang, *ACS Nano* **2014**, *8*, 458.